Functional Characterization of Musashi1 in Mouse Postnatal Development and Intestinal Homeostasis

By

Thelma Thabani Chiremba

Submitted to the graduate degree program in Molecular Biosciences and the Graduate Faculty of the University of Kansas in partial fulfillment of the requirements for the degree of Doctor of Philosophy.

_____

Chair: Kristi L. Neufeld

_____

Mizuki Azuma

_____

James Calvet

_____

Dan A. Dixon

_____

Berl R. Oakley

Date Defended: 10 December 2020

The dissertation committee for Thelma Thabani Chiremba certifies
that this is the approved version of the following dissertation:

Functional Characterization of Musashi1 in Mouse Postnatal Development and Intestinal Homeostasis

Kristi L. Neufeld

Date Approved: 10 December 2020

Abstract

Tightly regulated gene expression is essential for normal development and maintenance of tissue homeostasis. RNA-binding proteins (RBPs) are essential facilitators of spatiotemporal gene expression control by regulating post-transcriptional activity of target RNAs. Of particular interest to our lab is the RBP Musashi1 (Msi1), which displays aberrant expression in multiple cancer types, including colorectal cancers. Msi1 controls translation, stability, and alternative splicing of developmentally relevant target mRNAs. Previous in-vitro studies in our lab implicated Msi1 in the regulation of intestinal tissue homeostasis. To elucidate functions of Msi1 in the intestinal epithelium, our lab generated a mouse model that allows conditional and inducible Msi1 overexpression. In this dissertation, I report that young mice ubiquitously overexpressing Msi1 ($Msi1^{O/E}$) had an overall stunted growth phenotype and experienced premature death. These $Msi1^{O/E}$ mice failed to maintain normal organ proportions, with particular organs either too small or too large when compared to control mice. For example, the small intestine tissue of $Msi1^{O/E}$ mice was smaller, whereas the brain was larger. Therefore, my work suggests a potential role of Msi1 in regulating postnatal development of various mouse organs.

Focusing on the intestinal tissue, I demonstrate that ubiquitous $Msi1^{O/E}$ mice had decreased proportions of proliferating intestinal epithelial cells (IECs) and reduced growth of small intestine villi and colon crypts. These findings were consistent with the shortened intestinal tissue phenotype. Furthermore, I show that dampened *Cdc20* expression could underlie the intestinal growth defects and diminished IEC proliferation. Most importantly, I report novel results showing that Msi1 controls IEC differentiation in a region-specific manner. The ileum sections of $Msi1^{O/E}$ mice displayed more pronounced alterations in IEC differentiation and Notch signaling when compared to the jejunum and colon sections. In addition, I observed enhanced expression of intestinal ion transporters in $Msi1^{O/E}$ mice. These ion transporters

regulate movement of ions across the intestinal epithelia and facilitate reabsorption of water into IECs. Taken together, my findings implicate Msi1 in intestinal tissue development, and homeostasis, as well as highlight distinct roles of Msi1 along the intestinal tract.

Using an intestine-specific Msi1 overexpressing mouse line (Vil-Msi1$^{O/E}$), I show that our novel mouse model is a versatile tool that can be utilized to elucidate developmental and pathological functions of Msi1 in any tissue of interest. Notably, the Vil-Msi1$^{O/E}$ mice had a greater longevity than ubiquitous Msi1$^{O/E}$ mice. This finding suggests that the early premature death observed in ubiquitous Msi1$^{O/E}$ mice might be due to contributions from tissues or cell types distinct from intestinal epithelia. Furthermore, the greater longevity of Vil-Msi1$^{O/E}$ mice indicates that this model will be a useful tool in studies which require mice to be viable for a longer time, such as those focusing on tumor formation and screening of new therapeutics.

Lastly, Msi1 is an attractive therapeutic target due to its enhanced expression in various cancer types and association with tumor progression. In this dissertation, I tested several small molecule inhibitors of Msi1 in tissue culture and identified three compounds that were effective at pharmacologically-relevant concentrations.

Acknowledgments

I am extremely grateful to my advisor, Dr. Kristi Neufeld, for her invaluable guidance and unwavering support during the course of my dissertation. Her enthusiastic encouragement, unparalleled patience, and profound belief in my abilities motivated me to do my best. Thank you for being an incredible mentor and role model; your great sense of humor made the learning process enjoyable even during the stressful and challenging times.

I am deeply indebted to my dissertation committee members, Dr. Mizuki Azuma, Dr. James Calvet, Dr. Dan Dixon, and Dr. Berl Oakley, for their insightful suggestions. Assistance given by my past committee members, Dr. Matthew Buechner, Dr. Alexander Moise, and Dr. Rob Ward, was instrumental in advancing my research.

Many thanks to my fellow colleagues, Dr. Christian Gomez, Dr. Taybor Parker, Dr. Aaron Rudeen, and Eldric Carreon for their constructive feedback during lab meetings. I am particularly grateful for the technical and data collection assistance provided by William McGuinness, Vinamratha Rao, and Kayla Castillo. You all made our work environment welcoming and fun.

I would like to thank the various funding sources that made this work possible. This dissertation was supported by the National Institutes of Health (R01 CA178831 and P30CA168524), the Provost's Strategic Initiative Grant (University of Kansas Research Investment Council), and the University of Kansas Cancer Center Pilot Grant. I received a conference travel award from the University of Kansas Research Excellence Initiative program. Personal stipends were provided by the University of Kansas Graduate Research and Teaching Assistantships. I also gratefully acknowledge my fellow graduate students and professors from the University of Kansas Molecular Biosciences Department for their helpful contributions during my seminar presentations.

To all my friends, thank you for your encouragement and motivation. Particularly supportive were my good friends Abigail and Dr. Abel Chikanda, and their daughters Anotida

and Annemarie. I am grateful to my dear friends Rujeko Chinomona, Haeyoung Kim, and Dr. Ian Munhenzva for lending a sympathetic ear whenever I needed it. I also wish to thank Nancy Guinane and her family for being the best host family during my undergraduate at Grinnell College, and for their continued support.

Finally, I would like to extend my deepest gratitude to my family for their constant love, support and understanding. I will forever be grateful to my parents, Monica and Peter, for all the sacrifices they have made for me and for always encouraging me in my endeavors. To my sisters and brothers-in-law, thank you for your wise counsel and reassurance throughout my dissertation work. Special thanks to my biggest supporters, my nieces and nephews, who never failed to cheer me up during the rough times.

Dedication

To my mother, Monica Machira, for always being my inspiration.

Table of contents

List of figures

List of tables

List of abbreviations

Apc	Adenomatous Polyposis Coli
Atp12a	H+/K+ transporting, non-gastric, alpha polypeptide
CDX	Caudal-type homeobox 2
ChgA	Chromogranin A
CLD	Chloride-losing diarrhea
Cre	Cre recombinase
Ct	Cycle threshold
CTCF	Corrected total cellular fluorescence
dpi	Days post-injection
Dra	Down-regulated in adenoma
DSS	Dextran sodium sulfate
ENaC	Epithelial sodium channel
ERT2	Tamoxifen-inducible estrogen receptor
Hes1	Hairy and enhancer of split
Hnf	Hepatocyte nuclear factor
IEC	Intestinal epithelial cell
ISC	Intestinal stem cell
Jag1	Jagged1
Lac	Lactase
Lgr5	Leucine-rich repeat-containing G-protein coupled receptor 5

Math1	Mouse atonal homolog1
Msi1	Musashi1
$Msi1^{O/E}$	Msi1-overexpressing, ubiquitous
Muc2	Mucin2
Nhe3	Sodium-hydrogen antiporter
O/E	Overexpression
RBP	RNA-binding protein
RRM	RNA-recognition motif
Sis	Sucrase-isomaltase
Slc26a3	Solute carrier family 26 member 3
Slc29a3	Solute carrier family 9 member 3
TAM	Tamoxifen
Ubc	Ubiquitin
Vil	Villin
$Vil\text{-}Msi1^{O/E}$	Villin-Msi1-overexpressing, intestine specific
wpi	Weeks post-injection

CHAPTER 1: INTRODUCTION

Regulation of gene expression and disease

Precise spatiotemporal gene expression is essential for normal tissue development and functioning. Biological events such as gastrulation, organogenesis and tissue self-renewal require proper coordination of cellular processes in response to internal and environmental cues. These processes include cell growth, proliferation, differentiation, movement and death (1–3). The internal and environmental cues can be biochemical or biophysical, and examples include growth factors, hormones, cytokines or changes in the extracellular matrix composition (4,5). When a cell receives a signal, it triggers specific intracellular signaling pathways that can alter gene expression and ultimately modify cellular activity. Thus, gene expression changes in response to activation and deactivation of signaling pathways must be tightly regulated to allow appropriate cellular behavior.

Aberrant gene expression and cellular activity is implicated in many diseases and disorders. Cleft palate, one of the most common human birth defects, is caused by improper fusion of the upper facial prominences as a result of disrupted cell movement (6,7). Other birth defects with underlying genetic factors include microcephaly (8), congenital heart defect (9), congenital short-bowel syndrome (10), and Down syndrome (11). Although the severity differs among individuals, birth defects can have profound immediate and long-term effects on a child's development and quality of life. For example, if not surgically corrected, cleft palates can adversely affect speech and auditory development in children (12,13).

In addition to birth defects, dysregulated gene expression is associated with tumorigenesis. Tumors arise when a cell acquires mutations that promote cell proliferation or inhibit cell death, and this causes the cell to become unresponsive to mechanisms that normally regulate tissue cell numbers. Cancer is the second leading cause of mortality after heart disease in both men and women in the United States (14). It is estimated that more than

600,000 cancer deaths will occur nationally in 2020 (15). Like birth defects, cancer poses significant health and financial challenges at both individual and societal levels (16,17). As such, identifying and characterizing molecular factors that regulate gene expression could elucidate potential therapeutic targets for genetic diseases.

RNA-binding proteins in gene expression control

Eukaryotic gene expression is a dynamic and intricate process with regulation at the transcriptional, RNA processing, translational and posttranslational levels. Each regulatory step involves multiple molecular factors that work cooperatively to determine when, where and to what extent a gene is expressed. RNA-binding proteins (RBPs) represent a unique group of essential regulators that function mostly at the post-transcriptional level. The human genome encodes at least 1,600 RBPs with diverse roles (18). RBPs bind to sequence-specific motifs in target RNAs, and modulate all aspects of RNA metabolism including splicing, 5'-capping, polyadenylation, stability, transport, and translation (19). Furthermore, emerging evidence suggests that RBPs can function at the transcriptional level by interacting with transcriptional factors and active gene promoters (20).

Given that RBPs are crucial regulators of gene expression, it is not surprising that perturbations in their regulatory mechanisms are linked to many diseases. For example, aberrant RBP expression and function is observed in cancer (21), birth defects (22), neurodegenerative disorders (23), and autoimmune diseases (24). One such RBP is Musashi1 (Msi1), which displays altered expression in many cancers, including colorectal (25), brain (26), lung, prostate and breast cancers (27). In addition to tumorigenesis, Msi1 is also involved in the pathogenesis of Alzheimer's disease (23) and Zika virus-induced microcephaly (28). The involvement of Msi1 in such a diverse range of diseases is possibly due to its large pool of target mRNAs that play central roles in many processes such as cell cycle (29), differentiation (30) and metabolism (21). The best characterized role of Msi1 is translational regulation through

binding to specific sequences in the 3'-untranslated region (3'-UTR) of target mRNAs and repressing translation initiation (31).

The discovery of Musashi

The *musashi (msi)* gene was first identified in *Drosophila melanogaster* as an RBP that is required for proper development of the adult external sensory organ (32). During normal mechanosensory bristle development, a sensory organ precursor (SOP) cell divides asymmetrically to generate two progenitor precursors: a non-neuronal IIa cell and a neuronal IIb cell (Fig. 1.1A). Then the IIa precursor cell further divides asymmetrically into a socket cell and a shaft cell that eventually make up the external part of the bristle. Two successive asymmetric divisions of the IIb cell produce a neuron, a glia, and a sheath cell. Nakamura et al. (1994) generated flies with a loss-of-function msi mutation by excising part of the *msi* coding sequence using the P-transposable element system. Unlike wild-type flies, the $msi^{-/-}$ mutants developed external sensory organs that had two IIa cells, but lacked the IIb cell (Fig. 1.1B). This resulted in flies with two mechanosensory bristles originating from a single SOP cell. Consequently, the gene responsible for this double-bristled phenotype was named "*musash*i" after Miyamoto Musashi, a famous Japanese samurai who initiated the use of two swords when fighting, in favor of the traditional single-sword style.

Initial predictions for potential targets of *D. melanogaster* msi (d-msi) came from studies that showed similar or opposite phenotypes to the *msi* loss-of-function mutants. Tramtrack (ttk) is a zinc finger-containing transcriptional repressor that functions downstream of Notch signaling during fate determination of the SOP cell (33). Unlike *msi* mutants, loss of *ttk* expression resulted in the duplication of the IIb cell at the expense of the IIa cell. In contrast, *ttk* overexpressing mutants had a similar phenotype to *msi* loss-of-function mutants (33,34). Msi and ttk expression do not overlap during development of the adult external sensory organ as indicated by immunohistochemistry staining. Ttk is expressed in the non-neural IIa, socket and

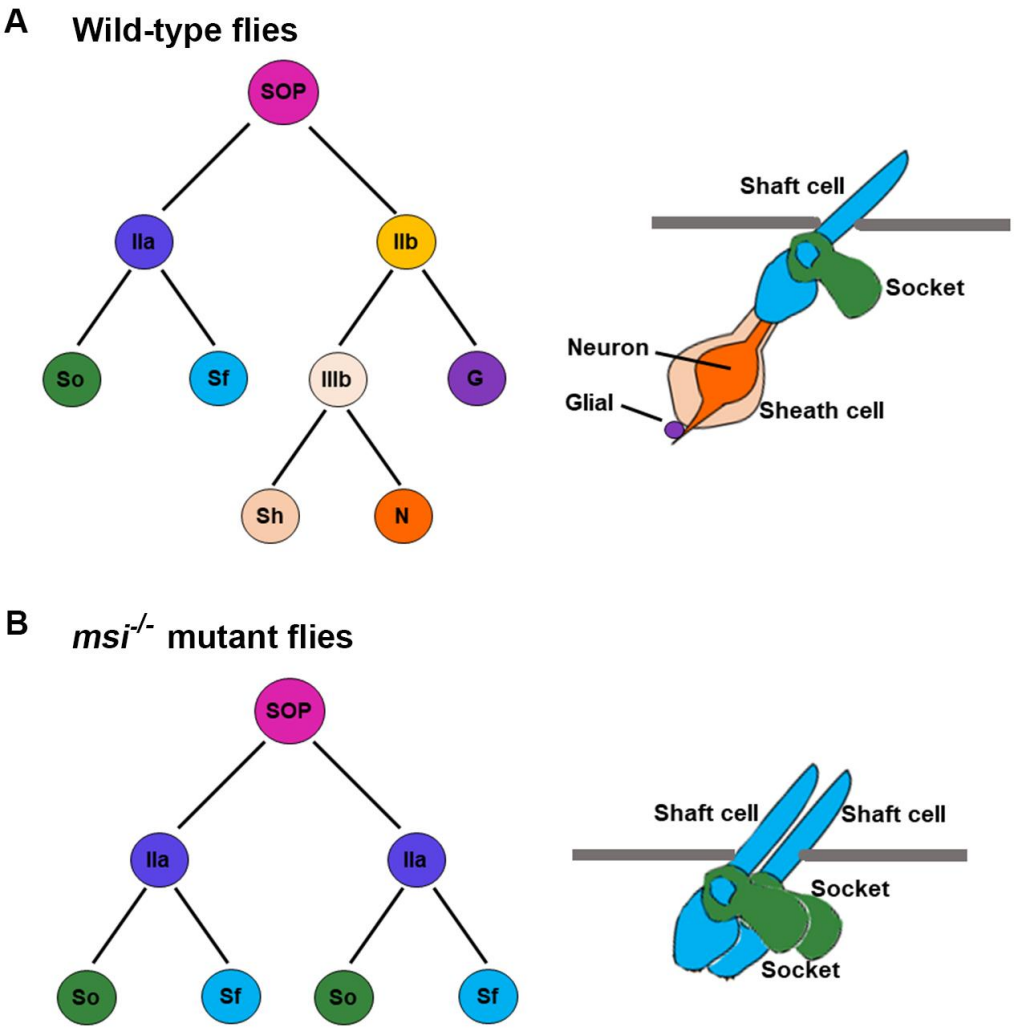

Figure 1.1: Msi1 is required for proper development of the external sensory organ in *Drosophila melanogaster*. (A) Normal asymmetric division of the sensory organ precursor cell (SOP) produces two progenitor precursor cells (IIa and IIb), which divides further, asymmetrically, to produce 5 different daughter cell types. [Socket cell = So, Shaft cell= Sf, Glia = G, Sheath cell = Sh, Neuron = N] **(B)** Loss of *msi* results in duplication of IIa cells at the expense of IIb cell, and the resulting flies have 2 socket and 2 shaft cells. *Adapted with permission from Okano et al., (2002) J Cell Sci.* (104)

shaft cells, but is not expressed in the neural IIb cell or its daughter cells (34). While, msi is expressed in the nuclei of neural progenitor cells (32). Therefore, the staining pattern and phenotypes of mutant flies suggested that msi and ttk have antagonistic roles in sensilla development, possibly through post-transcriptional processing of ttk mRNA by msi.

A possible regulatory role of msi on *ttk* expression was later revealed in a study that investigated the role of msi in *D. melanogaster* eye development (35). Msi is expressed in the nuclei of all developing photoreceptor cells. Additional analysis showed that msi functions cooperatively and redundantly with seven in absentia (sina) to ensure proper neural differentiation in photoreceptor cells. Eyes from *msi* and *sina* double loss-of-function mutants had severe differentiation and morphological abnormalities as well as enhanced ttk protein expression when compared to individual mutants. Reducing *ttk* expression significantly rescued these developmental defects. Thus, this study implied that sina and msi negatively regulate *ttk* expression at the post-transcriptional level during neurogenesis of photoreceptor cells.

These early studies in *D. melanogaster* suggested that msi could be involved in regulating translation or stability of target mRNAs. Since the discovery of *msi* almost two and half decades ago, much effort has been put forward to characterize msi expression, protein structure, target mRNAs, and regulatory mechanism using various model organisms.

Identification of Msi in other organisms

D-msi has orthologs in several species including human (36), mouse (37), rat (38), *Xenopus laevis* (39), and zebrafish (40). Two MSI protein family members have been identified thus far, and they are encoded by genes located within different chromosomes. Mouse-Msi1 (m-Msi1) and mouse-Msi2 (m-Msi2) share a 69% amino acid sequence identity, and an overall 75% charge identity (41). Although the expression of the two proteins overlaps in brain, intestines and other tissues, they also have distinct tissue distributions (37,41). Msi2 is expressed in more tissue types than Msi1. Functional redundancy of m-Msi1 and m-Msi2 has been reported in the

intestinal epithelium (21) and brain (42). However, the two proteins also have distinct roles even in cells or tissues where their expression overlaps, such as in the ovaries (43) and pancreatic β-cells (44). Human MSI1 and MSI2 share similar expression patterns as their mouse orthologs (NCBI gene).

The Neufeld group has historically focused its research efforts on the tumor suppressor *Adenomatous Polyposis Coli* (*Apc*). More recently, we began studying Msi1 because *Msi1* expression was highly upregulated (~13-fold) in mouse intestinal epithelium tissue upon loss of *Apc* (45). Elevated Msi1 protein levels were also observed in mouse intestinal tumors expressing truncated, loss-of-function Apc (46).

Characterization of mammalian Msi1 and determinants for binding to mRNA targets

Human *MSI1* and m-*Msi1* genes encode 362-amino acid (39 kDa) protein products that have 99.4% (360/362) and 99.7% (361/362) amino acid sequence and charge similarities, respectively (UCSC genome browser and NCBI protein blast). Msi1 has two tandem RNA recognition motifs (RRM1 and RRM2), also known as RNA-binding domains, (Fig. 1.2A) (36,37,47). RRMs are conserved 80-90 amino acid domains that are ubiquitously present in RBPs, albeit in different numbers (48,49). These RRMs facilitate interaction between an RBP and its target RNAs through binding to sequence-specific motifs within the RNA. The two Msi1 RRMs are highly homologous with 45% sequence and 65% charge identities (50). Their structures are shown in Fig. 1.2B (50–53).

The β-strands in the RRMs provide a surface for Msi1 to interact with a target mRNA (52). RRM1 β-strands are more positively charged than RRM2 β-strands, and this charge difference makes it more favorable for RRM1 to interact with the negatively-charged mRNA. The significance of RRM1 in target recognition and binding was highlighted by studies in which the substitution of three RRM1 phenylanine residues with leucines obliterated Msi1 binding to targets (30,54). These phenylanine residues (F23, F63 and F65; Fig. 1.2B) stabilize the protein-

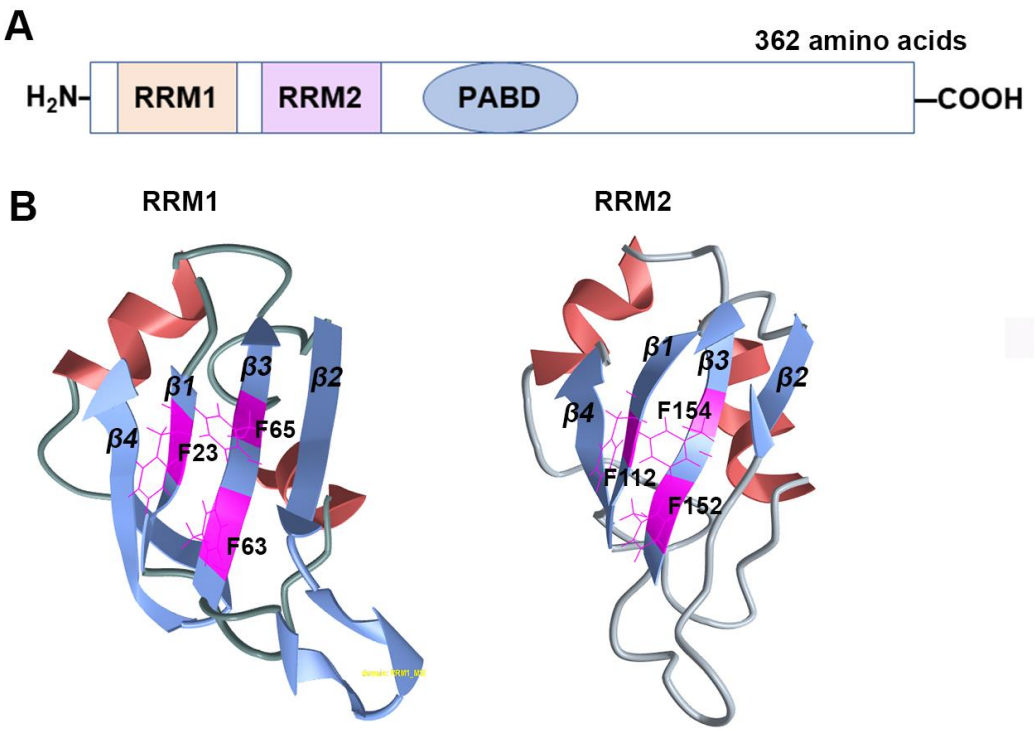

Figure 1.2: Structure of Msi1 protein and RNA-recognition motifs. (A) Linear representation of human and mouse Msi1 showing the two RNA-recognition motifs (RRM1 and RRM2) and the poly(A)-binding protein domain (PABD).m**(B)** Structures of Msi1 RRMs. Side chains of three phenylanine residues (F23, F63 and F65) that are essential for RRM1 binding to targets are shown. *Illustrations for RRMs were modified from deposited structures (PDB 2RS2 and 2MSS) in the NCBI Structure Summary MMDB database. Adapted from Miyanoiri et al., 2003.*

mRNA complex by providing aromatic-aromatic stacking interactions with specific nucleotide bases in the mRNA (50,55). In addition, the β1- and β3-strands in RRM1 are more flexible than those in RRM2; thus, provide ideal flexibility which facilitates induced fit interactions between Msi1 and a target mRNA as well as better conditions for robust stacking interactions (52). As a result, RRM1 has a higher binding affinity to target RNAs than RRM2 (30,47).

The binding specificity of Msi1 to targets is determined by RRM1 (52,55). This is probably due to the higher binding affinity of RRM1. Although RRM2 provides additional binding affinity, it does not alter the specificity to mRNA targets. As such, RRM1 has been proposed as a potential therapeutic target for small-molecule inhibitors that are designed to compete with mRNA for binding to Msi1. Chapter 7 describes results from a project in which I screened several small-molecule Msi1inhibitors that were designed and synthesized by our collaborators.

Mouse Numb mRNA is a target of Msi1 protein

The first sequence-specific binding motif for m-Msi was identified as (G/A)U_{1-3}AGU via an in vitro SELEX assay (Systematic Evolution of Ligands by Exponential enrichment) (30). *Numb* mRNA was used to validate the sequence motif because *Numb* had been proposed as a likely Msi1 target based on evidence that Numb is required for neural differentiation, and both Msi1 and Numb are expressed in undifferentiated *D. melanogaster* and mouse neural progenitor cells (32,37,56). Numb protein, a Notch signaling antagonist, is localized asymmetrically to the SOP cell membrane, and is differentially proportioned to one of the intermediate progenitor cells following SOP cell division (56). Sequence analysis revealed that the 3'-UTR of m-*Numb* mRNA contains the consensus sequence motif, and Msi1 can bind to m-*Numb* both in vitro and in vivo (30). Mutating the motif abolished binding of Msi1 to targets, indicating that the sequence is essential for Msi1 activity (26,29,30,54). Later studies confirmed the Msi1 SELEX-motif and showed that a conserved UAG trinucleotide forms the core of the Msi1 binding site and underlies the binding specificity of Msi1 to mRNA targets (27,50,55,57).

Mechanism for translational inhibition by Msi1

To elucidate the post-transcriptional regulatory role of Msi1, Imai et al. (2001) analyzed effects of ectopic expression of Msi1 on m-*Numb* mRNA and protein levels in NIH 3T3 cells that do not express endogenous Msi1. There were no significant alterations in m-*Numb* mRNA levels. However, a 78% reduction in endogenous m-Numb protein quantity was observed. These findings indicated that Msi1 negatively regulates *Numb* translation without affecting its mRNA stability.

It was later shown that Msi1 regulates target mRNA translation by competing with the eukaryotic translation initiation factor eIF4G for binding poly(A)-binding protein (PABP) (31). Msi1 can be immunoprecipitated with PABP, and RNase treatment does not disrupt this association, implying a direct interaction between the two proteins. The C-terminus of Msi1 contains a PABP-binding domain (PABD) (Figure 1.2A), and Msi1 also binds to the same region within PABP as eIF4G. Addition of incremental amounts of Msi1 decreases the amount of PABP that can be immunoprecipitated with eIF4G in a dose-dependent manner. These results suggested that Msi1 represses translation initiation of targets by inhibiting the PABP-eIF4G interaction. Supporting this analysis, immunostaining showed discrete cytoplasmic puncta of Msi1 in addition to a more diffuse cytoplasmic staining. Strong colocalization of Msi1 with PABP, eIF4G, eIF4E, and markers for mRNA processing bodies indicated that the puncta were stress granules that contained stalled translation initiation complexes as a result of Msi1 inhibiting 80s ribosomal complex formation. Lastly, recombinant Msi1 without the PABD does not inhibit translation; thus, the interaction between Msi1 and PABP is required for Msi1 regulatory activity.

Identification of additional Msi1 targets

Other validated mammalian Msi1 targets that were identified using the SELEX motif (G/A)U_{1-3}AGU include *APC* (54), the cycle inhibitor *p21/CDKN1A/WAF1* (29), and *Tensin3 (TNS3)*, a negative regulator of cell migration (26). Similar to *Numb*, the Msi1-binding motif is

located within the 3'-UTRs of *APC*, *p21*, and *Tns3* mRNAs, and Msi1 overexpression reduced APC, p21, and Tns3 protein levels. However, unlike *p21*, *Numb*, and *Tns3*, overexpressing Msi1 increased the amount of *APC* mRNA in a dose-dependent manner (54). These results suggested that Msi1 could also be involved in regulating the stability of specific targets. However, it remains to be determined how Msi1 can stabilize certain targets while not affecting others.

Four major studies have been conducted thus far to identify additional direct targets of Msi1. First, an in vitro study that utilized HEK293T cells, a human embryonic kidney-derived cell line, and ribonucleoprotein immunoprecipitation followed by microarray analysis (RIP-Chip) identified 64 mRNAs that were preferentially associated with MSI1 (58). 62 out of the 64 mRNAs have at least one MSI1 consensus binding motif in their 3'-UTRs. Two additional large scale in vitro studies also employed the unbiased RIP-Chip, and individual-nucleotide resolution cross-linking and immunoprecipitation (iCLIP) techniques to identify multiple direct mRNA targets of Msi1 in two brain cancer-derived cell lines (57,59). Uren et al., (2015) found multiple intronic binding sites in direct targets, suggesting that Msi1 could have other post-transcriptional regulatory roles. Furthermore, the enrichment of the UAG trinucleotide sequence in Msi1 binding sites raised the possibility that Msi1 could target stop codons and interfere with translation termination. However, the iCLIP results showed that Msi1 rarely binds to UAGs that serve as stop codons; thus, Msi1 is likely not involved in translation termination (57).

Recently, 2,371 endogenous wild-type Msi1 targets were identified in a large scale CLIP-Seq study that utilized cells isolated from mouse intestinal epithelium (21). *Pten* (*Phosphatase and tensin homolog*) and *β-catenin*, an antagonist of the mTOR pathway and a transcriptional effector of the canonical Wnt signaling pathway, respectively, were the only targets of Msi1 that were validated in this study. Msi1 overexpression repressed translation of both targets. Although the majority of targets that were identified in these four studies have yet to be fully validated, gene ontology analyses revealed that the proteins encoded by the targets are involved in the

regulation of many cellular processes including cell proliferation, cell differentiation, cell cycle, apoptosis, cell metabolism, post-translational protein modification, protein localization, and cell movement.

Other post-transcriptional regulatory functions of Msi1

Similar to previous findings (57), Li et al., (2015) identified additional binding motifs for Msi1 in the 5'-UTRs, coding sequences, introns and 3'-UTRs (Fig. 1.4G). Interaction of Msi1 with non-3'-UTR motifs suggested additional RNA regulatory functions of Msi1. Although Msi1 was originally identified as a translational repressor, several studies have shown that Msi1 can enhance translation of direct targets such as *Robo3* (*Roundabout guidance receptor 3*) (60), *cMet* (61), *Pdgfrα* (*Platelet-derived growth factor receptor alpha*), *Egfr* (*Epidermal growth factor receptor*), and *Igf1r* (*Insulin-like growth factor 1 receptor*) (57). Msi1 binding sites are present in the 3'-UTRs of all five targets. The protein expression of these targets increases when Msi1 is overexpressed in cultured cells or mouse models, and diminishes upon the knockdown or knockout of Msi1. It is not clearly understood how Msi1 promoted translation of *Robo3*, *Pdgfrα*, *Egfr*, and *Igf1r* because the increase in protein amounts was not accompanied by upregulated mRNA levels (57,60).

It is possible that, even though these are direct targets of Msi1, the translational enhancement observed is an indirect effect of Msi1 on protein stability. It has been shown that Msi1 indirectly downregulates expression and activity of the 26S proteasome subunit in breast cancer and glioblastoma cells by binding to and inhibiting translation of *Nuclear transcription factor Y subunit alpha* (*NF-YA*), a transcription factor which is required for expression of human proteasome genes (62,63). Thus, the enhanced protein expression observed could be due to decreased proteasome activity.

In some cases, heightened mRNA stability of direct targets is linked to enhanced protein levels upon upregulation of Msi1. In vivo overexpression of Msi1 in the intestinal epithelium

resulted in increased mRNA and protein expression of *Cyclin D1* (*Ccnd1*), *Cyclin-dependent kinase 6* (*Cdk6*), and *SRY-Box transcription factor 4* (*Sox4*) (64). The increase in both mRNA and protein levels was due to slower mRNA transcript decay rates in the presence of Msi1. Similar findings of increased mRNA stability and translation were observed for *tachykinin* (*TAC1*) (65), and *intercellular adhesion molecule-1* (*ICAM1*) (66) in breast cancer and glioblastoma cells, respectively. Furthermore, *Ccnd1*, *Cdk6*, *Sox4*, and *TAC1* have Msi1 binding sites in their 3'-UTRs. It is poorly understood how Msi1 can use conserved sequence motifs to bind to the same region of mRNA targets and either promote or inhibit translation, and also have selective effects on mRNA stability. It is possible that there are additional sequences that have not been identified yet which allow Msi1 to regulate the stability and/or enhance translation of a specific set of targets.

The binding of Msi1 to intronic sequences facilitates alternative splicing of mRNA targets in mouse retina (67). Msi1 binding sites are enriched downstream of exons of various genes that are alternatively spliced during photoreceptor cell development, and in vitro experiments showed that Msi1 expression increases the inclusion of specific exons of the photoreceptor genes. It is important to note that the direct regulatory role of Msi1 on alternative splicing requires nuclear localization of Msi1 and is also cell-type dependent. Endogenous Msi1 is expressed in both nuclei and cytoplasm of mouse intestinal epithelial cells, although the cytoplasmic expression is higher (21). mRNA targets that showed Msi1-intronic interactions in the wild-type state had increased exon inclusion following Msi1 overexpression when compared to transcripts that did not have intronic binding sites. Thus, this result implies that Msi1 is involved in alternative splicing in mouse intestinal epithelial cells. Although a considerable number of intronic binding sites for Msi1 were identified in U251 glioblastoma cells (57), further analysis revealed a modest direct effect of Msi1 on alternative splicing. This modest role in regulating alternative splicing could be due to the predominant cytoplasmic-localization of Msi1

in neural cells (27). Taken together, these studies suggest that Msi1 has context-dependent regulatory effects on stability, translation, and alternative-splicing of direct mRNA targets.

Msi1 expression: roles in development and disease

Msi1 expression is enriched in stem and progenitor cells of various mammalian tissues including brain (37), mammary (68), hair (69), stomach (38), pancreas (44), testis (70), and intestine (71). The expression pattern of Msi1 and its large pool of developmentally relevant target mRNAs implicate Msi1 in tissue development and in the renewal of adult tissues. For example, targeted Msi1 disruption in the developing mouse brain resulted in obstructive hydrocephalus, improper cell proliferation and differentiation (42), and impaired neural cell motility (60). Moreover, Msi1 deficiency diminished regeneration of the intestinal epithelial tissue following irradiation-induced injury in adult mice (72). The importance of Msi1 in early development is further emphasized by findings that Msi1 expression is higher in some embryonic tissues; for example, in mouse brain, but decreases as the organism matures (37).

Aberrant Msi1 expression has been implicated in the pathogenesis of several human cancers, including glioblastoma (26,57,59,73), colorectal (21,25), breast (62,74), lung and prostate cancers (27). Most of these tumors exhibit Msi1 levels higher than that of uninvolved tissue, implicating upregulated Msi1 expression and activity in driving oncogenesis. The potential oncogenic effects of Msi1 were supported by evidence that Msi1 overexpression can transform normal cells. Exogenous Msi1 expression in cultured primary rat intestinal cells enhanced cell proliferation, activated Wnt and Numb signaling pathways, and induced tumors in a xenograft mouse model (75). In contrast, the knockdown of Msi1 impaired growth of xenografts derived from different cancer cell lines (25,59,73,74), indicating that Msi1 upregulation is essential for sustaining cancer cell proliferation and growth. Furthermore, high Msi1 expression increased the growth of mouse intestinal organoids (21,64). In addition, elevated Msi1 promoted cell migration (64,76,77), and augmented chemoresistance (76,78) of

various cancer cell types. Taken together, these studies show that independent manipulation of Msi1 expression can alter cell biology and thus, implicate Msi1 as a potential therapeutic target.

Regulation of Msi1 expression

Given that Msi1 is upregulated in a wide-variety of cancers, several studies have sought to identify molecular factors that regulate Msi1 expression. At the transcriptional level, Msi1 is positively regulated by Notch (79), and Wnt (75) signaling pathways in the intestinal epithelium. The promoter region of *Msi1* contains two binding sites for Tcf/Lef1, the downstream transcription activators of Wnt signaling, and overexpression of the ligand Wnt3a in primary rat intestinal epithelial cells resulted in increased Msi1 mRNA and protein levels. These findings suggested that Msi1 is a Wnt target gene (75). Furthermore, our group previously showed that APC, through its role as a Wnt signaling antagonist, can repress the Wnt-induced expression of *MSI1* in human colonocytes (54). In contrast, no alterations in Msi1 expression were observed when Wnt3a was overexpressed in breast cancer cells, despite increased expression of other well-established Wnt target genes (80). This discrepancy implies that the effect of Wnt3a on Msi1 expression is tissue- and context- dependent. More work in other tissues is needed to further elucidate the relationship between Msi1 and Wnt signaling pathway.

With regards to Notch signaling, Msi1 expression is positively regulated in colorectal cancer cells by Notch3 and Delta-like ligand 4 (Dll4), a Notch receptor and ligand, respectively (79). In contrast, the knockdown of Notch3 diminished Msi1 expression and the Dll4-induced expression of Msi1. Taken together, these studies suggest that Notch and Wnt signaling pathways co-operatively control the transcriptional expression of Msi1 in intestinal epithelial cells.

Additional factors that modulate the transcriptional expression of Msi1 include thyroid hormone (T3), Tenascin C (TNC), and Regulatory Factor X (Rfx) transcription factors. T3 regulates *Msi1* transcription in developing rat brain, and the ectopic expression of T3 restored

Msi1 mRNA and protein expression in hypothyroid brains (81). The sixth intron of the *Msi1* gene contains a regulatory region for Rfx transcription factors, and is essential for positive regulation of Msi1 expression in mouse neural stem and progenitor cells (82,83). Lastly, the extracellular matrix protein TNC enhances Msi1 expression in breast cancer cells (80). These studies further emphasize the notion that Msi1 expression is regulated by various factors in a cell- and context-dependent manner.

Positive post-transcriptional regulation of Msi1 is provided by HuR and HuD, two members of the highly conserved ELAV family of RBPs. ELAV proteins are involved in almost all aspects of mRNA metabolism, and are neuronal-specific RBPs, with the exception of the ubiquitously-expressed HuR (84). *Msi1* mRNA has a very long 3'-UTR which has conserved regulatory binding sites for HuR and HuD (85,86). HuR and Msi1 expression patterns are positively correlated in glioblastoma tumors, and HuR stabilizes *Msi1* mRNA and promotes its translation (86). Similarly, HuD significantly reduced the degradation rate of *Msi1* mRNA in neural stem and progenitor cells (85). HuR and HuD are overexpressed in neuronal tumors and this could explain the upregulation of Msi1 in the same cancer types.

Several tumor suppressor microRNAs (miRNAs) have been identified as negative post-transcriptional regulators of *Msi1* mRNA stability and translation. These miRNAs include miR-34a, miR-101, miR-128, miR-137, miR-138, and miR-331 (87–89). miRNAs are small, single-stranded, and non-coding RNAs that bind to target mRNAs and either repress translation or promote mRNA degradation. Msi1 expression is inversely correlated to that of the miRNAs, with Msi1 expression being higher in tumors, whereas that of the miRNAs is downregulated (87,88). Induced expression of miRNA mimics in glioblastoma cells significantly reduced *Msi1* mRNA levels, and almost completely obliterated Msi1 protein expression (88). Moreover, the downregulation of Notch and Wnt signaling by miR-137 in colorectal cancer cells could add to the diminished *Msi1* expression that is observed upon the overexpression of miR-137 mimics

(87). It has also been shown that the repression of *Msi1* by miR-137 during neurogenesis promotes neural cell differentiation in favor of the self-renewal effect of Msi1 (90).

Taken together, these studies suggests that Msi1 is a proto-oncogene whose expression is tightly regulated by tumor suppressor miRNAs and APC during normal homeostasis. In addition, loss-of-function mutations in *APC* and/or downregulation of these miRNAs could underlie the aberrant expression and activity of Msi1 in tumors.

Signaling pathways that are directly influenced by Msi1

The most characterized pathway that is directly regulated by Msi1 is the evolutionary conserved canonical Notch signaling pathway, which controls cell differentiation (91) and epithelial-mesenchymal transition (EMT) (92,93) in various cell types. Overexpression of Msi1 in primary cells from mouse (30) and rat (75) potentiated Notch signaling through translational inhibition of Numb. Remarkably, the effects of Msi1 on *Numb* and Notch signaling seem to be cell-context dependent. Instead of enhanced Numb protein levels, diminished amounts were observed in gastric cells of Msi1-knockout mice (94). Furthermore, *Numb* translation efficiency was not significantly altered in neural stem cells that were isolated from a Msi1-overexpressing mouse model (27). These differential effects of Msi1 on *Numb* translation have been suggested to be due to alternative splicing of *Numb* mRNA transcripts in a cell-specific manner (94). Another member of Notch signaling which is influenced by Msi1 is Jagged1 (Jag1) (27), a ligand and inducer of Notch. Activation of Notch by Jag1 is necessary for EMT and metastasis of breast cancer cells (95). Msi1 translationally repressed Jag1 expression and restricted EMT in mammary epithelial cells via inhibition of Notch signaling (27). Thus, these studies imply that Msi1's effect on Notch signaling greatly depends on the cell and tissue type.

Wnt signaling is another pathway that has been proposed to be regulated by Msi1. In addition to stimulating Notch signaling, the overexpression of Msi1 promoted growth and proliferation of primary rat intestinal cells through activation of Wnt signaling (75). Furthermore,

our identification of *APC* mRNA as a MSI1 target suggested that MSI1 could potentiate Wnt signaling through repression of *APC* translation (54). Supporting these two independent in vitro studies, were results from a Msi1-overexpressing mouse model showing upregulated expression of a few Wnt target genes in the intestinal mucosae (64). In contrast, no alterations in Wnt signaling or expression of Wnt target genes were observed in two mouse models that either overexpressed Msi1 (21) or had a complete Msi1 knock-out (72). This discrepancy in Wnt signaling could be due to differences between in vitro and in vivo models, and the use of different promoters to induce or knockout Msi1. This topic will be discussed further in Chapter 2 where I describe the various Msi1 mouse models that have been generated and characterized thus far.

Another pathway that is directly regulated by Msi1 is the PI3K/Akt/mTOR signaling cascade, consisting of Phosphatidylinositide-3 kinases, their downstream mediator Akt, and mammalian target of rapamycin (mTOR). The PI3K/Akt/mTOR signaling regulates many cellular processes including cell survival, growth, proliferation and metabolism (96,97). Msi1 knockdown in glioblastoma cells resulted in decreased cell proliferation and survival partly due to increased protein levels of PTEN (Phosphatase and tensin homolog), an inhibitor of PI3K/Akt/mTOR signaling (73). Furthermore, transgenic overexpression of Msi1 in a mouse model activated PI3K/Akt/mTOR signaling through direct translational inhibition of *Pten* (21). This activation was necessary for enhanced intestinal epithelial cell proliferation and crypt growth that was observed in the Msi1 overexpressing mouse. Given that most mRNA targets of Msi1 reported in literature (21,57–59) have yet to be fully validated, it is possible that Wnt, Notch, and PI3K/Akt/mTOR pathways represent a very small subset of signaling pathways that are directly regulated by Msi1.

The use of mouse models in studying Msi1

Most of our knowledge regarding MSI1 has been generated from studies performed in animal models, including mouse models. Given the high homology between human MSI1 and m-Msi1, it is not surprising that findings from mouse studies have mostly recapitulated results from human-derived cells. Thus, experiments in mouse models have enhanced the general understanding of the pathogenesis of human cancers and neurological diseases that display altered MSI1 expression. The main types of mouse models that have been used to study Msi1 are xenograft and genetically engineered mice.

The term xenograft refers to the transplant of an organ, tissue or cells to an individual of another species. The main types of xenograft models are cell-derived xenograft (CDX) and patient-derived xenograft (PDX) mice. CDX models involve the injection of normal or cancer cells, from established cell lines, into a mouse. Whereas, the PDX models involves the use of human tumor samples. PDX models are a useful tool in pre-clinical trials because they provide a medium for testing the efficiency and potential toxicity of drugs before they are tested in humans (98). For example, a therapy targeting Msi1 inhibited pancreatic cancer cell growth in a PDX model (61). Although xenograft models are useful in this sense, they have a huge disadvantage in that the xenografts are transplanted into immunocompromised mice, namely SCID (severe combined immune deficient) or athymic Nude mice (99,100). These mice lack immune cells and therefore, do not reject transplanted cells or tissue. However, the lack of immune cells in the injected tumor cell's microenvironment can severely limit findings because immune cells can recognize tumor cells and eliminate them (101–103). Thus, because the immune system can affect tumor growth and survival, results from studies performed in Nude and SCID mice are not completely translatable to immune-competent patients. Therefore, genetically engineered mouse models, also known as transgenic models, have become more popular for studies that seek to understand the basic characterization of a gene, whether in development or the progression of a disease.

Aims of my dissertation research

The main focus of my dissertation was to characterize a novel mouse model that can be induced to overexpress Msi1 in tissues of interest at a desired developmental stage. Several mouse models for Msi1 were generated and reported during the course of my project. These mice have been used to investigate functions of Msi1 in tissue development, homeostasis, oncogenesis, and neurological disorders. I review and compare the genetic modifications and findings from these models in Chapter 2.

The design, generation, verification, and growth phenotype of our inducible and ubiquitous Msi1-overexpressing mice are discussed in Chapter 3. Given that our group had previously reported a potential role of Msi1 in the maintenance of intestinal homeostasis (54), the rest of my dissertation project was focused on characterizing the intestinal phenotype of these ubiquitous Msi1-overexpressing mice. Results from analyses that were performed in the intestinal epithelium tissue are reported in Chapter 4. In addition, I investigated the role of Msi1 in regulating expression of intestinal ion transporters. The preliminary results from this investigation are described in Chapter 5.

Following detailed analyses of the intestinal phenotype of our inducible, ubiquitous Msi1-overexpressing model, I transitioned my studies to an inducible, intestine-specific mouse model. I discuss preliminary results from this investigation in Chapter 6.

Lastly, another part of my dissertation was to test small molecule inhibitors for potential therapy in cancers that display elevated Msi1 expression. This project was a collaborative study that involved two other groups led by Dr. Liang Xu and Dr. John Karanicolas who designed, synthesized and further tested these inhibitors. I used bioluminescence cell-based assays to screen the small molecule inhibitors. In addition, I analyzed potential Msi1 inhibitor compounds for dose-dependent effects on Msi1 activity. Experimental results from these cell-based assays are described in Chapter 7.

References

1. Bu P, Evrard YA, Lozano G, Dent SYR. Loss of Gcn5 acetyltransferase activity leads to neural tube closure defects and exencephaly in mouse embryos. Mol Cell Biol. 2007 May 1;27(9):3405–16.

2. Han X, Zhang J, Liu Y, Fan X, Ai S, Luo Y, et al. The lncRNA *Hand2os1* / *Uph* locus orchestrates heart development through regulation of precise expression of *Hand2*. Development. 2019 Jul 1;146(13):dev176198.

3. Wilczynski B, Liu Y-H, Yeo ZX, Furlong EEM. Predicting spatial and temporal gene expression using an integrative model of transcription factor occupancy and chromatin state. PLoS Comput Biol. 2012 Dec 6;8(12):e1002798.

4. Pocaterra A, Santinon G, Romani P, Brian I, Dimitracopoulos A, Ghisleni A, et al. F-actin dynamics regulates mammalian organ growth and cell fate maintenance. J Hepatol. 2019 Jul;71(1):130–42.

5. Sistigu A, Di Modugno F, Manic G, Nisticò P. Deciphering the loop of epithelial-mesenchymal transition, inflammatory cytokines and cancer immunoediting. Cytokine Growth Factor Rev. 2017 Aug;36:67–77.

6. Losa M, Risolino M, Li B, Hart J, Quintana L, Grishina I, et al. Face morphogenesis is promoted by Pbx-dependent EMT via regulation of *Snail1* during frontonasal prominence fusion. Development. 2018 Mar 1;145(5):dev157628.

7. Medio M, Yeh E, Popelut A, Babajko S, Berdal A, Helms JA. Wnt/β-catenin signaling and Msx1 promote outgrowth of the maxillary prominences. Front Physio. 2012 Sep 21;3:375.

8. Journiac N, Gilabert-Juan J, Cipriani S, Benit P, Liu X, Jacquier S, et al. Cell metabolic alterations due to Mcph1 mutation in microcephaly. Cell Rep. 2020 Apr;31(2):107506.

9. Qiao X-H, Wang Q, Wang J, Liu X-Y, Xu Y-J, Huang R-T, et al. A novel NR2F2 loss-of-function mutation predisposes to congenital heart defect. Eur J Med Genet. 2018 Apr;61(4):197–203.

10. Van Der Werf CS, Wabbersen TD, Hsiao N, Paredes J, Etchevers HC, Kroisel PM, et al. CLMP is required for intestinal development, and loss-of-function mutations cause congenital short-bowel syndrome. Gastroenterology. 2012 Mar;142(3):453-462.e3.

11. Zhang J, Zhou W, Liu Y, Li N. Integrated analysis of DNA methylation and RNA-sequencing data in Down syndrome. Mol Med Rep. 2016 Nov;14(5):4309–14.

12. Rivelli RA, Casadio V, Bennun RD. Audiological alterations in patients with cleft palate. J Craniofac Surg. 2018 Sep;29(6):1486–9.

13. Schönmeyr B, Wendby L, Sharma M, Raud-Westberg L, Restrepo C, Campbell A. limited chances of speech improvement after late cleft palate repair. J Craniofac Surg.. 2015 Jun;26(4):1182–5.

14. Heron M. Deaths: Leading Causes for 2017. NVSS. 2019;68(6):77.

15. Siegel RL, Miller KD, Jemal A. Cancer statistics, 2020. CA A Cancer J Clin. 2020 Jan;70(1):7–30.

16. Mols F, Thong MSY, Vissers P, Nijsten T, van de Poll-Franse LV. Socio-economic implications of cancer survivorship: Results from the PROFILES registry. Eur J Cancer. 2012 Sep;48(13):2037–42.

17. Reeve BB, Potosky AL, Smith AW, Han PK, Hays RD, Davis WW, et al. Impact of cancer on health-related quality of life of older Americans. J Natl Cancer Inst. 2009 Jun 16;101(12):860–8.

18. Castello A, Fischer B, Eichelbaum K, Horos R, Beckmann BM, Strein C, et al. Insights into RNA biology from an atlas of mammalian mRNA-binding proteins. Cell. 2012 Jun;149(6):1393–406.

19. McLaughlin E, Hime G, Sutherland J, Siddall N. RNA binding proteins in spermatogenesis: an in depth focus on the Musashi family. Asian J Androl. 2015;17(4):529.

20. Xiao R, Chen J-Y, Liang Z, Luo D, Chen G, Lu ZJ, et al. Pervasive chromatin-RNA binding protein interactions enable RNA-based regulation of transcription. Cell. 2019 Jun;178(1):107-121.e18.

21. Li N, Yousefi M, Nakauka-Ddamba A, Li F, Vandivier L, Parada K, et al. The Msi Family of RNA-binding proteins function redundantly as intestinal oncoproteins. Cell Rep. 2015 Dec;13(11):2440–55.

22. Jayasena CS, Bronner ME. Rbms3 functions in craniofacial development by posttranscriptionally modulating TGF-β signaling. J Cell Biol. 2012 Oct 29;199(3):453–66.

23. Sengupta U, Montalbano M, McAllen S, Minuesa G, Kharas M, Kayed R. Formation of toxic oligomeric assemblies of RNA-binding protein: Musashi in Alzheimer's disease. Acta Neuropathol Commun. 2018 Dec;6(1):113.

24. Pistono C, Monti MC, Marchesi N, Boiocchi C, Campagnoli LIM, Morlotti D, et al. Unraveling a new player in multiple sclerosis pathogenesis: The RNA-binding protein HuR. Mult Scler Relat Disord. 2020 Jun;41:102048.

25. Sureban SM, May R, George RJ, Dieckgraefe BK, McLeod HL, Ramalingam S, et al. Knockdown of RNA binding protein Musashi-1 leads to tumor regression in vivo. Gastroenterology. 2008 May;134(5):1448-1458.e2.

26. Chen H-Y, Lin L-T, Wang M-L, Laurent B, Hsu C-H, Pan C-M, et al. Musashi-1 enhances glioblastoma cell migration and cytoskeletal dynamics through translational inhibition of Tensin3. Sci Rep. 2017 Dec;7(1):8710.

27. Katz Y, Li F, Lambert NJ, Sokol ES, Tam W-L, Cheng AW, et al. Musashi proteins are post-transcriptional regulators of the epithelial-luminal cell state. eLife. 2014;3:e03915

28. Chavali PL, Stojic L, Meredith LW, Joseph N, Nahorski MS, Sanford TJ, et al. Neurodevelopmental protein Musashi-1 interacts with the Zika genome and promotes viral replication. Science. 2017 Jul 7;357(6346):83–8.

29. Battelli C, Nikopoulos GN, Mitchell JG, Verdi JM. The RNA-binding protein Musashi-1 regulates neural development through the translational repression of p21WAF-1. Mol Cell Neurosci. 2006 Jan;31(1):85–96.

30. Imai T, Tokunaga A, Yoshida T, Hashimoto M, Mikoshiba K, Weinmaster G, et al. The neural RNA-binding protein Musashi1 translationally regulates mammalian numb gene expression by interacting with its mRNA. Mol Cell Bio. 2001 Jun 15;21(12):3888–900.

31. Kawahara H, Imai T, Imataka H, Tsujimoto M, Matsumoto K, Okano H. Neural RNA-binding protein Musashi1 inhibits translation initiation by competing with eIF4G for PABP. J Cell Biol. 2008 May 19;181(4):639–53.

32. Nakamura M, Okano H, Blendy JA, Montell C. Musashi, a neural RNA-binding protein required for drosophila adult external sensory organ development. Neuron. 1994 Jul;13(1):67–81.

33. Guo M, Bier E, Jan LY, Jan YN. tramtrack acts downstream of numb to specify distinct daughter cell fates during asymmetric cell divisions in the drosophila PNS. Neuron. 1995 May;14(5):913–25.

34. Ramaekers G, Usui K, Usui-Ishihara A, Ramaekers A, Ledent V, Ghysen A, et al. Lineage and fate in Drosophila : role of the gene tramtrack in sense organ development. Dev Genes Evol. 1997 Jul 4;207(2):97–106.

35. Hirota Y, Okabe M, Imai T, Kurusu M, Yamamoto A, Miyao S, et al. Musashi and Seven in absentia downregulate Tramtrack through distinct mechanisms in Drosophila eye development. Mech Dev. 1999 Sep;87(1–2):93–101.

36. Good P, Yoda A, Sakakibara S, Yamamoto A, Imai T, Sawa H, et al. The human Musashi homolog 1(MSI1) gene encoding the homologue of Musashi/Nrp-1, a neural RNA-binding protein putatively expressed in CNS stem cells and neural progenitor cells. Genomics. 1998 Sep;52(3):382–4.

37. Sakakibara S, Imai T, Hamaguchi K, Okabe M, Aruga J, Nakajima K, et al. Mouse-Musashi-1, a neural RNA-binding protein highly enriched in the mammalian CNS stem cell. Dev Biol. 1996 Jun;176(2):230–42.

38. Nagata H, Akiba Y, Suzuki H, Okano H, Hibi T. Expression of Musashi-1 in the rat stomach and changes during mucosal injury and restitution. FEBS Letters. 2006 Jan 9;580(1):27–33.

39. Richter K, Good PJ, Dawid IB. A developmentally regulated, nervous system-specific gene in Xenopus encodes a putative RNA-binding protein. New Biol. 1990;2(6):556-65.

40. Shibata S, Umei M, Kawahara H, Yano M, Makino S, Okano H. Characterization of the RNA-binding protein Musashi1 in zebrafish. Brain Res. 2012 Jun;1462:162–73.

41. Sakakibara S, Nakamura Y, Satoh H, Okano H. RNA-Binding Protein Musashi2: developmentally regulated expression in neural precursor cells and subpopulations of neurons in mammalian CNS. J Neurosci. 2001 Oct 15;21(20):8091–107.

42. Sakakibara S, Nakamura Y, Yoshida T, Shibata S, Koike M, Takano H, et al. RNA-binding protein Musashi family: Roles for CNS stem cells and a subpopulation of ependymal cells revealed by targeted disruption and antisense ablation. PNAS. 2002 Nov 12;99(23):15194–9.

43. Sutherland J, Sobinoff A, Gunter K, Fraser B, Pye V, Bernstein I, et al. Knockout of RNA binding protein MSI2 impairs follicle development in the mouse ovary: characterization of MSI1 and MSI2 during folliculogenesis. Biomolecules. 2015 Jun 26;5(3):1228–44.

44. Szabat M, Kalynyak TB, Lim GE, Chu KY, Yang YH, Asadi A, et al. Musashi expression in β-cells coordinates insulin expression, apoptosis and proliferation in response to endoplasmic reticulum stress in diabetes. Cell Death Dis. 2011 Nov;2(11):e232–e232.

45. Sansom OJ, Reed KR, Hayes AJ, Ireland H, Brinkmann H, Newton IP, et al. Loss of Apc in vivo immediately perturbs Wnt signaling, differentiation, and migration. Genes Dev. 2004 Jun 15;18(12):1385–90.

46. Potten CS, Booth C, Tudor GL, Booth D, Brady G, Hurley P, et al. Identification of a putative intestinal stem cell and early lineage marker; musashi-1. Differentiation. 2003 Jan;71(1):28–41.

47. Kurihara Y, Nagata T, Imai T, Hiwatashi A, Horiuchi M, Sakakibara S, et al. Structural properties and RNA-binding activities of two RNA recognition motifs of a mouse neural RNA-binding protein, mouse-Musashi-1. Gene. 1997 Feb;186(1):21–7.

48. Deo RC, Bonanno JB, Sonenberg N, Burley SK. Recognition of polyadenylate RNA by the Poly(A)-binding protein. Cell. 1999 Sep;98(6):835–45.

49. Ripin N, Boudet J, Duszczyk MM, Hinniger A, Faller M, Krepl M, et al. Molecular basis for AU-rich element recognition and dimerization by the HuR C-terminal RRM. Proc Natl Acad Sci USA. 2019 Feb 19;116(8):2935–44.

50. Ohyama T, Nagata T, Tsuda K, Kobayashi N, Imai T, Okano H, et al. Structure of Musashi1 in a complex with target RNA: the role of aromatic stacking interactions. Nucleic Acids Res. 2012 Apr;40(7):3218–31.

51. Nagata T, Kanno R, Kurihara Y, Uesugi S, Imai T, Sakakibara S, et al. Structure, backbone dynamics and interactions with RNA of the C-terminal RNA-binding domain of a mouse neural RNA-binding protein, Musashi1. J Mol Biol. 1999;287:315–30.

52. Miyanoiri Y, Kobayashi H, Imai T, Watanabe M, Nagata T, Uesugi S, et al. Origin of higher affinity to RNA of the N-terminal RNA-binding domain than that of the C-terminal one of a mouse neural protein, Musashi1, as revealed by comparison of their structures, modes of interaction, surface electrostatic potentials, and backbone dynamics. J Biol Chem. 2003 Oct 17;278(42):41309–15.

53. Madej T, Lanczycki CJ, Zhang D, Thiessen PA, Geer RC, Marchler-Bauer A, et al. MMDB and VAST+: tracking structural similarities between macromolecular complexes. Nucl Acids Res. 2014 Jan;42(D1):D297–303.

54. Spears E, Neufeld KL. Novel double-negative feedback loop between Adenomatous Polyposis Coli and Musashi1 in colon epithelia. J Biol Chem. 2011 Feb 18;286(7):4946–50.

55. Zearfoss NR, Deveau LM, Clingman CC, Schmidt E, Johnson ES, Massi F, et al. A Conserved Three-nucleotide Core motif defines Musashi RNA binding specificity. J Biol Chem. 2014 Dec 19;289(51):35530–41.

56. Rhyu MS, Jan LY, Jan YN. Asymmetric distribution of numb protein during division of the sensory organ precursor cell confers distinct fates to daughter cells. Cell. 1994 Feb;76(3):477–91.

57. Uren PJ, Vo DT, de Araujo PR, Pötschke R, Burns SC, Bahrami-Samani E, et al. RNA-binding protein Musashi1 is a central regulator of adhesion pathways in glioblastoma. Mol Cell Biol. 2015 Sep 1;35(17):2965–78.

58. de Sousa Abreu R, Sanchez-Diaz PC, Vogel C, Burns SC, Ko D, Burton TL, et al. Genomic analyses of Musashi1 downstream targets show a strong association with cancer-related processes. J Biol Chem. 2009 May 1;284(18):12125–35.

59. Vo DT, Subramaniam D, Remke M, Burton TL, Uren PJ, Gelfond JA, et al. The RNA-binding protein Musashi1 affects medulloblastoma growth via a network of cancer-related genes and is an indicator of poor prognosis. Am J Pathol. 2012 Nov;181(5):1762–72.

60. Kuwako K, Kakumoto K, Imai T, Igarashi M, Hamakubo T, Sakakibara S, et al. Neural RNA-binding protein Musashi1 controls midline crossing of precerebellar neurons through posttranscriptional regulation of Robo3/Rig-1 expression. Neuron. 2010 Aug;67(3):407–21.

61. Fox RG, Lytle NK, Jaquish DV, Park FD, Ito T, Bajaj J, et al. Image-based detection and targeting of therapy resistance in pancreatic adenocarcinoma. Nature. 2016 Jun;534(7607):407–11.

62. Lagadec C, Vlashi E, Frohnen P, Alhiyari Y, Chan M, Pajonk F. The RNA-binding protein Musashi-1 regulates proteasome subunit expression in breast cancer- and glioma-initiating cells. Stem Cells. 2014 Jan;32(1):135–44.

63. Xu H, Fu J, Ha S-W, Ju D, Zheng J, Li L, et al. The CCAAT box-binding transcription factor NF-Y regulates basal expression of human proteasome genes. Biochim Biophys Acta Acta Mol Cell Res. 2012 Apr;1823(4):818–25.

64. Cambuli FM, Correa BR, Rezza A, Burns SC, Qiao M, Uren PJ, et al. A mouse model of targeted Musashi1 expression in whole intestinal epithelium suggests regulatory roles in cell cycle and stemness. Stem Cells. 2015 Dec;33(12):3621–34.

65. Nahas GR, Murthy RG, Patel SA, Ganta T, Greco SJ, Rameshwar P. The RNA-binding protein Musashi 1 stabilizes the oncotachykinin 1 mRNA in breast cancer cells to promote cell growth. FASEB J. 2016 Jan;30(1):149–59.

66. Lin J-C, Tsai J-T, Chao T-Y, Ma H-I, Liu W-H. Musashi-1 enhances glioblastoma migration by promoting ICAM1 translation. Neoplasia. 2019 May;21(5):459–68.

67. Murphy D, Cieply B, Carstens R, Ramamurthy V, Stoilov P. The Musashi 1 controls the splicing of photoreceptor-specific exons in the vertebrate retina. PLoS Genet. 2016 Aug 19;12(8):e1006256.

68. Clarke RB, Spence K, Anderson E, Howell A, Okano H, Potten CS. A putative human breast stem cell population is enriched for steroid receptor-positive cells. Dev Biol. 2005 Jan;277(2):443–56.

69. Sugiyama-Nakagiri Y, Akiyama M, Shibata S, Okano H, Shimizu H. Expression of RNA-binding protein Musashi in hair follicle development and hair cycle progression. Am J Pathol. 2006 Jan;168(1):80–92.

70. Sutherland JM, Fraser BA, Sobinoff AP, Pye VJ, Davidson T-L, Siddall NA, et al. Developmental expression of Musashi-1 and Musashi-2 RNA-binding proteins during spermatogenesis: analysis of the deleterious effects of dysregulated expression1. Biol Reprod. 2014 May 1;90(5):92,1-12

71. Kayahara T, Sawada M, Takaishi S, Fukui H, Seno H, Fukuzawa H, et al. Candidate markers for stem and early progenitor cells, Musashi-1 and Hes1, are expressed in crypt base columnar cells of mouse small intestine. FEBS Letters. 2003 Jan 30;535(1–3):131–5.

72. Yousefi M, Li N, Nakauka-Ddamba A, Wang S, Davidow K, Schoenberger J, et al. Msi RNA-binding proteins control reserve intestinal stem cell quiescence. J Cell Biol. 2016 Nov 7;215(3):401–13.

73. Muto J, Imai T, Ogawa D, Nishimoto Y, Okada Y, Mabuchi Y, et al. RNA-binding protein Musashi1 modulates glioma cell growth through the post-transcriptional regulation of Notch and PI3 Kinase/Akt signaling pathways. PLoS ONE. 2012 Mar 12;7(3):e33431.

74. Wang X-Y, Penalva LO, Yuan H, Linnoila RI, Lu J, Okano H, et al. Musashi1 regulates breast tumor cell proliferation and is a prognostic indicator of poor survival. Mol Cancer. 2010;9(1):221.

75. Rezza A, Skah S, Roche C, Nadjar J, Samarut J, Plateroti M. The overexpression of the putative gut stem cell marker Musashi-1 induces tumorigenesis through Wnt and Notch activation. J Cell Sci. 2010 Oct 1;123(19):3256–65.

76. Chiou G-Y, Yang T-W, Huang C-C, Tang C-Y, Yen J-Y, Tsai M-C, et al. Musashi-1 promotes a cancer stem cell lineage and chemoresistance in colorectal cancer cells. Sci Rep. 2017 Dec;7(1):2172.

77. Gong P, Wang Y, Gao Y, Gao M, Liu L, Qu P, et al. Msi1 promotes tumor progression by epithelial-to-mesenchymal transition in cervical cancer. Hum Pathol. 2017 Jul;65:53–61.

78. Chen H-Y, Lin L-T, Wang M-L, Lee S-H, Tsai M-L, Tsai C-C, et al. Musashi-1 regulates AKT-derived IL-6 autocrinal/paracrinal malignancy and chemoresistance in glioblastoma. Oncotarget. 2016 Jul 5;7(27):42485–501.

79. Pasto A, Serafin V, Pilotto G, Lago C, Bellio C, Trusolino L, et al. NOTCH3 signaling regulates Musashi-1 expression in metastatic colorectal cancer cells. Cancer Res. 2014 Apr 1;74(7):2106–18.

80. Oskarsson T, Acharyya S, Zhang XH-F, Vanharanta S, Tavazoie SF, Morris PG, et al. Breast cancer cells produce tenascin C as a metastatic niche component to colonize the lungs. Nat Med. 2011 Jul;17(7):867–74.

81. Cuadrado A, García-Fernández LF, Imai T, Okano H, Muñoz A. Regulation of tau RNA maturation by thyroid hormone is mediated by the neural RNA-binding protein Musashi-1. Mol Cell Neurosci. 2002 Jun;20(2):198–210.

82. Kawase S, Kuwako K, Imai T, Renault-Mihara F, Yaguchi K, Itohara S, et al. Regulatory Factor X transcription factors control Musashi1 transcription in mouse neural stem/progenitor cells. Stem Cells Dev. 2014 Sep 15;23(18):2250–61.

83. Kawase S, Imai T, Miyauchi-Hara C, Yaguchi K, Nishimoto Y, Fukami S, et al. Identification of a novel intronic enhancer responsible for the transcriptional regulation of musashi1 in neural stem/progenitor cells. Mol Brain. 2011;4(1):14.

84. Colombrita C, Silani V, Ratti A. ELAV proteins along evolution: Back to the nucleus? Mol Cell Neurosci. 2013 Sep;56:447–55.

85. Ratti A. A role for the ELAV RNA-binding proteins in neural stem cells: stabilization of Msi1 mRNA. J Cell Sci. 2006 Apr 1;119(7):1442–52.

86. Vo DT, Abdelmohsen K, Martindale JL, Qiao M, Tominaga K, Burton TL, et al. The oncogenic RNA-binding protein Musashi1 is regulated by HuR via mRNA translation and stability in glioblastoma cells. Mol Cancer Res. 2012 Jan 1;10(1):143–55.

87. Smith AR, Marquez RT, Tsao W-C, Pathak S, Roy A, Ping J, et al. Tumor suppressive microRNA-137 negatively regulates Musashi-1 and colorectal cancer progression. Oncotarget. 2015 May 20;6(14):12558–73.

88. Vo DT, Qiao M, Smith AD, Burns SC, Brenner AJ, Penalva LOF. The oncogenic RNA-binding protein Musashi1 is regulated by tumor suppressor miRNAs. RNA Biol. 2011 Sep;8(5):817–28.

89. Yang L-Y, Song G-L, Zhai X-Q, Wang L, Liu Q-L, Zhou M-S. MicroRNA-331 inhibits development of gastric cancer through targeting musashi1. WJGO. 2019 Sep 15;11(9):705–16.

90. Velasco MX, Kosti A, Guardia GDA, Santos MC, Tegge A, Qiao M, et al. Antagonism between the RNA-binding protein Musashi1 and miR-137 and its potential impact on neurogenesis and glioblastoma development. RNA. 2019 Jul;25(7):768–82.

91. Fre S, Huyghe M, Mourikis P, Robine S, Louvard D, Artavanis-Tsakonas S. Notch signals control the fate of immature progenitor cells in the intestine. Nature. 2005 Jun;435(7044):964–8.

92. Chigurupati S, Arumugam TV, Son TG, Lathia JD, Jameel S, Mughal MR, et al. Involvement of Notch signaling in wound healing.PLoS ONE. 2007 Nov 14;2(11):e1167.

93. Zavadil J, Cermak L, Soto-Nieves N, Böttinger EP. Integration of TGF-β/Smad and Jagged1/Notch signalling in epithelial-to-mesenchymal transition. EMBO J. 2004 Mar 10;23(5):1155–65.

94. Takahashi T, Suzuki H, Imai T, Shibata S, Tabuchi Y, Tsuchimoto K, et al. Musashi-1 post-transcriptionally enhances phosphotyrosine-binding domain-containing m-Numb protein expression in regenerating gastric mucosa. PLoS ONE. 2013 Jan 4;8(1):e53540.

95. Sethi N, Dai X, Winter CG, Kang Y. Tumor-derived Jagged1 promotes osteolytic bone metastasis of breast cancer by engaging Notch signaling in bone cells. Cancer Cell. 2011 Feb;19(2):192–205.

96. Cho D, Mier JW, Atkins MB. PI3K/Akt/mTOR pathway: a growth and proliferation pathway. In: Bukowski RM, Figlin RA, Motzer RJ, editors. Renal cell carcinoma: molecular targets and clinical applications. Totowa, NJ: Humana Press; 2009. p. 267–85.

97. Porta C, Paglino C, Mosca A. Targeting PI3K/Akt/mTOR signaling in Cancer. Front Oncol 2014 Apr 14;4:64

98. Murayama T, Gotoh N. Patient-derived xenograft models of breast cancer and their application. Cells. 2019 Jun 20;8(6):621.

99. Bosma GC, Custer RP, Bosma MJ. A severe combined immunodeficiency mutation in the mouse. Nature. 1983;301:527–30.

100. Pantelouris EM. Absence of thymus in a mouse mutant. Nature.1968 Jan 27;217:370-371

101. Crowe NY, Smyth MJ, Godfrey DI. A critical role for natural killer t cells in immunosurveillance of Methylcholanthrene-induced sarcomas. :9.

102. Smyth MJ, Thia KYT, Street SEA, Cretney E, Trapani JA, Taniguchi M, et al. Differential Tumor Surveillance by Natural Killer (NK) and NKT Cells. J Exp Med. 2002 July 1;196(1):119-127.

103. Shankaran V, Ikeda H, Bruce AT, White JM, Swanson PE, Old LJ, et al. IFNg and lymphocytes prevent primary tumour development and shape tumour immunogenicity. Nature. 2001;410:1107-111

104. Okano H, Imai T, Okabe M. Musashi: a translational regulator of cell fate. J Cell Sci. 2002 April 1;115(7):1355–9. https://jcs.biologists.org/content/joces/115/7/1355.full.pdf

CHAPTER 2: REVIEW OF MOUSE MODELS FOR MSI1

INTRODUCTION

In this chapter I review transgenic mouse models for Msi1 that have been reported in the literature. Given that mouse Msi1 and human MSI1 share 99.4% and 99.7% amino acid sequence and charge similarities, respectively, mouse models provide a highly translatable tool for elucidating expression patterns and functions of MSI1. Msi1 mouse models can be divided into three categories; reporter, knockout, and knock-in overexpressing models.

Reporter mice for Msi1

To generate a reporter mouse, a fluorescent or non-fluorescent reporter gene is inserted into a target gene for use in analyzing the endogenous expression pattern of the target gene. In addition, reporter mice can be used for cell lineage tracing and cell sorting studies (1,2). Four reporter mice for Msi1 have been described thus far, and these are *Msi1-CreER^{T2}* (3), *Msi1-eGFP* (4), *Msi1$^{eYFP/+}$* (5), and *Msi1^{CreERT2}* (6) (Table 2.1). Enhanced green fluorescent protein (eGFP) and its derivative enhanced yellow fluorescent protein (eYFP) are commonly used as expression reporters in both in vitro and in vivo studies. CreER^{T2} is Cre-recombinase fused with a mutant ligand-binding domain of the estrogen receptor, and is active when bound to tamoxifen (TAM) (7). A reporter mouse expressing *CreER^{T2}* can be used for either fluorescent or non-fluorescent reporter expression by breeding with a mouse carrying the reporter transgene. Examples of fluorescent reporters include GFP, YFP, and RFP (red fluorescent protein), while LacZ which encodes β-galactosidase is frequently used for non-fluorescent analysis.

For the *Msi1-CreER^{T2} and Msi1$^{eYFP/+}$* mice, the *CreER^{T2}* and *eYFP* sequences were inserted downstream of the first ATG start codon in exon 1 of *Msi1* and their expression is dependent on the endogenous Msi1 promoter (3,5). Similarly, *eGFP* expression in *Msi1-eGFP*

Table 2.1: Reporter mouse models for Msi1. [a] Main tissue studied.

Mouse model	Tissue expression	Notes
Msi1-CreER^{T2} (3)	[a] Brain, retina, testis	Tamoxifen inducible. Can be bred with mice harboring loxP-flanked reporter genes for expression and lineage tracing analysis. **Embryonic stage**: administered tamoxifen at E10.5 in pregnant *Msi1-CreER^{T2} ;Rosa26-lsl-LacZ* mice. Revealed strong LacZ expression in the entire nervous system (analysis at E12.5), in olfactory epithelium (analysis at E17.5), and in differentiated cells of the forebrain cortex, cerebellum, and brain stem cells (analysis at E17.5). **Postnatal**: administered at 4 weeks of age. High LacZ expression in the retina photoreceptor cell layer in *Msi1-CreER^{T2} ;Rosa26-lsl-LacZ* reporter mice. LacZ reporter-expressing neural stem cells (NSCs) in the subventricular zone (SVZ). Lineage tracing analysis at 60 days after tamoxifen showed LacZ-positive cells in the SVZ, olfactory bulb and rostral migration system. Using *Rosa26^{YFP}* reporter mice for lineage tracing, YFP expression was observed in NSCs of SVZ (2 months post-tamoxifen), in precursor cells for dentate granule cells of the hippocampus (2 months post-tamoxifen), and common progenitor cells of the olfactory receptor neurons and sustentacular cells (8 months post-tamoxifen).
Msi1-eGFP (4)	[a] Small intestine, brain, lung, colon, heart, ovary, skin, muscle, liver, pancreas, JP, ID	Not inducible. 8-12-week old mice analyzed. Actively-cycling intestinal stem cells (crypt basal columnar, CBC) express low *Msi1-eGFP*, while slow-cycling “+4” intestinal stem cells express high *Msi1-eGFP*.
Msi1$^{eYFP/+}$ (5)	[a] Pancreas, brain neural cells	Not inducible. YFP-reporter expression observed in brain neural cells, and in pancreatic cancer stem cells. This mouse line can be used to analyze Msi1-reporter expression pattern in other tissues that normally express Msi1.
Msi1^{CreERT2} (6)	Small intestine	Tamoxifen inducible. Analysis at 15 hours after tamoxifen administration, showed high *Msi1^{CreERT2}*-expressing cells at the “+4” position and these cells have multipotent stem cell properties. Instead of being quiescent, the “+4” Msi1-expressing intestinal stem cells are actively cycling, and are resistant to radiation-induced DNA damage, which enables them to repopulate the intestinal epithelium following radiation. Can be bred with mice harboring loxP-flanked reporter genes for expression and lineage tracing experiments. This paper used *R26$^{Lox-Stop-Lox-LacZ}$* and *R26^{mTmG}* mice.

mice is driven by the Msi1 promoter (4), but it is not clear whether it utilizes the same ATG start codon in exon 1 as the *Msi1-CreER^{T2}* and *Msi1$^{eYFP/+}$* mice. Insertion of a reporter gene at the start codon can result in truncation or inactivation of the target gene. For example, there was no Msi1 protein expressed from the *Msi1-CreER^{T2}* allele, only the *CreER^{T2}* was translated (3). This suggests that the modified allele behaved as a knock-out. In fact, homozygous *Msi1-CreER^{T2}* mice had a similar hydrocephalus phenotype to that of a previously reported Msi1 knockout mouse (8). Thus, heterozygous reporter mice are often used to avoid unintended phenotypes which can result from the complete inactivation of a target gene.

Unlike the reporter genes in *Msi1-CreER^{T2}*, *Msi1-eGFP*, and *Msi1$^{eYFP/+}$* mice, the *CreER^{T2}* gene in the *Msi1^{CreERT2}* model was inserted just before the endogenous Msi1 stop codon (6). Insertion of a 2A peptide (P2A) sequence between the last exon of *Msi1* and the *CreER^{T2}* transgene allowed expression of both genes from the *Msi1* promoter. A process known as ribosome skipping occurs during translation of a transcript that has two gene sequences linked by the P2A sequence (9–11). For example, in the *Msi1-P2A-CreER^{T2}* RNA transcript, a hydrolysis process occurs when a ribosome encounters the last *P2A* codon. This results in release of the Msi1-P2A polypeptide and allows the ribosome to “skip” and start translating the *CreER^{T2}* sequence.

Given that expression of a reporter gene is controlled by the promoter of the endogenous target gene, the cell and tissue expression pattern of the reporter are considered to be equivalent to the expression pattern of the target gene. RNA expression of the *Msi1-CreER^{T2}* reporter transcript was detected in the eyes, brain, and testis (3). There was no *Msi1-CreER^{T2}* expression in the stomach, small intestine, colon, liver, kidney, muscle, ovary or uterus. This expression pattern differed significantly from that of the *Msi1-eGFP* RNA transcript, which was expressed in the brain, lung, colon, heart, ovary, skin, muscle, liver, and pancreas (4). A possible explanation for this discrepancy in expression of the reporters could be due to tissue-

specific expression of different isoforms of Msi1. Two splice variants of the *Msi1* gene have been identified in both mouse and human (12,13). The *Msi1-CreER^{T2}* mice utilized the first transcription start codon in exon 1, whereas the isoform expressed in the intestine lacked exon 1 (3). This suggests that the intestine isoform uses an alternate start codon which was likely inactivated by the insertion of the *CreER^{T2}* sequence. I am unable to fully compare the reporter expression for all four models because expression of YFP in *Msi1$^{eYFP/+}$* mice was analyzed in neuronal cells only, while the *Msi1^{CreERT2}* model was used for intestinal epithelial tissue analysis only. However, the difference in tissue expression patterns between the *Msi1-eGFP* and *Msi1-CreER^{T2}* models suggests caution should be used when analyzing expression of a reporter gene in tissues where a target gene is alternatively spliced.

The Msi1 reporter mice are great tools for investigating expression and functions of Msi1 in various tissue types. Using the *Msi1-CreER^{T2}* mice for lineage tracing experiments, Takeda and colleagues showed that Msi1 is expressed in embryonic and adult brain neural stem and progenitor cells (3). In addition, this study showed that *Msi1-CreER^{T2}*-expressing neural stem cells can produce differentiated cells in the forebrain cortex, cerebellum, and brain stem in mouse embryos. Analysis of the intestinal tissue of *Msi1-eGFP* mice showed that Msi1 is expressed in both active and quiescent intestinal stem cells (ISCs). This expression pattern in ISCs has also been shown using antibody staining (6,14). The authors found that the expression level of GFP was higher in quiescent ISCs than in active ISCs, and that the ISCs with varying GFP levels had different gene signatures. Supporting these findings, were experiments using the *Msi1^{CreERT2}* mice which detected enriched Msi1 expression in quiescent ISCs (6). Results from *Msi1-eGFP* and *Msi1^{CreERT2}* mice suggest that quiescent ISCs are not completely dormant, but cycle slowly, at a much lower rate than active ISCs. Further studies using *Msi1^{CreERT2}* mice revealed that ISCs expressing elevated Msi1 contribute to intestinal regeneration following irradiation-induced injury. Although the reporter genes in *Msi1-eGFP* and

Msi1^{CreERT2} mice were inserted at different sites in the endogenous Msi1 locus, the mice had a similar expression pattern for Msi1 in the quiescent ISCs.

Another major application for reporter mice is in the investigation of the role of Msi1 in tumorigenesis. The *Msi1*$^{eYFP/+}$ mouse provided a model for analyzing Msi1 functions in the pathogenesis of pancreatic cancer by crossing them with mice that had p53-inactivating and Kras-stabilizing mutations (5). These two mutations are necessary for the initiation and progression of pancreatic cancer (15–17). The authors identified rare pancreatic tumor cells which co-expressed high levels of YFP and aldehyde dehydrogenase (ALDH), a pancreatic cancer stem cell marker (5). In addition, the rare tumor cells formed more spheroids in tissue culture than non-YFP expressing tumor cells. Taken together, findings from this study implied that Msi1 could be used as a marker of pancreatic cancer stem cells.

Msi1-deficient mice

Three models with reduced Msi1 expression have been reported; *Msi1*$^{-/-}$ (8), *Msi1*$^{flox/flox}$ (or *Msi1KO*) (18,19), and *Msi1*$^{f/f}$ (5) (Table 2.2). Deletion of *Msi1* in C57BL/6 strain mice did not cause embryonic lethality; however, the majority of the *Msi1*$^{-/-}$ mice died within one to two months after birth (8). This early postnatal lethality was due to hydrocephalus, which was likely caused by improper axon guidance and midline crossing in the forebrain of *Msi1*$^{-/-}$ mice. Further studies that utilized the *Msi1*$^{-/-}$ line used them in the outbred CD-1 background (20,21). This choice of outbred mice was possibly a way to overcome the lethal effects of knocking out Msi1 in the inbred C57BL6/J line (8). Inbred and outbred stocks are maintained by sibling and non-sibling mating, respectively. As a result, CD-1 mice are more genetically diverse than C57BL/6 mice, and can tolerate genetic manipulations due to their allelic variation (22,23). The CD-1 *Msi1*$^{-/-}$ mice have been used to study additional functions of Msi1 in the brain and stomach tissues (20,21). It was shown that Msi1 binds to *Roundabout homolog 3 (Robo3)* mRNA and

Table 2.2: Msi1-deficient mouse models. [a] Main tissue studied.

Mouse model	Tissue expression	Notes
Msi1$^{-/-}$ (5, 8, 20, 21)	[a] Brain, pancreas, stomach	Not inducible. No severe phenotype during embryogenesis, except for agenesis of the corpus callosum due to errors in axon guidance and midline crossing at E17. Hydrocephalus in adult brain characterized by abnormal brain morphology including dilated ventricles, intracerebral hemorrhage, and hypoplastic septa (8). Msi1 promotes Robo3 protein expression, and are both required for midline crossing of precerebellar neurons (20). Decreased m-Numb protein levels in the gastric epithelium of *Msi1*$^{-/-}$ mice after ethanol-induced injury resulted in delayed regeneration of the gastric lining (20). This decrease in m-Numb expression was not observed in brain, colon, liver, lung or testis of *Msi1*$^{-/-}$ mice.
Msi1$^{flox/flox}$ (*Msi1KO*) (18,19)	Intestine	Tamoxifen inducible. 8-12-week old mice analyzed. No effect on intestinal cell proliferation, differentiation or tissue homeostasis observed in tamoxifen-injected *Villin-CreER;Msi1KO* mice. However, *Villin-CreER;Msi1KO* mice had delayed regeneration after irradiation injury, indicating that Msi1 expression is required for proper repopulation of the intestinal epithelium.
Msi1$^{f/f}$ (5)	Pancreas	Tamoxifen inducible. Used for studying Msi1 contribution to pancreatic cancer progression and effects on mouse survival in a pancreatic cancer mouse model with deleted Msi2.

increases Robo3 protein levels (20). Robo3 is essential for proper neuronal migration and axonal midline crossing of precerebellar neurons in the mouse brain (24,25). Thus, Msi1 regulation of *Robo3* translation mediates these two neuronal cell processes during development. In the stomach, it was shown that Msi1 is required for proper regeneration of the stomach lining following ethanol-induced mucosal injury (21). Delayed repair of the gastric epithelium in Msi1$^{-/-}$ mice was attributed to diminished Numb protein expression. It had previously been shown that Msi1 inhibits *Numb* translation (26); thus, the decrease in Numb protein levels in the gastric epithelium was unexpected (21). However, further studies, including from our lab (Figure 4.7), have shown that Msi1 has differential effects on *Numb* mRNA and these effects seem to be tissue- and context-dependent (21,27,28).

The *Msi1*$^{-/-}$ mice have also been used in pancreatic cancer studies; however, it is not clear whether they were in the CD-1 or C57BL/6 background (5). Deletion of Msi1 in mice expressing truncated p53 and stabilized Kras (necessary for pancreatic tumor development), resulted in decreased pancreatic tumor volume, increased survival of mice, and impaired progression of tumors to the adenocarcinoma stage. These phenotypes could partially be attributed to reduced expression of c-MET, a receptor tyrosine kinase, in *Msi1*$^{-/-}$ pancreatic tumors. Binding of c-Met to its ligand hepatocyte growth factor results in activation of a signaling pathway which promotes cell proliferation, survival and migration. Overexpression of c-Met and aberrant HGF-c-Met signaling have been implicated in invasion and metastasis of several cancer types (29,30) . Identification of *c-Met* RNA as a target of Msi1 and the reduced c-MET protein levels seen in Msi1$^{-/-}$ cells imply that Msi1 mediates pancreatic cancer progression possibly by regulating c-Met translation, among other many targets.

Deletion of *Msi1* using the Cre-inducible and LoxP system allows targeted deletion of Msi1 in adult mice in a tissue-specific manner. Mice with floxed-Msi1 alleles can be bred to mice expressing Cre or Cre-ER^{T2} recombinase under the control of a desired promoter. *Msi1KO* mice

were generated by breeding the *Msi1*$^{flox/flox}$ mice with the *Villin-CreER* mice, resulting in intestine-specific deletion of Msi1 (19). The intestinal phenotype of *Msi1KO* mice was not different from that of controls, suggesting that Msi1 is not essential for intestinal tissue proliferation, differentiation, and homeostasis. However, regeneration of the intestinal epithelial tissue after radiation-induced injury was impaired in Msi1-deficient mice. This result agrees with findings from the *Msi1*^{CreERT2} reporter mice which showed that high *Msi1*^{CreERT2}-reporter expressing "+4" ISCs promote intestinal regeneration (6). Lastly, *Msi1KO* mice have be used to show the functional redundancy between Msi1 and its closely-related family member Musashi2 (Msi2) in intestinal tissue. Deletion of both Msi1 and Msi2 was required to reduce tumor growth and burden in mice expressing truncated *Adenomatous polyposis coli* (*Apc*) (18). In addition, loss of both proteins severely impaired intestinal regeneration following radiation-induced injury when compared to individual deletion of either protein (19). Taken together, findings from Msi1 knockout mice highlight essential roles for Msi1 in tissue development and regeneration. These studies also show that Msi1 promotes growth of tumors originating from different tissue types.

Mouse models with enhanced Msi1 expression

In addition to my studies, three mouse models overexpressing Msi1 have been described thus far. These are *v-Msi1* (31), *Tre-Msi1* (18), and *TgMsi1* (32) (Table 2.3). The *v-Msi1* and *Tre-Msi1* mice were used to investigate the functions of Msi1 in the intestinal epithelium and in tumorigenesis. The *v-Msi1* model is a knock-in mouse that constitutively overexpresses *Msi1* cDNA under the control of the *villin1 (Vil1)* promoter specifically in the intestinal epithelium starting from embryonic day 11. The *Tre-Msi1* model utilized the ubiquitous doxycycline-inducible *collagen (Col1a1)* promoter to drive Msi1 expression in all adult mouse cells. A detailed comparison of these two mouse models is provided in the discussion section of Chapter 4.

Table 2.3: Mouse models with enhanced Msi1 expression

Mouse model	Tissue expression	Notes
v-Msi1 (24)	Small intestine, colon	Not inducible. Wnt signaling pathway was not strongly upregulated in v-Msi1 mice. Enhanced c-Myc, Cyclin D1 and activated β-catenin protein levels in v-Msi1 intestinal epithelium. Msi1 binds to and stabilizes *Cdk6* and *Cyclin D1* mRNAs resulting in increased protein levels.
Tre-Msi1 (18, 19)	Small intestine, colon	Doxycycline inducible. 2-3 month old mice were analyzed. Intestinal epithelial cells were used in CLIP-Seq experiments. 2,425 and 9,827 Msi1 mRNA targets were identified from control and *Tre-Msi1 intestinal epithelial cells respectively. Pten* and *β-catenin* were validated as Msi1 targets, and Msi1 represses their translation. No activation of Wnt signaling following Msi1 induction.
TgMsi1 (27, 31)	Testis	Not inducible. Abnormal spermatozoa morphology. Identified *Erh* as a target of Msi1. Also showed that Importin-5 (IPO5) is a binding partner of Msi1 and it facilitates Msi1 the translocation of Msi1 to the nucleus.

TgMsi1 is a testis-specific Msi1-overexpressing mouse model in which the *lactate dehydrogenase C* (*LDHC*) promoter drives expression of the Msi1 transgene (32). *TgMsi1* mice had reduced testicular size, abnormal sperm morphology, delayed germ cell differentiation, and increased apoptosis during spermatogenesis. Analysis of Msi1 expression in human seminoma and testicular cancer cell lines in the same study suggested that Msi1 could be involved in the development of testicular cancer. However, the absence of germ cell tumors in *TgMsi1* mice indicated that Msi1 overexpression alone is not enough to induce testicular cancer. Further studies using the *TgMsi1* model revealed that Msi1 regulates translation of RNA targets which encode proteins involved in spermatogenesis, such as *Msi2* and *Enhancer of rudimentary homology (Erh)* (28).

Summary

Msi1 mouse models provide invaluable tools for analyzing expression patterns and elucidating functions of Msi1 in normal and diseased tissues. Most of the Msi1 mouse models described in this chapter were published after the Neufeld lab had generated its own inducible Msi1 knock-in transgenic model (*Rosa26*$^{Msi1/Msi1}$). I describe the generation and characterization of our *Rosa26*$^{Msi1/Msi1}$ mouse in Chapters 3, 4, and 5.

REREFENCES

1. Kretzschmar K, Watt FM. Lineage Tracing. Cell. 2012 Jan;148(1–2):33–45.
2. Li N, Nakauka-Ddamba A, Tobias J, Jensen ST, Lengner CJ. Mouse label-retaining cells are molecularly and functionally distinct from reserve intestinal stem cells. Gastroenterology. 2016 Aug;151(2):298-310.e7.
3. Takeda H, Koso H, Tessarollo L, Copeland NG, Jenkins NA. *Musashi1 - CreER*^{T2} : A new cre line for conditional mutagenesis in neural stem cells. Genesis. 2013 Feb;51(2):128–34.
4. Cambuli FM, Rezza A, Nadjar J, Plateroti M. Brief report: Musashi1-eGFP mice, a new tool for differential isolation of the intestinal stem cell populations. Stem Cells. 2013 Oct;31(10):2273–8.

5. Fox RG, Lytle NK, Jaquish DV, Park FD, Ito T, Bajaj J, et al. Image-based detection and targeting of therapy resistance in pancreatic adenocarcinoma. Nature. 2016 Jun;534(7607):407–11.

6. Sheng X, Lin Z, Lv C, Shao C, Bi X, Deng M, et al. Cycling stem cells are radioresistant and regenerate the intestine. Cell Rep. 2020 Jul;32(4):107952.

7. Feil R, Wagner J, Metzger D, Chambon P. Regulation of Cre recombinase activity by mutated estrogen receptor ligand-binding domains. Biochem Biophys Res Commun. 1997 Aug;237(3):752–7.

8. Sakakibara S, Nakamura Y, Yoshida T, Shibata S, Koike M, Takano H, et al. RNA-binding protein Musashi family: Roles for CNS stem cells and a subpopulation of ependymal cells revealed by targeted disruption and antisense ablation. PNAS. 2002 Nov 12;99(23):15194–9.

9. Donnelly MLL, Luke G, Mehrotra A, Li X, Hughes LE, Gani D, et al. Analysis of the aphthovirus 2A/2B polyprotein 'cleavage' mechanism indicates not a proteolytic reaction, but a novel translational effect: a putative ribosomal 'skip.' J Gen Virol. 2001 May 1;82(5):1013–25.

10. de Felipe P, Luke GA, Hughes LE, Gani D, Halpin C, Ryan MD. E unum pluribus: multiple proteins from a self-processing polyprotein. Trends Biotechnol. 2006 Feb;24(2):68–75.

11. Tang W, Ehrlich I, Wolff SBE, Michalski A-M, Wolfl S, Hasan MT, et al. faithful expression of multiple proteins via 2A-Peptide self-processing: a versatile and reliable method for manipulating brain circuits. J Neurosci. 2009 Jul 8;29(27):8621–9.

12. Sakakibara S, Imai T, Hamaguchi K, Okabe M, Aruga J, Nakajima K, et al. Mouse-Musashi-1, a neural RNA-binding protein highly enriched in the mammalian CNS stem cell. Dev Biol. 1996 Jun;176(2):230–42.

13. Ma L, Shan Y, Ma H, Elshoura I, Nafees M, Yang K, et al. Identification of a novel splice variant of the human musashi-1 gene. Oncol Lett. 2018 Oct;16(4):5441-8

14. Kayahara T, Sawada M, Takaishi S, Fukui H, Seno H, Fukuzawa H, et al. Candidate markers for stem and early progenitor cells, Musashi-1 and Hes1, are expressed in crypt base columnar cells of mouse small intestine. FEBS Letters. 2003 Jan 30;535(1–3):131–5.

15. Hruban RH. K-ras Oncogene Activation in Adenocarcinoma of the Human Pancreas. study of 82 carcinomas using a combination of mutant-enriched polymerase chain reaction analysis and allele-specific oligonucleotide hybridization. Am J Pathol. 1993 Aug;143(2):545-54

16. Redston MS, Caldas C, Seymour AB, Hruban RH, Kern SE. Homocopolymer tracts in DNA microdeletions. Cancer Res. 1994;54:3025–33.

17. Kahlert C, Melo SA, Protopopov A, Tang J, Seth S, Koch M, et al. Identification of double-stranded genomic DNA spanning all chromosomes with mutated *KRAS* and *p53* DNA in the serum exosomes of patients with pancreatic cancer. J Biol Chem. 2014 Feb 14;289(7):3869–75.

18. Li N, Yousefi M, Nakauka-Ddamba A, Li F, Vandivier L, Parada K, et al. The Msi family of RNA-binding proteins function redundantly as intestinal oncoproteins. Cell Rep. 2015 Dec;13(11):2440–55.

19. Yousefi M, Li N, Nakauka-Ddamba A, Wang S, Davidow K, Schoenberger J, et al. Msi RNA-binding proteins control reserve intestinal stem cell quiescence. J Cell Biol. 2016 Nov 7;215(3):401–13.

20. Kuwako K, Kakumoto K, Imai T, Igarashi M, Hamakubo T, Sakakibara S, et al. Neural RNA-binding protein musashi1 controls midline crossing of precerebellar neurons through posttranscriptional regulation of Robo3/Rig-1 Expression. Neuron. 2010 Aug;67(3):407–21.

21. Takahashi T, Suzuki H, Imai T, Shibata S, Tabuchi Y, Tsuchimoto K, et al. Musashi-1 post-transcriptionally enhances phosphotyrosine-binding domain-containing m-Numb protein expression in regenerating gastric mucosa. PLoS ONE. 2013 Jan 4;8(1):e53540.

22. Tuttle AH, Philip VM, Chesler EJ, Mogil JS. Comparing phenotypic variation between inbred and outbred mice. Nat Methods. 2018 Dec;15(12):994–6.

23. Reichenbach DK, Li Q, Hoffman RA, Williams AL, Shlomchik WD, Rothstein DM, et al. Allograft outcomes in outbred mice: allograft outcomes in outbred mice. Am J Transplant. 2013 Mar;13(3):580–8.

24. Jen JC, Chan W-M, Bosley TM, Wan J, Carr JR, Rub U, et al. Mutations in a human ROBO gene disrupt hindbrain axon pathway crossing and morphogenesis. Science. 2004 Jun 4;304(5676):1509–13.

25. Marillat V, Sabatier C, Failli V, Matsunaga E, Sotelo C, Tessier-Lavigne M, et al. The Slit Receptor Rig-1/Robo3 controls midline crossing by hindbrain precerebellar neurons and axons. Neuron. 2004 Jul;43(1):69–79.

26. Imai T, Tokunaga A, Yoshida T, Hashimoto M, Mikoshiba K, Weinmaster G, et al. The neural RNA-binding protein Musashi1 translationally regulates mammalian numb gene expression by interacting with its mRNA. Mol Cell Biol. 2001 Jun 15;21(12):3888–900.

27. Katz Y, Li F, Lambert NJ, Sokol ES, Tam W-L, Cheng AW, et al. Musashi proteins are post-transcriptional regulators of the epithelial-luminal cell state. eLife 2014;3:e03915

28. Sutherland JM, Sobinoff AP, Fraser BA, Redgrove KA, Davidson T, Siddall NA, et al. RNA binding protein Musashi-1 directly targets *Msi2* and *Erh* during early testis germ cell development and interacts with IPO5 upon translocation to the nucleus. FASEB J. 2015 Jul;29(7):2759–68.

29. Chakraborty S, Balan M, Flynn E, Zurakowski D, Choueiri TK, Pal S. Activation of c-Met in cancer cells mediates growth-promoting signals against oxidative stress through Nrf2-HO-1. Oncogenesis. 2019 Feb;8(2):7.

30. Hughes PE, Rex K, Caenepeel S, Yang Y, Zhang Y, Broome MA, et al. *In Vitro* and *In Vivo* activity of AMG 337, a potent and selective MET kinase inhibitor, in MET-dependent cancer models. Mol Cancer Ther. 2016 Jul;15(7):1568–79.

31. Cambuli FM, Correa BR, Rezza A, Burns SC, Qiao M, Uren PJ, et al. A mouse model of targeted Musashi1 expression in whole intestinal epithelium suggests regulatory roles in cell cycle and stemness. Stem Cells. 2015 Dec;33(12):3621–34.

32. Sutherland JM, Fraser BA, Sobinoff AP, Pye VJ, Davidson T-L, Siddall NA, et al. Developmental Expression of Musashi-1 and Musashi-2 RNA-Binding Proteins During Spermatogenesis: Analysis of the Deleterious Effects of Dysregulated Expression1. Biol Reprod. 2014 May 1;90(5):92,1-12

CHAPTER 3: GENERATION AND GROWTH PHENOTYPE OF UBIQUITOUS MSI1-OVEREXPRESSING MICE

The data and opinions in this chapter were published previously and reformatted for this dissertation:

Chiremba TT, Neufeld KL. Constitutive Musashi1 expression impairs mouse postnatal development and intestinal homeostasis. Mol Biol Cell. 2020 Nov 11. Ahead of print. Available: https://www.molbiolcell.org/doi/abs/10.1091/mbc.E20-03-0206#

ABSTRACT

The RNA-binding protein Musashi1 (Msi1) is involved in post-transcriptional regulation of developmentally-relevant RNAs, and has been implicated in tumorigenesis. Our lab previously identified a mutual-inhibitory relationship between Msi1 and the tumor suppressor Adenomatous polyposis coli (Apc) in cell culture studies. We hypothesized that the interaction between Msi1 and Apc regulates homeostasis in the intestinal epithelium tissue. To test this hypothesis in vivo, we generated a versatile mouse model that facilitates Cre-inducible and tissue-specific overexpression of Msi1. Here, I show that ubiquitous Msi1 induction in ~5 week old mice delays overall growth, alters organ-to-body proportions, and causes premature death. This work implicates Msi1 in mouse postnatal development of multiple organs, including the intestinal tissue.

INTRODUCTION

Evolutionary conserved RNA-binding protein Msi1 can regulate developmentally relevant genes. In addition, enhanced Msi1 expression is observed in various cancer types including glioblastoma (1–4), colorectal (5,6), breast (7,8) lung and prostate cancers (9). Over 80% of colorectal cancers have inactivating mutations in the *Adenomatous polyposis coli (Apc)* gene,

which encodes a tumor suppressor and Wnt signaling antagonist. Msi1 is highly upregulated in mouse intestinal tissue upon *Apc* loss (10) and in intestinal tumors expressing mutated Apc (11) These results, together with the identification of Msi1 as a Wnt target gene (12), led us to consider if a functional relationship exists between Msi1 and Apc. Our previous in vitro studies demonstrated that *APC* mRNA is a target of MSI1, and revealed a mutual-inhibitory relationship between MSI1 and APC in human colonocytes that express wild-type APC (13). We proposed that this relationship is critical for maintaining a balance between proliferation and differentiation of intestinal epithelial cells, and is disrupted in intestinal tumors expressing truncated Apc.

Our original intention of generating an inducible Msi1 gain-of-function mouse model was to characterize the oncogenic properties of Msi1 in an in vivo setting. Given the broad range of cancers that exhibit upregulation of Msi1, we also aimed to develop a mouse model that could be a valuable tool to the field as whole in delineating the pathological functions of Msi1 in cancers originating from different tissues. Unexpectedly, I identified altered organ and animal size in our tamoxifen-inducible ubiquitous Msi1-overexpressing mice and therefore, embarked on a study to determine effects of Msi1 overexpression on postnatal development. Here I report that young transgenic mice ubiquitously expressing Msi1 failed to thrive and died prematurely. My data show that these mice had stunted body and organ sizes indicating that ectopic Msi1 expression disrupted their normal postnatal development.

RESULTS

Generation of conditional and inducible Msi1-overexpressing mice

Upregulated Msi1 levels have been detected in tumors originating from many tissues including colon and brain (4,5,9). To study the consequences of Msi1 upregulation in a living organism, we developed a double-transgenic mouse model that enabled conditional and

inducible overexpression of Msi1, dependent on Cre-recombinase activity (Figure 3.1). Briefly, a Msi1 transgene, controlled by a strong promoter, but with a loxP-flanked transcription termination sequence blocking expression, was inserted into the *Rosa26* locus (Figure 3.1A, Figure 3.2A). When these "*Rosa26*$^{Msi1/Msi1}$" mice are bred with mice that express active Cre-recombinase, Msi1 overexpression is induced.

For the current study, homozygous Msi1 transgenic mice were bred with hemizygous *UBC-CreER*^{T2} mice which express an inactive form of Cre-recombinase in all cells under control of the ubiquitin promoter (Figure 3.1B; (14)). We utilized a whole-body mouse model for Msi1 overexpression because we were interested in the potential for tumorigenesis in any tissue. Following Cre activation with a single tamoxifen TAM) injection, double-transgenic mice (*Rosa26*$^{Msi1/+}$*;UBC-CreER*^{T2}) overexpressed Msi1 ubiquitously. Littermate control mice (*Rosa26*$^{Msi1/+}$) were heterozygous for the Msi1 transgene (Figure 3.1, C and D), but were *UBC-CreER*^{T2} null; therefore, they expressed only endogenous Msi1 even after TAM injection. Single- and double-transgenic mice were phenotypically indistinguishable before TAM administration. For simplification, TAM-injected *Rosa26*$^{Msi1/+}$ and *Rosa26*$^{Msi1/+}$*;UBC-CreER*^{T2} mice will be referred to as control and Msi1$^{O/E}$ (Msi1-overexpressing) mice, respectively.

To test for mutations that might have occurred in the *Rosa26*^{Msi1} transgene which were potentially acting on the Msi1 wild-type alleles in a dominant negative manner, we verified the sequence of the *Rosa26*^{Msi1} transgene. The *Msi1* transgene locus was PCR-amplified from genomic DNA extracted from tail biopsies of *Rosa26*$^{Msi1/Msi1}$ pups (Figure 3.2, B-D) and sequenced. I found no mutations in the transgene, and the sequence of the isolated locus was 100% identical to the published coding sequence of mouse Msi1 isoform 1 (Figure 3.2E).

For our initial analysis, mice were given one intraperitoneal injection of TAM at 4-5 weeks of age, and then sacrificed 3 days later (days post-injection, dpi). Immunofluorescence analysis showed elevated Msi1 protein levels in lung, heart, liver, kidney, small intestine, and

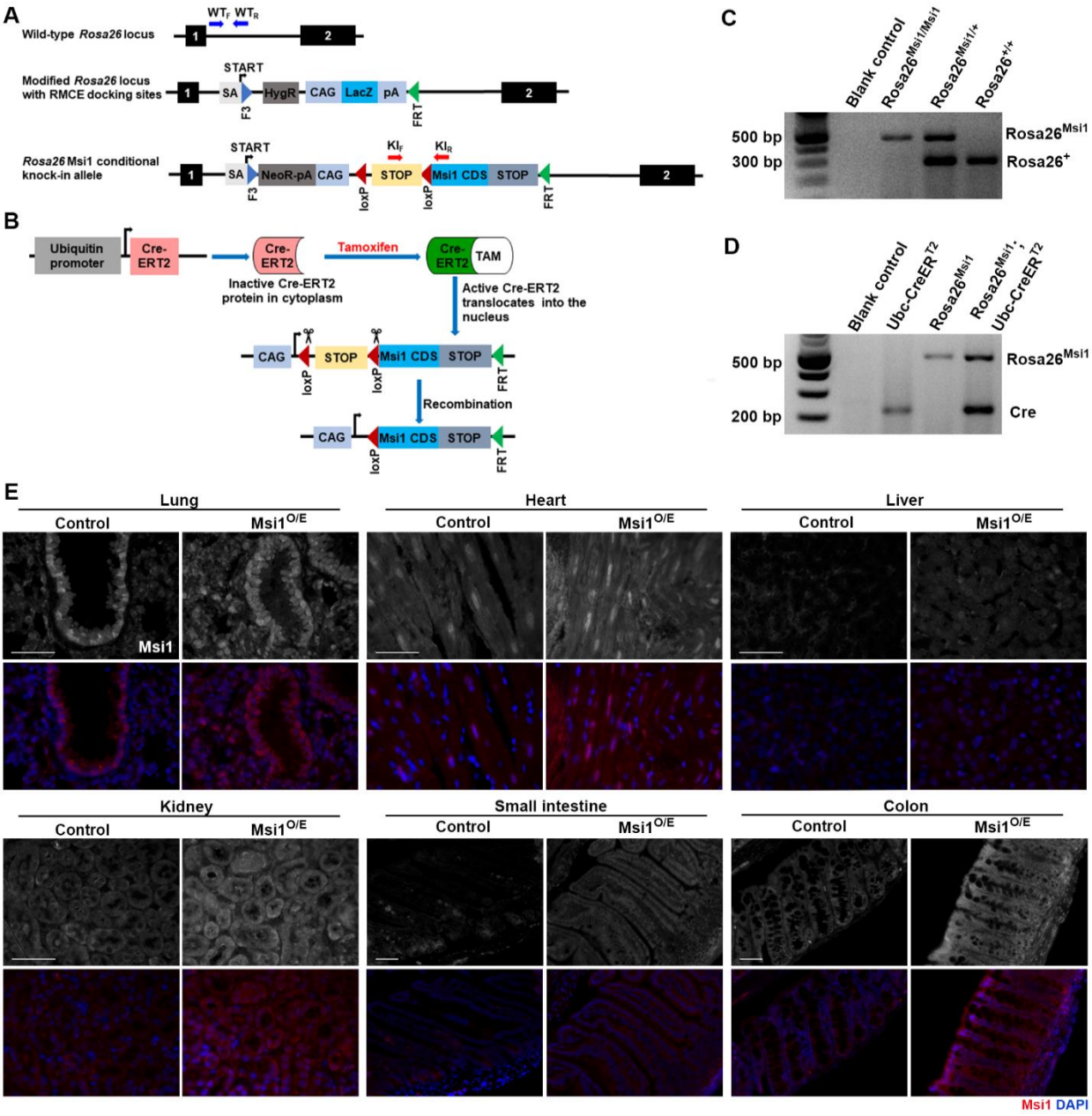

Figure 3.1: A knock-in mouse model for inducible Msi1 overexpression. (A) Schematic representation of CAG-loxP-STOP-loxP-*Msi1*CDS-STOP transgene insertion into a modified *Rosa26* locus equipped with F3/FRT-RMCE docking sites. Binding sites for primers used in genotyping are shown. (not to scale) (B) Strategy for Cre-mediated recombination of the *Rosa26* Msi1 conditional knock-in allele. Genotyping analysis by PCR and gel electrophoresis for (C) Msi1 knock-in and (D) Cre recombinase transgenes. For blank controls, nuclease-free water was added to the PCR mix in place of mouse genomic DNA. (E) Representative immunofluorescence images for Msi1 (Gray, Red) and DAPI (Blue) in various tissues harvested from 3-dpi mice. Scale bars, 50 µm.

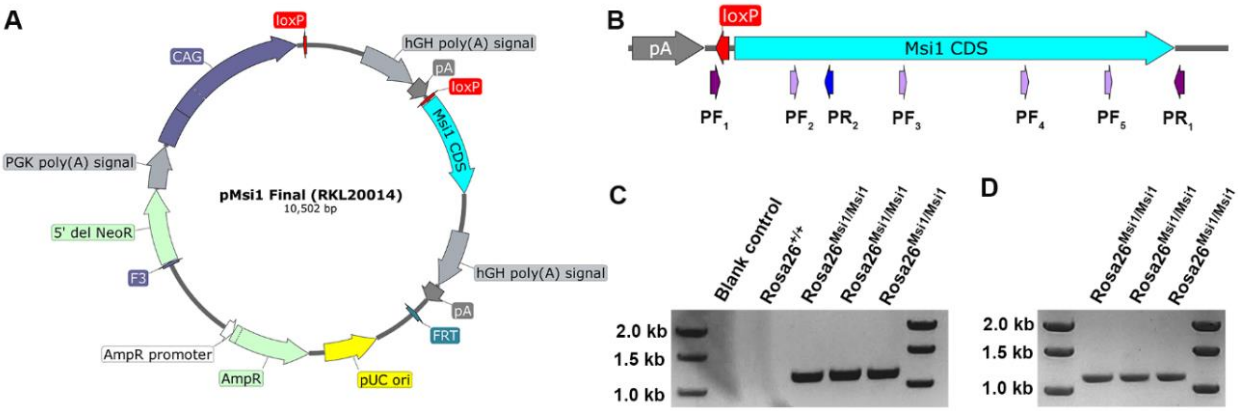

E

```
                1         10        20        30        40        50        60        70        80        90       100       110       120       130       140       150
                |---------+---------+---------+---------+---------+---------+---------+---------+---------+---------+---------+---------+---------+---------+---------|
NM_008629.2                                                                ATGGAGACTGACGCGCCCCAGCCCGGCCTCGCCTC-CCCGGACTCGCCGCACGACCCCTGCAAGATGTTCATCGGAGGACTCAGTTGGCAGACCACG
PF1                 NNNNNGNGNANNNNNNNNNNNNNNNTATCGCGGCCGCGCCACCATGGAGACTGACGCGCCCCAGCCCGGCCTCGCCTC-CCCGGACTCGCCGCACGACCCCTGCAAGATGTTCATCGGAGGACTCAGTTGGCAGACCACG
PR1 NNNNNNNNNNNNNNNNNNNNNNNNNNNNNNNNNNNNNNNCNTNNNNNAGTNNNNNNNNNNCNCANGNGNCTGANNNNNNNAGCCNNNTNNCTCCCGGACTNGCNGCNCGANCN-NGCAAGANNT-CATCGGAGGANTCANNNG-CANNCNACG
PF2
Consensus       .....................................................g...c..........gcc.....c.cccggact.gc.gc.cga.c...gcaaga..t.catcggagga.tca...g.ca..c.acg

                151       160       170       180       190       200       210       220       230       240       250       260       270       280       290       300
                |---------+---------+---------+---------+---------+---------+---------+---------+---------+---------+---------+---------+---------+---------+---------|
NM_008629.2 CAGGAA-GGGCTGCGCGAATACTTCGGCCAGTTCGGGGAGGTGAAAGAGTGTCTGGTGATGCGGGACCCCCTGACCAAAAGATCCAGGGGTTTCGGCTTCGTCACTTTCATGGACCAGGCGGGGGTGGATAAAGTGCTGGCGCAATCGCG
PF1 CAGGAA-GGGCTGCGCGAATACTTCGGCCAGTTCGGGGAGGTGAAAGAGTGTCTGGTGATGCGGGACCCCCTGACCAAAAGATCCAGGGGTTTCGGCTTCGTCACTTTCATGGACCAGGCGGGGGTGGATAAAGTGCTGGCGCAATCGCG
PR1 CAGGAAGGGCTGCGCGAATACT-CGGCCAGTTCGGGGAGGTGAAAGAGTGTCTGGTGATGCGGGACCCCC-NGACCAAAAGANCCAGGGGTTTCGGCTTCGTCACTTTCATGGACCAGGCGGGGGTGGATAAAGTGCTGGCGCAATCGCG
PF2                                                                                                                                                 NNNNNNNNNNNNNNNGGGTTTCGGCTTCGTCACTTTCATGGACCAGGCGGGGGTGGATAAAGTGCTGGCGCAATCGCG
Consensus       caggaa.gggctgcgcgaatact.cggccagttcggggaggtgaaagagtgtctggtgatgcgggacccc..gaccaaaaga.ccagGGGTTTCGGCTTCGTCACTTTCATGGACCAGGCGGGGGTGGATAAAGTGCTGGCGCAATCGCG

                301       310       320       330       340       350       360       370       380       390       400       410       420       430       440       450
                |---------+---------+---------+---------+---------+---------+---------+---------+---------+---------+---------+---------+---------+---------+---------|
NM_008629.2 GCACGAGCTCGACTCCAAAACAATTGACCCCAAGGTGGCCTTTCCTCGAAGAGCACAGCCTAAGATGGTCACTCGGACGAAGAAGATCTTCGTGGGGGGGCTGTCTGTGAACACCACGGTGGAAGATGTGAAACACTATTTCGAGCAGTT
PF1 GCACGAGCTCGACTCCAAAACAATTGACCCCAAGGTGGCCTTTCCTCGAAGAGCACAGCCTAAGATGGTCACTCGGACGAAGAAGATCTTCGTGGGGGGGCTGTCTGTGAACACCACGGTGGAAGATGTGAAACACTATTTCGAGCAGTT
PR1 GCACGAGCTCGACTCCAAAACAATTGACCCCAAGGTGGCCTTTCCTCGAAGAGCACAGCCTAAGATGGTCACTCGGACGAAGAAGATCTTCGTGGGGGGGCTGTCTGTGAACACCACGGTGGAAGATGTGAAACACTATTTCGAGCAGTT
PF2 GCACGAGCTCGACTCCAAAACAATTGACCCCAAGGTGGCCTTTCCTCGAAGAGCACAGCCTAAGATGGTCACTCGGACGAAGAAGATCTTCGTGGGGGGGCTGTCTGTGAACACCACGGTGGAAGATGTGAAACACTATTTCGAGCAGTT
Consensus       GCACGAGCTCGACTCCAAAACAATTGACCCCAAGGTGGCCTTTCCTCGAAGAGCACAGCCTAAGATGGTCACTCGGACGAAGAAGATCTTCGTGGGGGGGCTGTCTGTGAACACCACGGTGGAAGATGTGAAACACTATTTCGAGCAGTT

                451       460       470       480       490       500       510       520       530       540       550       560       570       580       590       600
                |---------+---------+---------+---------+---------+---------+---------+---------+---------+---------+---------+---------+---------+---------+---------|
NM_008629.2 CGGAAAGGTGGATGATGCCATGCTGATGTTCGACAAAACCACCAACAGGCACAGAGGGTTTGGATTTGTCACGTTTGAGAGCGAGGACATCGTAGAGAAAGTTTGTGAGATCCCACTTCCATGAAATCAACAACAAAATGGTGGAATGCAA
PF1 CGGAAAGGTGGATGATGCCATGCTGATGTTCGACAAAACCACCAACAGGCACAGAGGGTTTGGATTTGTCACGTTTGAGAGCGAGGACATCGTAGAGAAAGTTTGTGAGATCCCACTTCCATGAAATCAACAACAAAATGGTGGAATGCAA
PR1 CGGAAAGGTGGATGATGCCATGCTGATGTTCGACAAAACCACCAACAGGCACAGAGGGTTTGGATTTGTCACGTTTGAGAGCGAGGACATCGTAGAGAAAGTTTGTGAGATCCCACTTCCATGAAATCAACAACAAAATGGTGGAATGCAA
PF2 CGGAAAGGTGGATGATGCCATGCTGATGTTCGACAAAACCACCAACAGGCACAGAGGGTTTGGATTTGTCACGTTTGAGAGCGAGGACATCGTAGAGAAAGTTTGTGAGATCCCACTTCCATGAAATCAACAACAAAATGGTGGAATGCAA
Consensus       CGGAAAGGTGGATGATGCCATGCTGATGTTCGACAAAACCACCAACAGGCACAGAGGGTTTGGATTTGTCACGTTTGAGAGCGAGGACATCGTAGAGAAAGTTTGTGAGATCCCACTTCCATGAAATCAACAACAAAATGGTGGAATGCAA

                601       610       620       630       640       650       660       670       680       690       700       710       720       730       740       750
                |---------+---------+---------+---------+---------+---------+---------+---------+---------+---------+---------+---------+---------+---------+---------|
NM_008629.2 GAAAGCCCAGCCAAAGGAGGTGATGTCCCCGACAGGCTCAGCCCGGGGCAGGTCTCGGGTCATGCCCTACGGAATGGATGCCTTCATGCTGGGTATTGGGATGCTGGGTTACCCAGGGTTCCAAGCCACGACCTACGCCAGCCGGAGTTA
PF1 GAAAGCCCAGCCAAAGGAGGTGATGTCCCCGACAGGCTCAGCCCGGGGCAGGTCTCGGGTCATGCCCTACGGAATGGATGCCTTCATGCTGGGTATTGGGATGCTGGGTTACCCAGGGTTCCAAGCCACGACCTACGCCAGCCGGAGTTA
PR1 GAAAGCCCAGCCAAAGGAGGTGATGTCCCCGACAGGCTCAGCCCGGGGCAGGTCTCGGGTCATGCCCTACGGAATGGATGCCTTCATGCTGGGTATTGGGATGCTGGGTTACCCAGGGTTCCAAGCCACGACCTACGCCAGCCGGAGTTA
PF2 GAAAGCCCAGCCAAAGGAGGTGATGTCCCCGACAGGCTCAGCCCGGGGCAGGTCTCGGGTCATGCCCTACGGAATGGATGCCTTCATGCTGGGTATTGGGATGCTGGGTTACCCAGGGTTCCAAGCCACGACCTACGCCAGCCGGAGTTA
Consensus       GAAAGCCCAGCCAAAGGAGGTGATGTCCCCGACAGGCTCAGCCCGGGGCAGGTCTCGGGTCATGCCCTACGGAATGGATGCCTTCATGCTGGGTATTGGGATGCTGGGTTACCCAGGGTTCCAAGCCACGACCTACGCCAGCCGGAGTTA

                751       760       770       780       790       800       810       820       830       840       850       860       870       880       890       900
                |---------+---------+---------+---------+---------+---------+---------+---------+---------+---------+---------+---------+---------+---------+---------|
NM_008629.2 CACAGGCCTTGCCCCTGGTTACACCTACCAGTTCCCCGAATTCCGTGTAGAGCGGAGCCCTCTCCCGAGCGCCCCAGTCCTCCCCGAGCTCACAGCTATCCCTCTCACGGCTTATGGGCCCATGGCGGCGGCAGCGGCGGCGGCAGCTGT
PF1 CACAGGCCTTGCCCCTGGTTACACCTACCAGTTCCCCGAATTCCGTGTAGAGCGGAGCCCTCTCCCGAGCGCCCCAGTCCTCCCCGAGCTCACAGCTATCCCTCTCACGGCTTATGGGCCCATGGCGGCGGCAGCGGCGGCGGCAGCTGT
PR1 CACAGGCCTTGCCCCTGGTTACACCTACCAGTTCCCCGAATTCCGTGTAGAGCGGAGCCCTCTCCCGAGCGCCCCAGTCCTCCCCGAGCTCACAGCTATCCCTCTCACGGCTTATGGGCCCATGGCGGCGGCAGCGGCGGCGGCAGCTGT
PF2 CACAGGCCTTGCCCCTGGTTACACCTACCAGTTCCCCGAATTCCGTGTAGAGCGGAGCCCTCTCCCGAGCGCCCCAGTCCTCCCCGAGCTCACAGCTATCCCTCTCACGGCTTATGGGCCCATGGCGGCGGCAGCGGCGGCGGCAGCTGT
Consensus       CACAGGCCTTGCCCCTGGTTACACCTACCAGTTCCCCGAATTCCGTGTAGAGCGGAGCCCTCTCCCGAGCGCCCCAGTCCTCCCCGAGCTCACAGCTATCCCTCTCACGGCTTATGGGCCCATGGCGGCGGCAGCGGCGGCGGCAGCTGT

                901       910       920       930       940       950       960       970       980       990      1000      1010      1020      1030      1040      1050
                |---------+---------+---------+---------+---------+---------+---------+---------+---------+---------+---------+---------+---------+---------+---------|
NM_008629.2 AGTTCGAGGGACAGGCTCTCACCCCTGGACGATGGCTCCCCCTCCAGGTTCCACTCCCAGCCGCACAGGGGGCTTCCTAGGGACCACAAGCCCCGGCCCCATGGCTGAGCTCTACGGGGCAGCCAACCAGGACTCCGGGGTCAGCAGTTA
PF1 AGTTCGAGGGACAGGCTCTCACCCCTGGACGATGGCTCCCCCTCCAGGTTCCACTCCCAGCCGCAC-NGGGGCTTCCTAGGGACCACAAGCCCCNGGCCCATGGNTGAGCTCTA-NGGGCAGCCAACCAGGANTNCGGGGNCAGCAGTTA
PR1 AGTTCGAGGGACAGGCTCTCACCCCTGGACGATGGCTCCCCCTCCAGGTTCCACTCCCAGCCGCACAGGGGGCTTCCTAGGGACCACAAGCCCCGGCCCCATGGCTGAGCTCTACGGGGCAGCCAACCAGGACTCCGGGGTCAGCAGTTA
PF2 AGTTCGAGGGACAGGCTCTCACCCCTGGACGATGGCTCCCCCTCCAGGTTCCACTCCCAGCCGCACAGGGGGCTTCCTAGGGACCACAAGCCCCGGCCCCATGGCTGANCTCTACGGGGCAGCCAACCAGGACTCCGGGGTCAGCAGTTA
Consensus       AGTTCGAGGGACAGGCTCTCACCCCTGGACGATGGCTCCCCCTCCAGGTTCCACTCCCAGCCGCACagGGGGCTTCCTAGGGACCACAAGCCCCgGcCCCATGGcTGAgCTCTAcgGGGCAGCCAACCAGGAcTcCGGGGtCAGCAGTTA

                1051 1060      1070      1080      1090      1100      1110      1120      1130      1140      1150      1160      1170
                |---------+---------+---------+---------+---------+---------+---------+---------+---------+---------+---------+---------|
NM_008629.2 CATCAGCGCCGCCAGCCCCGCCCCCAGCACTGGTTTCGGCCACAGTCTTGGGGGTCCCTTGATTGC----CACAGCCTTCACCAATGGGTACCACTGA
PF1 CNTCANCNCN--CANCCCCNCCCCCANNACTNNTNN--GNNNCNGTCT--GGGGNCCCTTGATTGCNNANCNNNNCANNGNNCNNTGANNNNNNNNNN---NNNNNNNNNNNNNNNNNN
PR1 CATCAGCGCCGCCAGCCCCGCCCCCAGCACTGGTTTCGGCCACAGTCTTGGGGGTCCCTTGATTGC----CACAGCCT--------------CNCCNA---NNNNNNNNNN
PF2 CATCAGCGCCGCCAGCCCCGCCCCCAGCACTGGTTTCGGCCACAGTCTTGGGGGTCCCTTGATTGC----CACAGCCTTCACCAATGGGTACCACTGACGCNTNNNNNNNNNNNNNNNNNN
Consensus       CaTCAgCgCcgcCAgCCCCgCCCCCAgcACTggTttcgGccaCaGTCTtgGGGGtCCCTTGATTGC....CacagCcttcaccaatgggtaccactga...n.nnnnnnnnnnnnnnnnn
```

Figure 3.2: Generation of inducible Msi1-overexpressing mice. (A) Schematic representation of the Recombination-Mediated Cassette Exchange vector used for targeted transgenesis of the Msi1 knock-In allele. (not to scale). (B) Illustrates the position of primers that were used for sequencing the Msi1 transgene. Primers PF_1 and PR_1 were also used for isolating a PCR product containing the *Msi1* CDS. (C) Verification of the *Rosa26*^{Msi1} transgene product that was isolated from genomic DNA by PCR using primers PF_1 and PR_1. The 1,174 bp PCR amplicon included 1,089 bp of mouse *Msi1* CDS, and 61 bp upstream and 24 bp downstream of the transgene. The *Rosa26*$^{+/+}$ sample served as a negative control as primers PF_1 and PR_1 annealed to regions that are not present in the endogenous *Rosa26* locus. (D) Agarose gel electrophoretic analysis of purified PCR product. (E) Analysis of sequencing results. Sequencing results generated using PF_1, PR_1, and PF_2 were compared to the *mus musculus Msi1* CDS isoform 1 sequence (NM_008629.2, NCBI). Results generated from PF_3, PF_4, PF_5, and PR_1 (not shown) revealed no mutations in the transgenic *Msi1* CDS. Key for alignment: Black bases = high consensus for all 4 sequences, Red bases = consensus for 3 of the 4 sequences, Blue bases = low consensus (2 sequences match or 1 sequence is different from the other sequences).

colon tissues of Msi1$^{O/E}$ mice when compared to controls (Figure 3.1E). Ubiquitous upregulation of Msi1 was more pronounced in the kidney, small intestine, and colon epithelia of Msi1$^{O/E}$ mice relative to other tissues. Taken together, these results indicate efficient Msi1 induction as early as 3 days following TAM administration and show the successful generation of an inducible Msi1 knock-in transgenic mouse.

Severe growth retardation in Msi1-overexpressing mice

After confirming efficient Msi1 overexpression in various tissues of our TAM-injected double-transgenic mice, we set up a long-term experiment to determine whether Msi1 overexpression could induce tumor development in tissues that display elevated Msi1 expression during human tumorigenesis. Unexpectedly, ubiquitous Msi1 upregulation resulted in lethality in 15% of the mice by 14-dpi at which time all mice were euthanized because many had lost ~20% of their body weight and appeared morbid. The 14-day period from TAM injection to tissue harvesting was too short for analysis of potential tumor formation; therefore, we examined consequences of ubiquitous Msi1 overexpression on overall postnatal development of mice.

Although all mice had positive growth during the initial week following TAM-administration, weights of the Msi1$^{O/E}$ mice lagged behind their littermate controls (Figure 3.3A). Unexpectedly, we observed growth retardation in Msi1$^{O/E}$ mice starting at 2-dpi, with drastic weight loss from 10-dpi onwards. When compared to controls, Msi1$^{O/E}$ mice had significantly lower body weights and shorter body lengths at 14-dpi (Figure 3.3, B and C). This stunted growth phenotype was further emphasized by significantly shorter intestines at 7- and 14-dpi (Figure 3.3, D and E), and significantly smaller organs at 14-dpi (Figure 3.3F).

Although Msi1$^{O/E}$ mice showed a global decrease in body size, the reduction was not uniform as seen by their differentially altered organ proportions (Figures 3.3G, 3.3H and 3.4). When organ weights were normalized to body weights and then expressed as a percentage of similarly normalized organ proportions in wild-type mice; the spleen and lung proportions were

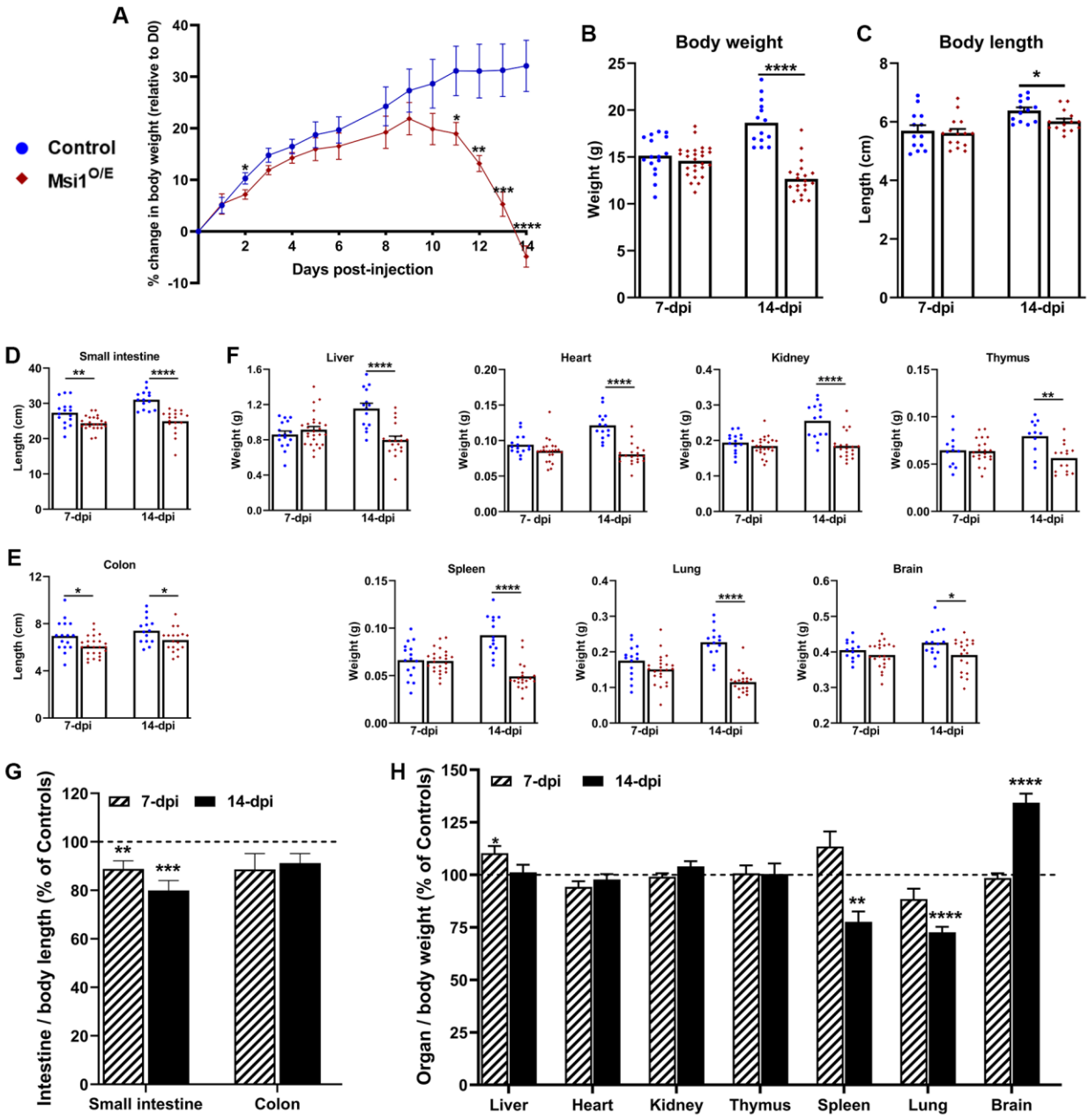

Figure 3.3: Gross morphology of Msi1-overexpressing mice. (A) Daily growth curve of mice from 0 to 14-dpi. Control (blue circle), n = 9, Msi1$^{O/E}$ (red diamond), n = 8. (B) Body weight, (C) body length, (D) small intestine length, (E) colon length, and (F) organ weights at 7- and 14-dpi. For B-F, each mouse is shown as individual blue circle (Control) or red diamond (Msi1$^{O/E}$). (G, H) Normalized organ proportions of Msi1$^{O/E}$ mice at 7- and 14-dpi as percentage of control littermate proportions. Dashed line at 100% represents normalized organ proportions of control mice. Graphical data represent mean ± SEM for each genotype (7-dpi, n = 11-26, 14-dpi, n = 11-20 mice). All data were analyzed using an unpaired two-tailed t-test. *p < 0.05, **p < 0.01, ***p < 0.001, ****p < 0.0001.

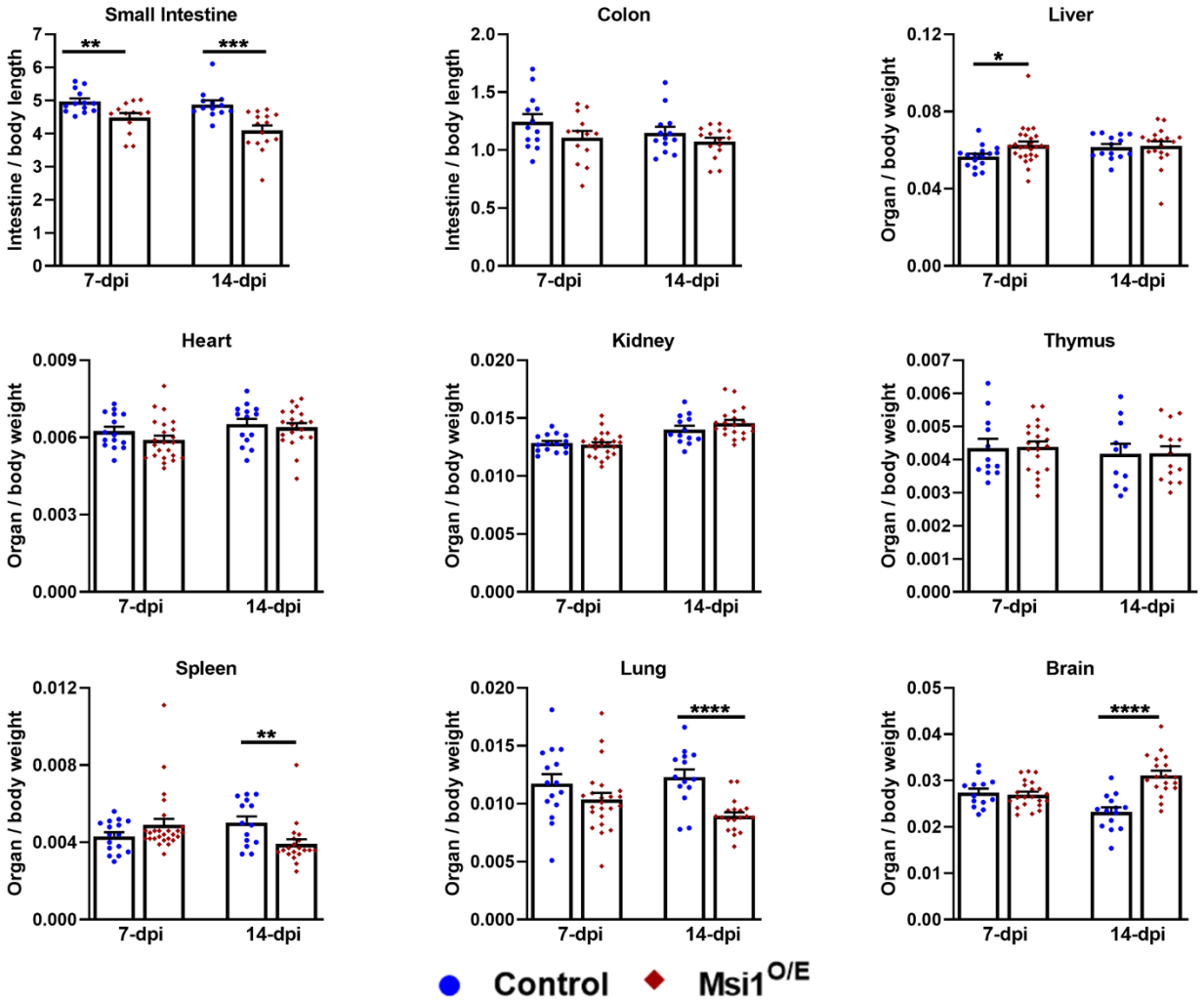

Figure 3.4: Msi1-overexpressing mice have altered organ proportions. (A, B) Intestinal to body length and (C) organ to body weight proportions at 7- and 14-dpi. (7-dpi = 11-26, 14-dpi = 11-20 mice). Mean ± SEM. Unpaired two-tailed t-test analysis. *p < 0.05, ***p* < 0.01, ****p* < 0.001, *****p* < 0.0001.

significantly lower in the Msi1$^{O/E}$ mice by 14-dpi (Figure 3.3H). In contrast, Msi1 overexpression resulted in increased relative brain size. There were no differences in normalized sizes of heart, kidney and thymus. Compared to control mice, small intestinal length to body length proportions of Msi1$^{O/E}$ mice were significantly reduced at both 7- and 14-dpi (Figure 3.3G). The colon proportions also trended to be reduced in Msi1$^{O/E}$ mice, but were not statistically different from littermate controls. Notably, only the liver and small intestine proportions were significantly altered in Msi1$^{O/E}$ mice at 7-dpi; with the liver proportion being larger (Figure 3.3H).

TAM toxicity and mere activation of Cre recombinase have each been linked to various phenotypes in mice (15,16). To investigate this possibility, I analyzed body and organ sizes of TAM-injected C57BL/6 wild-type mice either with or without the *UBC-CreER^{T2}* transgene. No significant differences in body weight, body length, intestinal lengths or organ weights were observed at 14-dpi; indicating that TAM administration or Cre expression alone was not sufficient to cause the stunted growth pattern I observed in Msi1$^{O/E}$ mice (Figure 3.5). Therefore, I conclude that the ubiquitous overexpression of Msi1 in developing mice results in severe growth retardation that is characterized by altered body and organ sizes.

DISCUSSION

In this study, I characterized a novel Cre-inducible mouse model that facilitates conditional transgenic overexpression of Msi1. Our main aim for generating this transgenic mouse was to investigate the oncogenic properties of Msi1 in vivo. The second goal was to provide the Msi1 research field with a valuable resource that can be used to further the overall understanding of the pathological roles played by Msi1 in tumors originating from different tissues. I utilized a tamoxifen-dependent *UBC-CreER^{T2}* strain to drive whole-body expression of our *Msi1* knock-in transgene in order to identify tissues that were altered by Msi1 overexpression and could be characterized further.

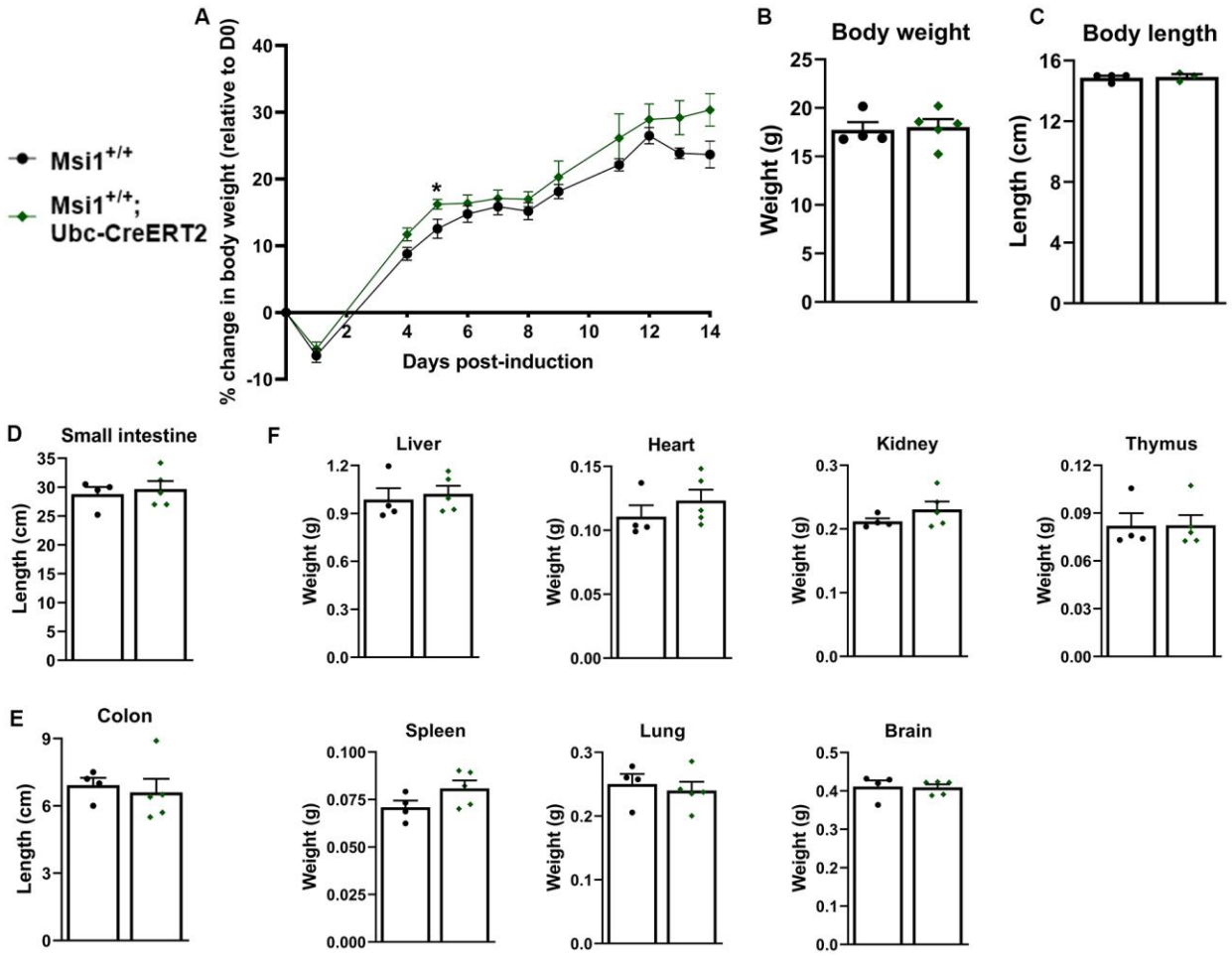

Figure 3.5: Tamoxifen or activation of Cre recombinase alone in C57BL/6 WT mice does not cause growth retardation or premature death by 14-dpi. (A) Daily growth curve of tamoxifen-injected *Msi1*$^{+/+}$ and *Msi1*$^{+/+}$*;UBC-CreERT2* mice from day 0 to 14-dpi. Comparison of (B) body weight, (C) body length, (D) small intestine length, (E) colon length, and (F) organ weights at 14-dpi. Sample size: *Msi1*$^{+/+}$ = 4, *Msi1*$^{+/+}$*;UBC-CreERT2* = 5. Mean ± SEM. Unpaired two-tailed t-test analysis. *$p < 0.05$.

Here I report that Msi1 expression was upregulated in various tissues, including kidney, lung, liver and intestinal epithelium, at 3 days after activation of Cre recombinase. However, the ubiquitous overexpression of Msi1 in juvenile mice (4-5 weeks old) resulted in a failure to thrive and premature death. Two weeks after Msi1 induction, the $Msi1^{O/E}$ mice had smaller body and organ weights, as well as shorter intestinal lengths when compared to littermate controls. Mouse pups are not fully developed when they are born and it has been shown that neonatal organs, including the intestines grow rapidly during the early postnatal period (~6 weeks) (17,18). Therefore, my findings suggest that whole-body overexpression of Msi1 severely impairs the postnatal development process in mice. However, this stunted growth phenotype of $Msi1^{O/E}$ mice was not seen in every tissue, but rather, showed selective alterations in organ proportions. It is possible that this selectivity was due to unequal organ sensitivities to upregulated Msi1 or differences in normal baseline Msi1 levels in different organs.

In summary, we have successfully developed a conditional and Cre-inducible Msi1 knock-in line by targeting the *Rosa26* locus. Msi1 overexpression appears to have a global inhibitory effect on mouse postnatal development, with prominent phenotypes observed in intestines, liver, spleen, lung and brain.

MATERIALS AND METHODS

Mouse husbandry

Mouse use was approved by the Institutional Animal Care and Use Committee at the University of Kansas. All mouse experiments adhered to federal regulations and institutional guidelines. Mice were maintained in the Animal Care Unit at the University of Kansas under the animal use statement 137-02 and were housed in cages with sex-matched littermates, except for breeding purposes, and fed *ad libitum* water and chow (ENVIGO, Teklad global #2918).

Generation of a Msi1 knock-in transgenic mouse

A conditional and tamoxifen-inducible Msi1 knock-in transgenic mouse was generated in collaboration with Taconic Artemis using Recombination-Mediated Cassette Exchange (RMCE) targeted transgenesis. The RMCE vector (pMsi1Final RKL20014, Figure S1A) contained a strong synthetic CAG promoter (Cytomegalovirus early enhancer element, chicken *β-Actin* promoter and rabbit *β-Globulin* first exon and intron), a loxP-flanked polyadenylated transcription termination (STOP) cassette, and mouse Msi1 open reading frame followed by a STOP cassette. This targeting vector was transfected into Taconic Artemis C57BL/6 embryonic stem (ES) cells equipped with F3/FRT-RMCE docking sites in the *Rosa26* locus. Successful recombinant clones containing the conditional Msi1 knock-in allele were selected using positive Neomycin resistance. Blastocysts isolated from impregnated BALB/c females were each injected with 10-15 positively-selected ES cells and subsequently transferred into pseudopregnant NMRI females to produce chimeric offspring (G0). Highly chimeric mice were backcrossed into wild-type C57BL/6 females. The presence of black, strain C57BL/6, offspring (G1) indicated successful germline transmission. To genotype G1 mice, PCR was performed on genomic DNA from tail snips and PCR amplicons were analyzed using a Caliper LabChip GX device. Homozygous and heterozygous Msi1 knock-in mice will be referred to as *Rosa26*$^{Msi1/Msi1}$ and *Rosa26*$^{Msi1/+}$, respectively.

Mice breeding and genotyping

Hemizygous B6.Cg-Tg(UBC-Cre-ERT2)1Ejb/2J (14) male breeders were purchased from The Jackson Laboratory (# 008085). *Rosa*$^{Msi1/Msi1}$ females were crossed with the *UBC-CreERT2* males to produce pups that were single transgenic *Rosa*$^{Msi1/+}$, or double transgenic *Rosa*$^{Msi1/+}$*;UBC-CreERT2*. Additional control mice were obtained from breeding a C57BL/6 wild-type female with a *UBC-CreERT2* male. Tail-snips from 3-weeks old pups were digested in 0.2mg/ml Proteinase K (ThermoFischer, #EO0491) at 55^{o}C overnight and heat-inactivated at

95°C for 10 min to extract genomic DNA. Primers used to genotype for Msi1 were: Msi1 WT Forward (WT_F) 5'- CTCTTCCCTCGTGATCTGCAACTCC-3'; Msi1 WT Reverse (WT_R) 5'-CATGTCTTTAATCTACCTCGATGG-3'; Msi1 knock-in Forward (KI_F) 5'-TGGCAGGCTTGAGATCTGG-3'; Msi1 knock-in Reverse (KI_R) 5'-CCCAAGGCACACAAAAAACC-3'. PCR conditions, using OneTaq DNA polymerase (NEB, #M0482S), were 95°C for 5 min, 35 cycles (95°C for 30 sec, 60°C for 30 sec, 72°C for 1 min) and 72°C for 10 min. Msi1 WT primers amplified a 299 bp sequence of the endogenous *Rosa26* locus (see Figure 1A). The binding sites for WT primers were also in the *Rosa26* knock-in allele, but there was no amplification due to the large transgenic vector inserted between the primer binding sites. The Msi1 knock-in primers amplified a 492 bp fragment. Primers used to identify Cre were: Cre_F 5'-CACCGCAGGTGTAGAGAAGG-3' and Cre_R 5'-CCAGAGTCATCCTTAGCGCC-3'. PCR conditions were 94°C for 3 min, 35 cycles (94°C for 30 sec, 59°C for 1 min, 68°C for 30 sec) and 68°C for 5 min and the Cre fragment size was 225 bp. To confirm the DNA quality of *Rosa26*$^{Msi1/+}$ mouse samples analyzed for Cre, an internal control fragment (492 bp) was amplified using the Msi1 knock-in primers.

Sequencing the Rosa26^{Msi1} transgene

The transgenic *Msi1* coding sequence (CDS) was isolated from genomic DNA by PCR using primers PF_1 and PR_1 (Figure S1B). Primers PF_1 and PR_2 amplified a 1,174 bp product which included 61 bp upstream and 24 bp downstream of the transgenic *Msi1* CDS (1,089 bp). The genomic DNA was extracted from tail-snips of 3-week old pups as mentioned above, and PCR was performed on samples from 3 independent *Rosa26*$^{Msi1/Msi1}$ transgenic mice, and 1 negative control *Rosa26*$^{+/+}$ (Msi1 wild-type) mouse. Primer sequences were: PF_1 5'- CTCCGTCGAC CTATAACTTCGTATAG-3' and PR_1 5'-CTTAAAATCTTAAGCTAGCACGCGTC-3'. PCR conditions, using Q5 High-Fidelity DNA Polymerase (NEB, #M0492S), were 98°C for 2 min 30 sec, 35 cycles (98°C for 10 sec, 68 °C for 30 sec, 72°C for 45 sec) and 72°C for 2 min. The PCR

product was then purified using a QlAquick PCR Purification Kit (Qiagen, #28104). Agarose gels were run before and after purification of the PCR product to verify the amplicon size. In addition to PF_1 and PR_1, primers PF_2, PF_3, PF_4, PF_5, and PR_2 (Figure S2B) were used to sequence the purified PCR product (Genewiz, NJ). Primer sequences were: PF_2 5'- GAAAGAGTGTCT GGTGATGC-3'; PF_3 5'-GATGCCATGCTGATGTTCG-3'; PF_4 5'- CTGGTTACACCTACC AGTTC-3'; PF_5 5'-CTTCCTAGGGACCACAAG-3'; and PR_2 5'- GATTGCGCCAGCACT TTATC-3'. Sequencing results were analyzed and compared to the NCBI reference sequence for mouse *Msi1* CDS isoform 1 (NM_008629.2); Assessed on 07/30/2020). Sequence alignment was performed using the MultAlin software (19).

Administration of Tamoxifen

4-5-week old mice, both sexes, were given intraperitoneal injections with a single dose of 75mg/kg body weight tamoxifen (TAM) solution (MP Biomedicals, #156738). TAM was prepared under sterile conditions by dissolving in 10:1 sunflower oil/ethanol mixture. 10% of the mixture was evaporated before administration into mice. Both control (*Rosa*$^{Msi1/+}$*)* mice and the Cre containing (*Rosa*$^{Msi1/+}$*;UBC-CreERT2*) mice were injected with TAM. Mice were euthanized by CO_2 asphyxiation followed by cervical dislocation at 3, 7 or 14 days post-tamoxifen injections. Age-matched littermates were used for all experiments.

Body weight, organ weights and length measurements

Mice were weighed daily at approximately the same time. Final body weights were measured immediately after mouse sacrifice. To obtain total body lengths, mice were laid face-down on a flat surface and body length was measured from the base of the skull to the anus. Organs were promptly excised and weighed, or their lengths measured. Organ to body weight proportions for liver, kidneys, thymus, spleen, lungs and brain were calculated by dividing the weight of the organ by the body weight of the mouse. Intestinal length to body length proportions were also

determined for the small intestine and colon. For comparison, organ proportions for each mouse were normalized to the average organ proportion of *Rosa*$^{Msi1/+}$ control mice.

Tissue sample preparation and Msi1 immunofluorescence

The small intestine and colon tissues were flushed with 10% saline-buffered formalin, cut lengthwise, individually rolled into “Swiss rolls”, and fixed in 10% saline-buffered formalin for 24 hr. Mouse heart, lung and kidney that were harvested at 3 days post-tamoxifen injections were fixed in 10% saline-buffered formalin for 24 hr, whereas liver samples were fixed for 48 hours. The tissue was then stored in 70% ethanol before paraffin embedding. In brief, 4µm tissue sections were deparaffinized 3x in xylene-substitute for a total of 30 min, rehydrated in a graded ethanol series (100, 95, 80, 70, 50%) for 5 min each, and permeabilized in methanol (0.1% Tween20) for 15 min on a shaker. Slides were washed 2x in absolute methanol for 5 min each, followed by a PBS wash. Antigen-retrieval was achieved by incubating slides in 0.01M citrate buffer (0.05% Tween20, pH 6.2) in a 90-95^{o}C water bath for 40 min. Slides were incubated for 2 hr in a PBS-blocking buffer containing 2% normal goat serum, 0.1% Triton X-100, 0.05% Tween20, 5% cold-fish skin gelatin, and 10% BSA (w/v). Sections were then incubated with primary antibodies overnight at 4^{o}C. A Msi1 (1:1000 Millipore, #MABE268 clone 7B11.1) primary antibody was used., Slides were rinsed 3x in PBS for 15 min total, incubated with Alexa Fluor secondary antibodies (1:1000 Invitrogen) for 1 hr at room temperature, and rinsed 3x in PBS before counterstaining with DAPI (Invitrogen, #P36962).

Microscope image acquisition and analysis

Immunofluorescence images were acquired using a Zeiss (Axiovert 135) microscope and Hamamatsu (C10600) digital camera. A Nikon (Eclipse 80i) microscope equipped with a ProgRes C3 (Jenoptik) digital camera was used to capture immunohistochemistry, H&E and Alcian blue images. RNA in situ hybridization images were acquired using a Leica (MZFLIII)

dissecting microscope and a Leica DFC 320 camera. Slides were assigned coded IDs and images were taken by an investigator who was blinded to sample genotype. Image brightness and levels were adjusted in Photoshop (Adobe), using identical settings for matched experiments

Statistical analysis

All data analysis was performed using GraphPad Prism 8 software. Data for body and organ weights, lengths or proportions, and RT-qPCR data were analyzed using an unpaired two-tailed t-test. Nested t-tests were used to analyze data for experiments where multiple technical measurements were taken from each mouse. These experiments included analysis of cell proliferation, morphological measurements and cell differentiation staining. Sample sizes for mice, crypts and villi analyzed are given in figure legends.

ACKNOWLEDGEMENTS

We thank William McGuinness for providing assistance with mouse husbandry. We extend our gratitude to TaconicArtemis GmbH for help with mouse design and generation, the KUMC histology core for use of tissue embedding equipment and the University of Kansas Animal Care Unit for mouse husbandry.

FUNDING

This work was supported by National Institutes of Health (R01 CA178831 and P30CA168524) and the Provost's Strategic Initiative Grant, Research Investment Council (University of Kansas).

REFERENCES

1. Muto J, Imai T, Ogawa D, Nishimoto Y, Okada Y, Mabuchi Y, et al. RNA-Binding Protein Musashi1 Modulates Glioma Cell Growth through the Post-Transcriptional Regulation of Notch and PI3 Kinase/Akt Signaling Pathways. PLoS ONE. 2012. 7(3):e33431.

2. Vo DT, Subramaniam D, Remke M, Burton TL, Uren PJ, Gelfond JA, et al. The RNA-binding protein Musashi1 affects medulloblastoma growth via a network of cancer-related genes and is an indicator of poor prognosis. Am J Pathol. 2012. 181(5): p. 1762–72.

3. Uren PJ, Vo DT, de Araujo PR, Pötschke R, Burns SC, Bahrami-Samani E, et al. RNA-binding protein Musashi1 is a central regulator of adhesion pathways in glioblastoma. Mol Cell Biol. 2015. 35(17): p. 2965–78.

4. Chen H-Y, Lin L-T, Wang M-L, Laurent B, Hsu C-H, Pan C-M, et al. Musashi-1 enhances glioblastoma cell migration and cytoskeletal dynamics through translational inhibition of Tensin3. Sci Rep. 2017. 7(1):8710.

5. Sureban SM, May R, George RJ, Dieckgraefe BK, McLeod HL, Ramalingam S, et al. Knockdown of RNA binding protein Musashi-1 leads to tumor regression in vivo. Gastroenterology. 2008. 134(5): p. 1448-1458.e2.

6. Li N, Yousefi M, Nakauka-Ddamba A, Li F, Vandivier L, Parada K, et al. The Msi family of RNA-binding proteins function redundantly as intestinal oncoproteins. Cell Rep. 2015. 13(11): p. 2440–55.

7. Wang X-Y, Penalva LO, Yuan H, Linnoila RI, Lu J, Okano H, et al. Musashi1 regulates breast tumor cell proliferation and is a prognostic indicator of poor survival. Mol Cancer. 2010. 9(1):221.

8. Lagadec C, Vlashi E, Frohnen P, Alhiyari Y, Chan M, Pajonk F. The RNA-binding protein Musashi-1 regulates proteasome subunit expression in breast cancer- and glioma-initiating cells. Stem Cells. 2014. 32(1): p. 135–44.

9. Katz Y, Li F, Lambert NJ, Sokol ES, Tam W-L, Cheng AW, et al. Musashi proteins are post-transcriptional regulators of the epithelial-luminal cell state. eLife. 2014;3:e03915.

10. Sansom OJ, Reed KR, Hayes AJ, Ireland H, Brinkmann H, Newton IP, et al. Loss of Apc in vivo immediately perturbs Wnt signaling, differentiation, and migration. Genes Dev. 2004 Jun 15;18(12):1385–90.

11. Potten CS, Booth C, Tudor GL, Booth D, Brady G, Hurley P, et al. Identification of a putative intestinal stem cell and early lineage marker; musashi-1. Differentiation. 2003 Jan;71(1):28–41.

12. Rezza A, Skah S, Roche C, Nadjar J, Samarut J, Plateroti M. The overexpression of the putative gut stem cell marker Musashi-1 induces tumorigenesis through Wnt and Notch activation. J Cell Science. 2010 Oct 1;123(19):3256–65.

13. Spears E, Neufeld KL. Novel Double-negative Feedback loop between Adenomatous Polyposis Coli and Musashi1 in colon epithelia. J Biol Chem. 2011 Feb 18;286(7):4946–50.

14. Ruzankina Y, Pinzon-Guzman C, Asare A, Ong T, Pontano L, Cotsarelis G, et al. Deletion of the developmentally essential gene ATR in adult mice leads to age-related phenotypes and stem cell loss. Cell Stem Cell. 2007 Jun;1(1):113–26.

15. Bohin N, Carlson EA, Samuelson LC. Genome toxicity and impaired stem cell function after conditional activation of CreERT2 in the intestine. Stem Cell Rep. 2018 Dec;11(6):1337–46.

16. Huh WJ, Khurana SS, Geahlen JH, Kohli K, Waller RA, Mills JC. tamoxifen induces rapid, reversible atrophy, and metaplasia in mouse stomach. Gastroenterology. 2012 Jan;142(1):21-24.e7.

17. Cheng H, Bjerknes M. Whole population cell kinetics and postnatal development of the mouse intestinal epithelium. Anat Rec. 1985 Apr;211(4):420–6.

18. Dehmer JJ, Garrison AP, Speck KE, Dekaney CM, Van Landeghem L, Sun X, et al. Expansion of intestinal epithelial stem cells during murine development. PLoS ONE. 2011 Nov 10;6(11):e27070.

19. Corpet F. Multiple sequence alignment with hierarchical clustering. Nucleic Acid Res. 1988 Nov 25;16(22):10881–90.

20. Chiremba TT, Neufeld KL. Constitutive Musashi1 expression impairs mouse postnatal development and intestinal homeostasis. Mol Biol Cell. 2020 Nov 11. Ahead of print. Available: https://www.molbiolcell.org/doi/abs/10.1091/mbc.E20-03-0206#

CHAPTER 4: CONSTITUTIVE MUSASHI1 EXPRESSION IMPAIRS MOUSE INTESTINAL HOMEOSTASIS

The data and opinions in this chapter were published previously and reformatted for this dissertation:

Chiremba TT, Neufeld KL. Constitutive Musashi1 expression impairs mouse postnatal development and intestinal homeostasis. Mol Biol Cell. 2020 Nov 11. Ahead of print. Available: https://www.molbiolcell.org/doi/abs/10.1091/mbc.E20-03-0206#

ABSTRACT

In this Chapter, I describe the intestinal phenotype of our novel ubiquitous Msi1-overexpressing mice. I show that Msi1-overexpressing mice had diminished intestinal epithelial cell (IEC) proliferation, and decreased growth of small intestine villi and colon crypts. Although Lgr5-positive intestinal stem cell numbers remained constant in Msi1-overexpressing tissue, an observed reduction in Cdc20 expression provides a potential mechanism underlying the intestinal growth defects. I further demonstrate that Msi1 overexpression affects IEC differentiation in a region-specific manner; with ileum tissue being influenced the most. Ilea of mutant mice displayed increased expression of enterocyte markers, but reduced expression of the goblet cell marker Muc2 and fewer Paneth cells. A higher Hes1:Math1 ratio in ilea from Msi1-overexpressing mice implicated Notch signaling in inducing enterocyte differentiation. Together, this work implicates Msi1 in mouse postnatal development of intestinal tissue, with Notch signaling alterations contributing to intestinal defects. This new mouse model will be a useful tool to further elucidate the role of Msi1 in other tissue settings.

INTRODUCTION

Msi1 is expressed in mouse and human intestinal epithelial cells (1,2). It has been shown that Msi1 facilitates regeneration of the intestinal epithelial tissues following irradiation-

induced injury in adult mice (3). However, no studies have investigated the role of Msi1 in the intestinal tissue during mouse postnatal development. Msi1 expression is upregulated in a considerable subset of colorectal cancers (4,5). Previously our lab identified a mutual-inhibitory relationship between MSI1 and APC, a tumor suppressor and Wnt signaling antagonist Adenomatous Polyposis Coli (6). We showed that *APC* mRNA is a target of MSI1, and MSI1 inhibits *APC* translation. Given that Msi1 is a Wnt target gene (7), my findings suggested a potential role for Msi1 in the regulation of intestinal epithelial cell (IEC) functions.

Using our inducible Msi1 knock-in model, I observed that mice ubiquitously overexpressing Msi1 ($Msi1^{O/E}$ mice) had smaller organs than control mice (Figure 3.3 and 3.4). Unexpectedly, the small intestines of $Msi1^{O/E}$ mice were the only tissues that showed significantly altered sizes at both 7- and 14-dpi. Therefore, I focused the rest of my study on analyzing effects of Msi1 overexpression in the intestinal epithelium.

RESULTS

Analysis of transgene expression and function in $Msi1^{O/E}$ intestinal epithelia

TAM and its active metabolite, N-desmethyltamoxifen, are cleared out of mouse brain at 7-dpi (8). To avoid confounding results that could be caused by residual TAM or $CreER^{T2}$ genome toxicity (9,10), I did not analyze the intestinal phenotype at time points earlier that 7-dpi. Furthermore, the gut-brain axis can influence intestinal functioning and pathology (11,12) and since Msi1 is expressed in the central nervous system of postnatal and adult mice (13), the 7-day wait period was essential for accurate comparison of the intestinal phenotypes of control and $Msi1^{O/E}$ mice.

It is well established that there is heterogeneity in tissue morphology, cell populations and gene expression along the proximal-to-distal axis of mouse intestinal tissue. Therefore,

I examined effects of Msi1 overexpression on the jejunum, ileum and colon as separate entities. First, I analyzed Msi1 RNA and protein expression in the intestinal epithelial tissue. Elevated *Msi1* mRNA levels were confirmed in IECs isolated from jejunum, ileum and colon segments of $Msi1^{O/E}$ mice compared to their injected control littermates (Figure 4.1, B and C). Furthermore, immunofluorescent staining showed increased Msi1 protein levels in intestinal tissue sections of $Msi1^{O/E}$ mice (Figure 4.1A). Bright fluorescent signal in the villi stroma of both control and $Msi1^{O/E}$ mice was due to nonspecific tissue autofluorescence (white arrows, Figure 4.1D) and absent from the intestinal epithelium.

I observed that recombination of the Msi1 knock-in transgene approached but did not reach 100% efficiency. I provide as an example, an image of small intestinal tissue of $Msi1^{O/E}$, which displayed some areas of low Msi1 protein expression (within dashed-white line, Figure 4.1E) comparable to endogenous Msi1 levels in control tissue. This mosaicism was not surprising, given recombination efficiencies reported for other Cre-LoxP systems (14).

To determine whether the transgenic Msi1 protein in $Msi1^{O/E}$ mice was functional, I analyzed Jagged1 (Jag1) expression. *Jag1* mRNA is a validated Msi1 target; Msi1 binds to *Jag1* mRNA and inhibits its translation, resulting in diminished Jag1 protein levels (3). I performed immunofluorescence staining for Jag1 and observed a significant decrease in Jag1 protein expression and fluorescence intensity in colon epithelia at 7-dpi (Figure 4.2, A and B). These results are consistent with Jag1 response to Msi1-overexpression in mouse neural stem cells (3) and indicate that the Msi1 transgene is functioning as expected.

Msi1 overexpression results in subtle effects on intestinal crypt and villi architecture

To assess whether the shorter intestines in $Msi1^{O/E}$ mice were related to changes in the overall structure of the intestinal epithelium, I analyzed crypt and villi morphology. Histological analyses of hematoxylin and eosin-stained tissue showed no overt differences between control

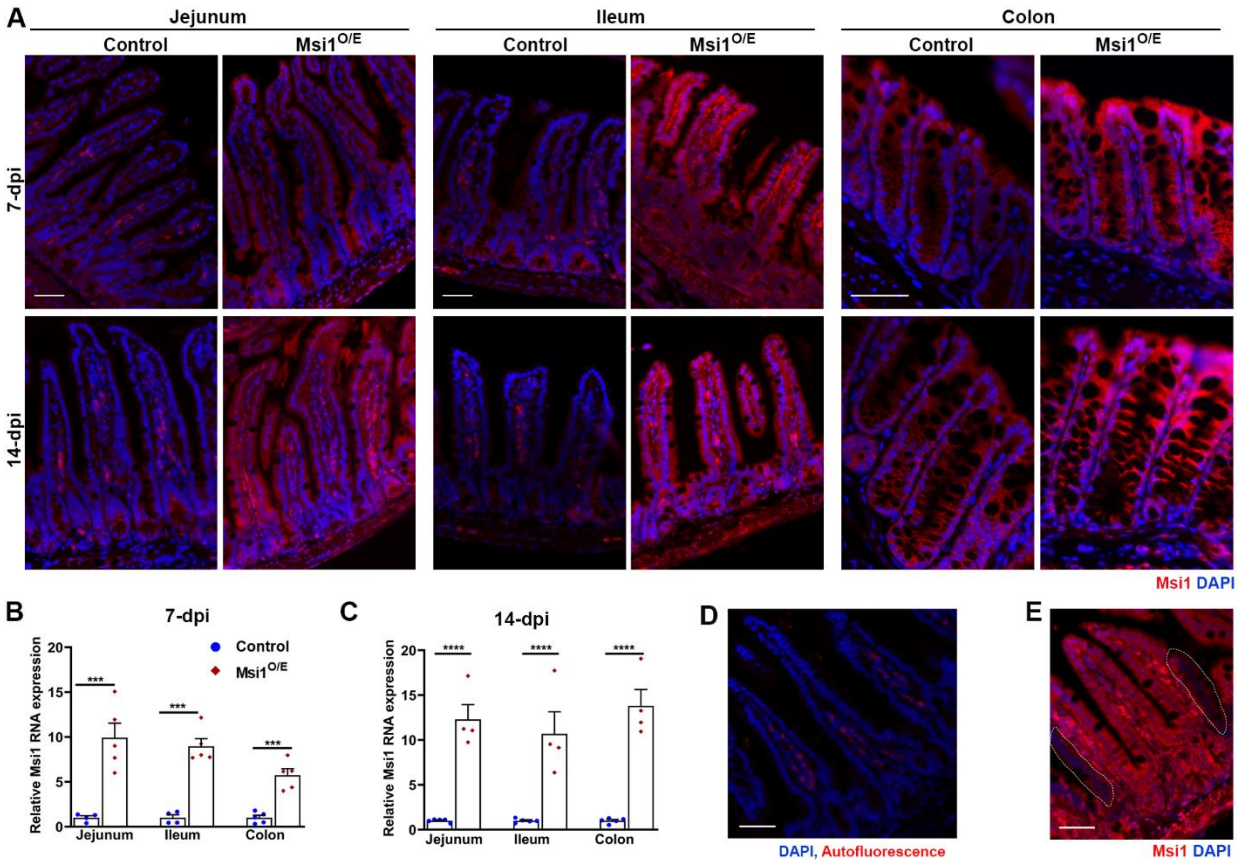

Figure 4.1. Upregulation of Msi1 expression in the Msi1 knock-in mouse model. (A) Evaluation of Msi1 overexpression in isolated intestinal epithelial cells by RT-qPCR. Data analyzed using an unpaired two-tailed t-test on ΔΔCt values. Expression was normalized to *Gapdh*. Graphical data represent mean ± SEM for each genotype (7-dpi, Control jejunum, n = 4, ileum, n = 4, colon, n = 5 ; $Msi1^{O/E}$, n = 5; 14-dpi, Control, n = 5, $Msi1^{O/E}$, n = 4 mice). Each mouse is shown as individual blue circle (Control) or red diamond ($Msi1^{O/E}$). There were 3 technical replicates assayed for each mouse. ***$p < 0.001$, ****$p < 0.0001$. (B) Representative merged immunofluorescent images for Msi1 (Red) and DAPI (nuclei staining, blue) in small intestine and colon epithelium tissues at 7- and 14-dpi. (C) Negative control (no primary antibody, only secondary antibody) immunofluorescent images showing autofluorescence (white arrows) in villi stroma. (D) Representative Msi1 immunofluorescent images illustrate areas of incomplete Cre-induced recombination of the CAG-loxP-STOP-loxP-*Msi1*CDS-STOP transgene. White-dashed outlines indicate cells expressing endogenous Msi1 levels in tamoxifen-injected $Msi1^{O/E}$ tissue.
Scale bars, 50 µm.

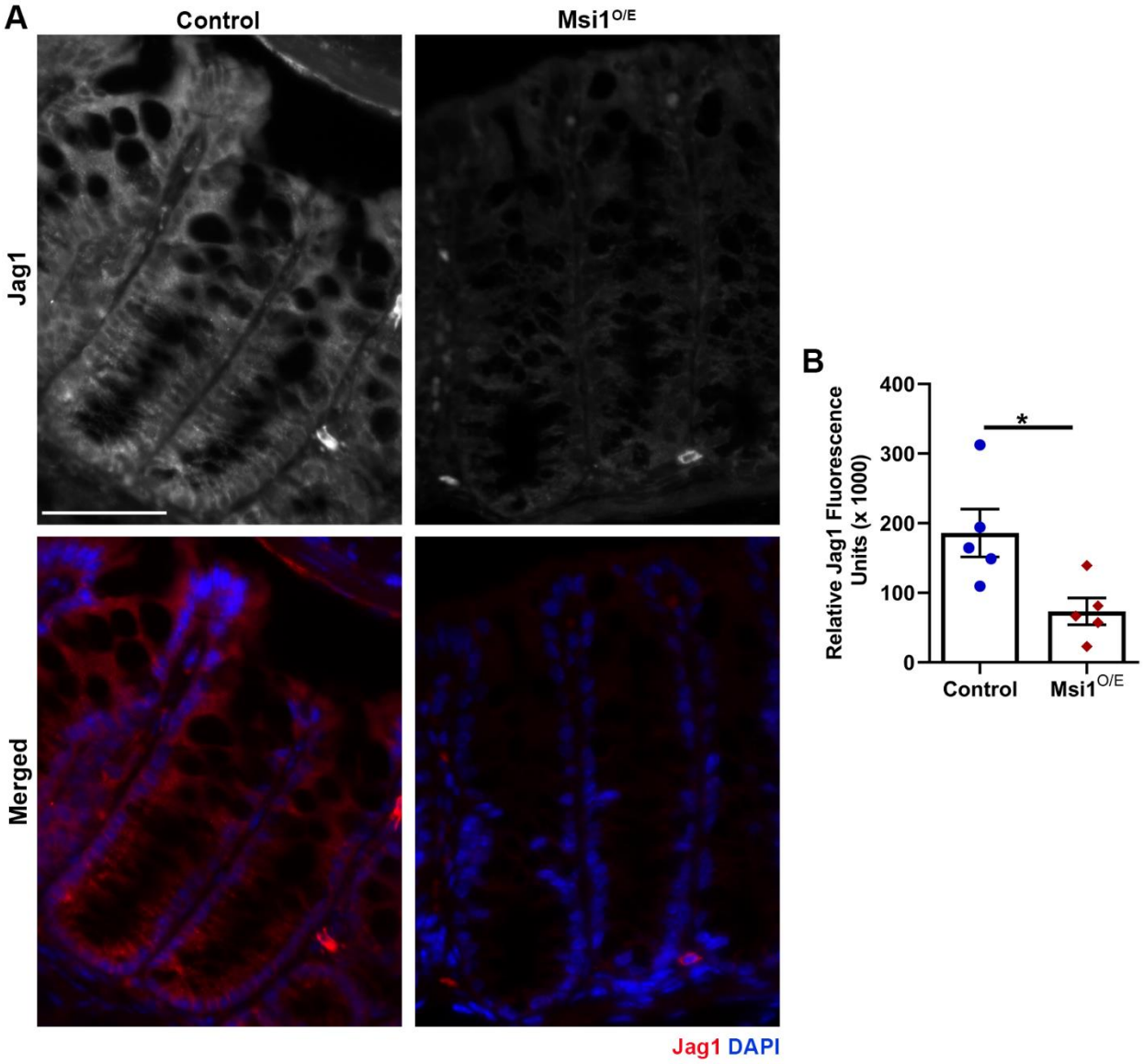

Figure 4.2: Decreased Jag1 protein expression in 7-dpi colon epithelial tissue of Msi1-overexpressing mice. (A) Representative immunofluorescence staining images for Jag1 (Gray, Red) and DAPI (Blue) in colon tissue at 7-dpi. Scale bars represent 50 µm. (B) Quantification of Jag1 immunofluorescence intensity. Each data point represents the mean relative Jag1 intensity in the crypt epithelia for a single mouse (5 mice per genotype). 13 images were analyzed for each mouse, and intensity was measured on the brightest four 150 μm^2 regions within the bottom two-thirds of crypts per image. Mean ± SEM. Nested two-tailed t-test analysis. *$p < 0.05$

and Msi-overexpressing mice (Figure 4.3A) indicating that normal gross crypt-villi architecture was maintained in the intestinal epithelial tissue of Msi1$^{O/E}$ mice.

Intestinal development during the first six weeks of postnatal life in wild-type C57BL/6 mice is characterized by a gradual increase in small intestine length, crypt depth and villus height (15). Therefore, I measured these parameters, along with crypt width and density in order to assess contributions of Msi1 to intestinal tissue development (Table 4.1). Analysis of size changes between 7- and 14-dpi revealed that villi height, and crypt depth and width of control mice had positive growth, while crypt density decreased (Figure 4.3, B-E). Although the overall patterns of Msi1$^{O/E}$ villi and crypt changes over the 7 day period tended to be similar to those of control tissue, the mean sizes of these changes were smaller and we observed some notable differences. For instance, the jejunum villi height and distal colon crypt depth of Msi1$^{O/E}$ mice had significant negative growth rates when compared to controls. Secondly, the proximal and distal colon crypts of Msi1$^{O/E}$ mice either changed in the opposite direction to that of control mice or barely changed between 7- and 14-dpi. In summary, although there were no exaggerated alterations in crypt-villi morphology of Msi1$^{O/E}$ mice, the overall decrease in intestinal growth observed was consistent with the shorter intestinal lengths.

Decreased proliferation in intestinal epithelia with Msi1 overexpression

To test the hypothesis that altered IEC proliferation could contribute to the shorter intestines and reduced intestinal growth rates of Msi1$^{O/E}$ mice, we stained and scored intestinal tissue for the proliferative cell marker Ki-67. Representative images of Ki-67 immunofluorescence at 7-dpi are shown in Figure 4.4A. The percentage of Ki-67-positive IECs in crypts of the jejunum, ileum and colon did not differ between control and Msi1$^{O/E}$ mice at 7-dpi (Figure 4.4B). In contrast, by 14-dpi, there were significantly fewer proliferative IECs in all three intestinal segments of Msi1$^{O/E}$ mice compared to controls (Figure 4.4, C and D). This decrease

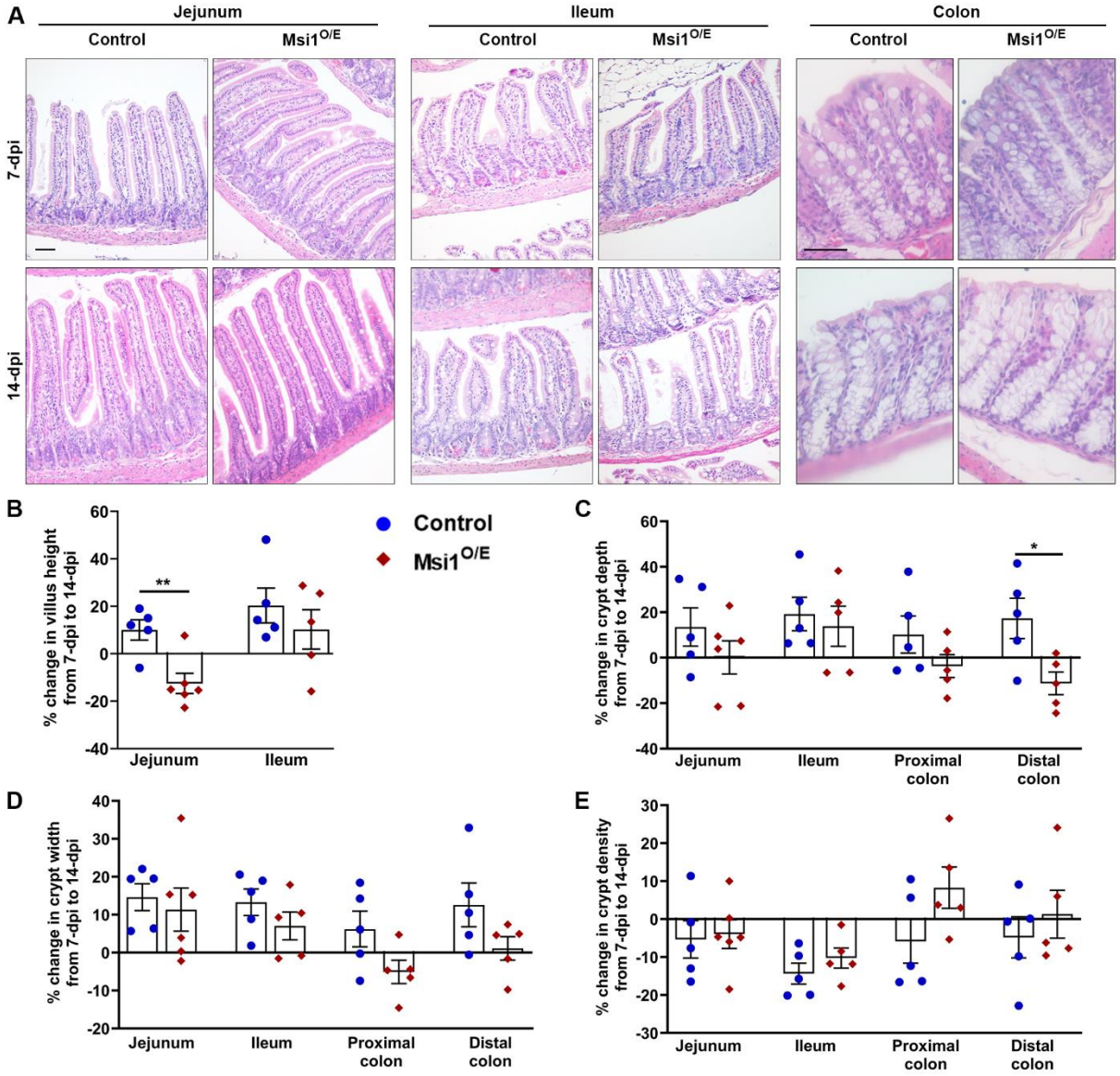

Figure 4.3. Effects of Msi1 upregulation on intestinal crypt and villi architecture. (A) Representative hematoxylin and eosin-stained images for small intestine and colon epithelia at 7- and 14- dpi. Scale bar, 50µm. Growth analysis as percentage change at 14-dpi relative to size at 7-dpi for (B) villi height, (C) crypt depth, (D) crypt width, and (E) crypt density. Each data point in the scatter plots indicates the mean percentage change for a single mouse (7-dpi, Control = 5, Msi1$^{O/E}$ jejunum = 6, ileum = 5, colon = 5; 14-dpi, Control = 5, Msi1$^{O/E}$ jejunum = 6, ileum = 5, colon = 5). Technical replicates per mouse: n ≥ 29 villi for height measurements; n ≥ 21 crypts for crypt depth and width measurements; n ≥ 15 images for crypt density analysis. Mean ± SEM. Nested two-tailed t-test analysis. *$p < 0.05$, **$p < 0.01$.

Table 4.1. Msi1 upregulation has varying effects on intestinal crypt and villi morphology. Mean measurements for crypt depth, width, density, and villi length are shown. Data analyzed using a nested two-tailed t-test. Sample size, n, in table is for biological replicates (7-dpi, Control = 5, $Msi1^{O/E}$ jejunum = 6, ileum = 5, colon = 5; 14-dpi, Control = 5, $Msi1^{O/E}$ jejunum = 6, ileum = 5, colon = 5). For technical replicates: n ≥ 21 crypts per mouse for crypt depth and width measurements; n ≥ 15 crypts images per mouse for crypt density; n ≥ 29 villi per mouse for villi height. Mean ± SEM. *P-values* for measurements that were statistically different between Control and $Msi1^{O/E}$ mice are in bold.

	7-days post-induction			14-days post-induction		
JEJUNUM	**Control**	**$Msi1^{O/E}$**	**p-value**	**Control**	**$Msi1^{O/E}$**	**p-value**
Crypt depth (μm)	76.8 ± 3.2	80.9 ± 5.8	0.428	87.1 ± 6.5	81.0 ± 5.9	0.5032
Crypt width (μm)	36.1 ± 2.2	33.9 ± 0.8	0.3445	41.3 ± 1.3	37.7 ± 1.9	0.1615
Crypt density (crypts/mm)	21.6 ± 1.1	24.0 ± 0.7	0.1346	20.1 ± 1.0	22.1 ± 0.8	0.1443
Villus height (μm)	209.3 ± 13.6	232.4 ± 5.2	0.1249	230.2 ± 8.9	203.2 ± 9.9	0.0754
	n=5	n=6		n=5	n=6	
ILEUM						
Crypt depth (μm)	81.7 ± 6.5	73.0 ± 3.4	0.2787	97.4 ± 6.0	83.2 ± 6.5	0.1471
Crypt width (μm)	34.6 ± 1.6	31.3 ± 1.1	0.1419	39.2 ± 1.2	33.6 ± 1.1	**0.0090****
Crypt density (crypts/mm)	23.6 ± 1.3	25.1 ± 1.0	0.3728	20.2 ± 0.6	22.6 ± 0.8	**0.0341***
Villus height (μm)	148.3 ± 8.8	158.7 ± 8.5	0.4254	178.4 ± 10.9	174.9 ± 13.2	0.8422
	n=5	n=5		n=5	n=5	
PROXIMAL COLON						
Crypt depth (μm)	84.8 ± 4.5	84.0 ± 6.2	0.9195	93.4 ± 6.9	80.9 ± 4.2	0.1609
Crypt width (μm)	28.7 ± 0.6	30.6 ± 0.7	0.0962	30.5 ± 1.3	29.0 ± 0.9	0.4137
Crypt density (crypts/mm)	30.7 ± 0.5	27.9 ± 0.5	**0.0002*****	28.9 ± 1.8	30.2 ± 1.5	0.6034
	n=5	n=5		n=5	n=5	
DISTAL COLON						
Crypt depth (μm)	124.2 ± 7.5	171.0 ± 4.6	**0.0007*****	145.7 ± 11.0	151.7 ± 8.5	0.6752
Crypt width (μm)	33.8 ± 0.9	33.9 ± 1.8	0.3614	38.0 ± 1.9	34.2 ± 1.0	0.1262
Crypt density (crypts/mm)	25.3 ± 1.0	26.3 ± 1.5	0.6011	24.1 ± 1.4	26.6 ± 1.7	0.2654
	n=5	n=5		n=5	n=5	

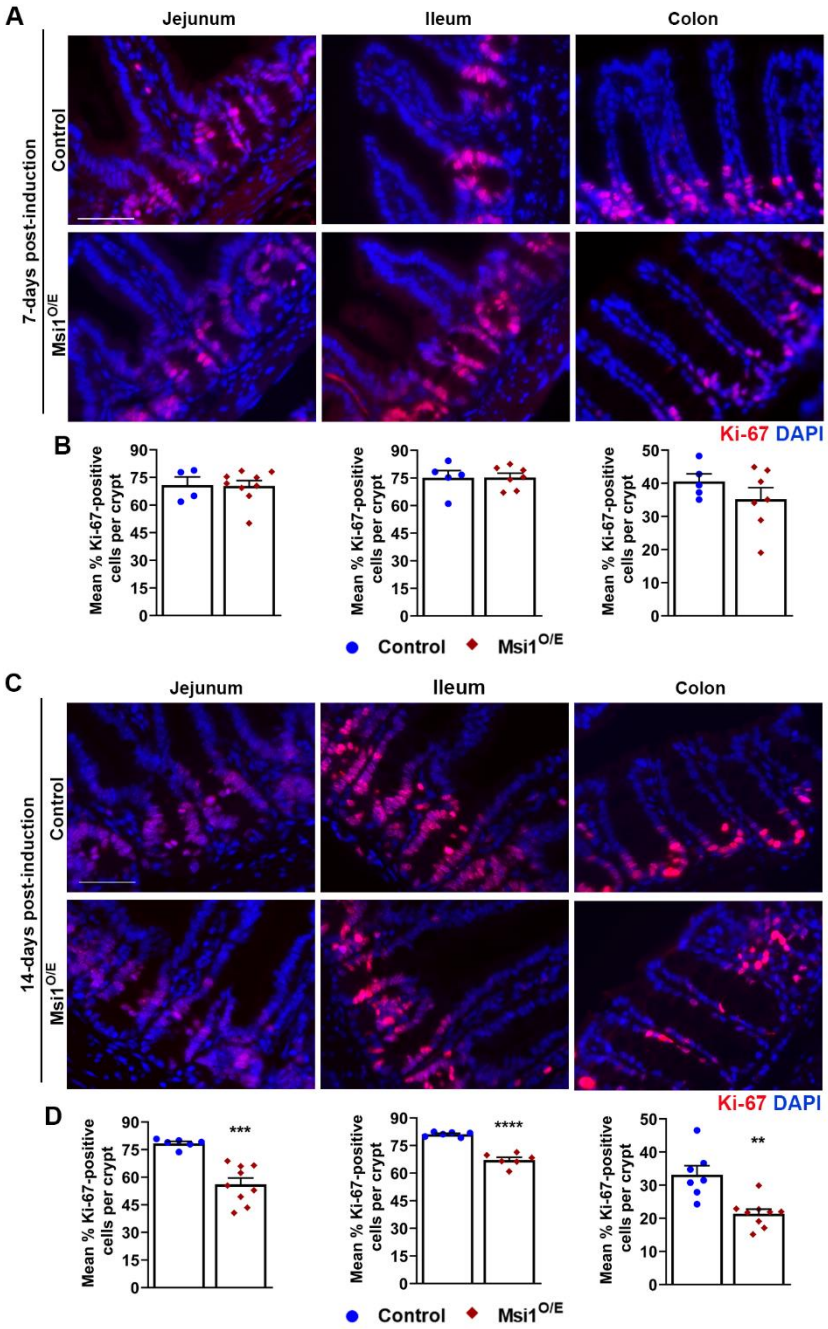

Figure 4.4: **Ubiquitous Msi1 overexpression results in decreased intestinal cell proliferation.** (A, C) Representative merged immunofluorescent images of Ki-67 (proliferative cell marker, red) and DAPI (nuclei staining, blue) for 7- and 14-dpi groups, respectively. Scale bar, 50μm. (B, D) Graphs of percentage of Ki-67-positive cells per crypt for 7- and 14-dpi, respectively. Each data point in the scatter plots represents the mean of Ki-67-positive cells per crypt for a single mouse (7-dpi, Control jejunum = 4, ileum and colon = 5, $Msi1^{O/E}$ jejunum = 9, ileum =7, colon = 7; 14-dpi, Control jejunum = 6, ileum = 6, colon = 7, $Msi1^{O/E}$ jejunum = 9, ileum = 6, colon = 9). For each mouse, 25 or more crypts were scored. Only those containing ≥30 total cells were analyzed. Mean ± SEM. Nested two-tailed t-test analysis. $^{**}p < 0.01$, $^{***}p < 0.001$, $^{****}p < 0.0001$.

in the population of Ki-67-positive cells is consistent with the stunted intestinal lengths and intestinal growth rates of Msi1$^{O/E}$ mice.

Increased goblet cell numbers in Msi1-overexpressing intestines

A possible mechanism for decreased IEC proliferation in mice overexpressing Msi1 is increased differentiation of transit-amplifying progenitor cells. To test this possibility, I first utilized Alcian blue to label goblet cells. Intestinal tissue from both control and Msi1-overexpressing mice displayed a general distribution of goblet cells similar to previous reports, with numbers increasing from jejunum to colon (Figures 4.5, A and B). Quantification revealed a significantly higher proportion of goblet cells in villi from Msi1$^{O/E}$ mouse ileum at 7-dpi, and both jejunum villi, and ileum crypts at 14-dpi. I was unable to quantify Alcian blue-positive cells in the colon segments due to the high percentage of goblet cells in that tissue (Figure 4.5B).

As a secondary method to evaluate goblet cells, I measured expression of Mucin2 (Muc2), a secretory mucin that is produced by goblet cells. In contrast to Alcian blue staining results, *Muc2* RNA levels were significantly reduced in IECs from Msi1$^{O/E}$ ileum compared to controls at 14-dpi (Figure 4.5C). Significant differences in *Muc2* expression in the other intestinal segments were not observed.

Msi1 overexpression has region-specific effects on intestinal cell differentiation

Next, I examined Paneth and enteroendocrine cell differentiation by immunostaining for lysozyme and Chromogranin A (Chga), respectively. Msi1$^{O/E}$ tissue had slightly fewer lysozyme-stained Paneth cells per crypt in all segments, with significant decreases in 7-dpi ileum (Figure 4.6A). In contrast, enteroendocrine cells from 7-dpi jejunum segments showed an increase, albeit insignificant, in Msi1$^{O/E}$ mice ($p=0.0698$, Figure 4.6D).

To quantify differentiation into the absorptive enterocyte lineage, I measured RNA levels of two enterocyte markers, *sucrase-isomaltase (Sis)* and *Lactase (Lac*) in IECs isolated from different intestinal sections (16). *Sis* but not *Lac* expression, was significantly decreased in

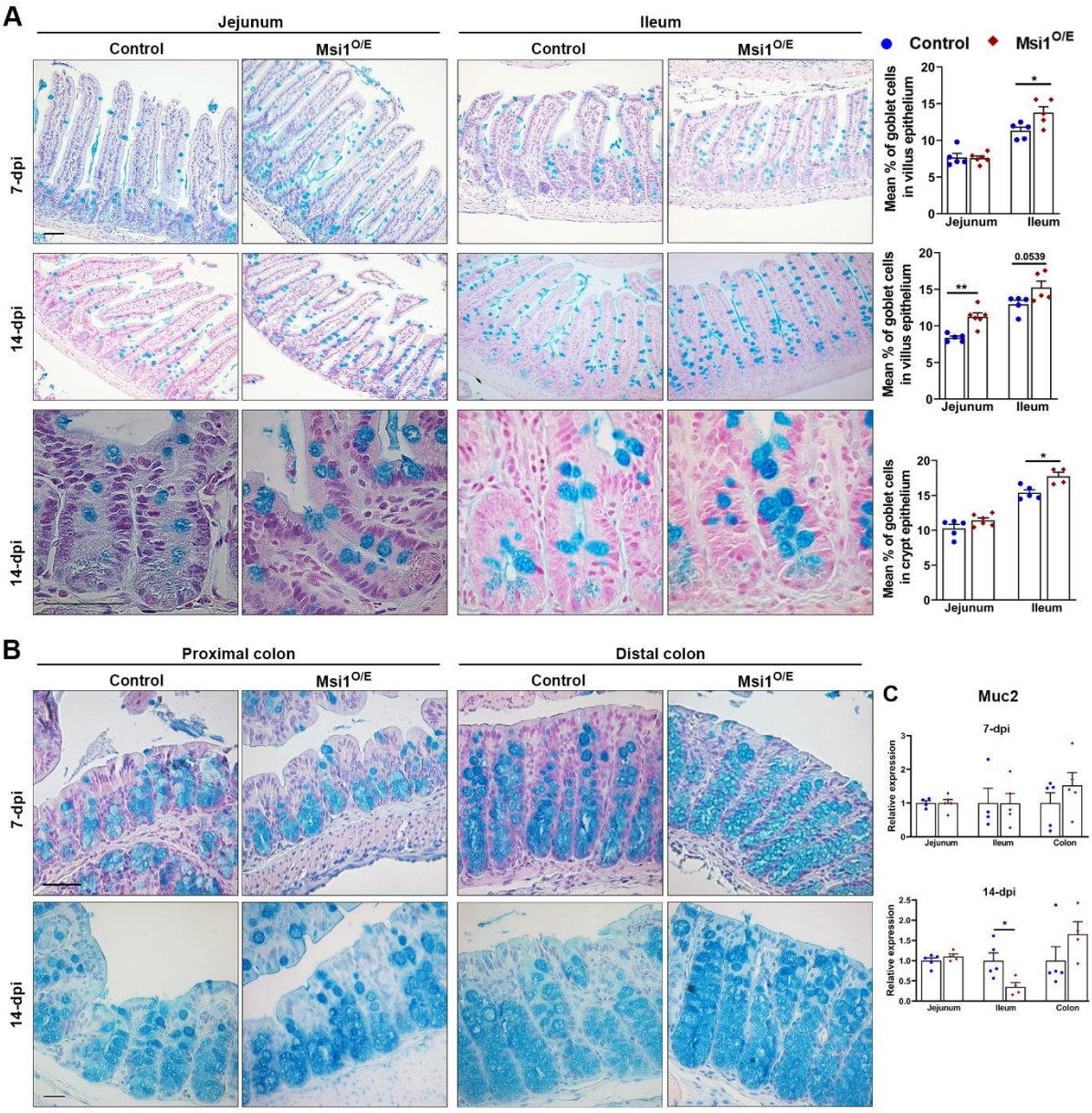

Figure 4.5: Altered goblet cell differentiation with Msi1 upregulation. (A) Representative images for goblet cells stained using Alcian blue and Nuclear Fast Red (left), and quantification of Alcian blue-positive cells in small intestine villi (right). (7-dpi, Control jejunum, n = 5, ileum, n = 6, Msi1$^{O/E}$ jejunum, n = 5, ileum, n = 5; 14-dpi, Control jejunum, n = 5, ileum, n = 5, Msi1$^{O/E}$ jejunum, n = 6, ileum, n = 5). N ≥ 30 villi per mouse. For crypts: (Control jejunum = 5, ileum = 5, Msi1$^{O/E}$ jejunum = 6, ileum = 4). N ≥ 27 crypts per mouse. **(B)** Representative images of goblet cell staining in mouse colon tissue at 7- and 14-dpi. **(C)** Analysis of *Muc2* RNAs in IECs harvested from 7- and 14-dpi mice. (7-dpi, Control jejunum, n = 4, ileum, n = 4, colon, n = 5; Msi1$^{O/E}$, n = 5; 14-dpi, Control, n = 5, Msi1$^{O/E}$, n = 4 mice). There were 3 technical replicates assayed for each mouse. Expression was normalized to *Gapdh*. Graphical data represent mean ± SEM for each genotype. Each mouse is shown as individual blue circle (Control) or red diamond (Msi1$^{O/E}$). Data in (A) analyzed using a nested two-tailed t-test, and in (C) analyzed using an unpaired two-tailed test. *p < 0.05. Scale bars, 50 μm.

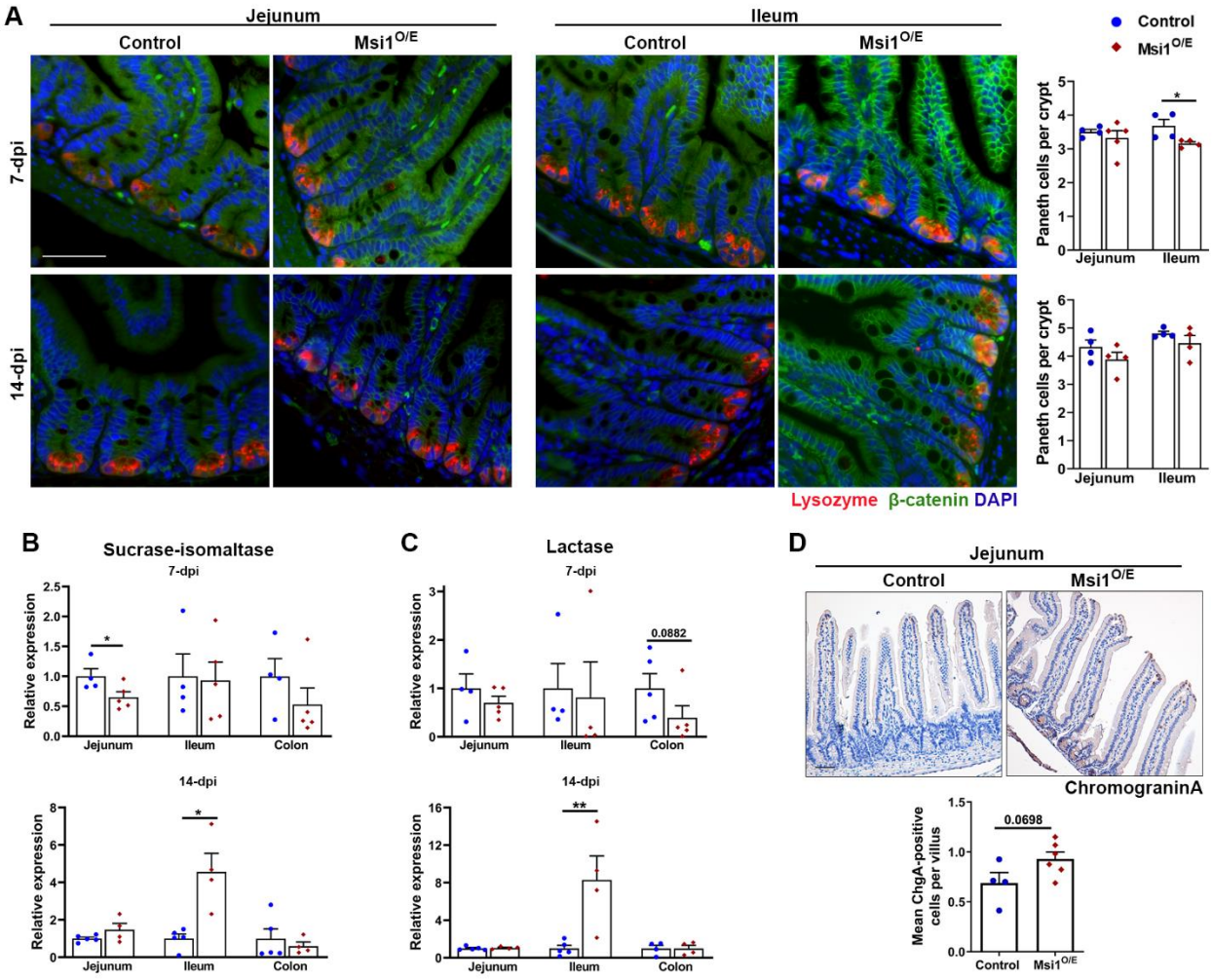

Figure 4.6: Msi1 overexpression alters intestinal epithelial cell differentiation (A) Representative merged immunofluorescent images for lysozyme (Paneth cell marker) staining and quantification of positive cells in small intestinal epithelia. (7-dpi, Control jejunum, n = 4, ileum, n =4, Msi1$^{O/E}$ jejunum, n = 5, ileum, n = 4; 14-dpi, Control jejunum, n = 4, ileum, n = 4, Msi1$^{O/E}$ jejunum, n = 4, ileum, n = 4). N ≥ 25 crypts per mouse. Analyses of **(B)** *Sucrase-isomaltase*, **(C)** *Lactase*, RNAs in IECs harvested from 7- and 14-dpi mice. (7-dpi, Control jejunum, n = 4, ileum, n = 4, colon, n = 5; Msi1$^{O/E}$, n = 5; 14-dpi, Control, n = 5, Msi1$^{O/E}$, n = 4 mice). 3 technical replicates assayed for each mouse. Expression was normalized to *Gapdh*. **(D)** Representative images of chromogranin A immunohistochemistry and quantification of enteroendocrine cell in 7-dpi jejunum tissue. (Control = 5, Msi1$^{O/E}$ jejunum = 6). N ≥ 57 villi per mouse.

Graphical data represent mean ± SEM for each genotype. Each mouse is shown as individual blue circle (Control) or red diamond (Msi1$^{O/E}$). Data in (A, C) analyzed using a nested two-tailed t-test, and in (B, D-H) analyzed using an unpaired two-tailed test. *p < 0.05, **p < 0.01. Scale bars, 50 μm.

jejunum IECs from Msi1$^{O/E}$ at 7-dpi (Figure 4.6, B and C). In contrast, both *Sis* and *Lac* RNA levels were significantly higher (4.5-fold and 8-fold increase, respectively) in 14-dpi ileum of mice overexpressing Msi1 (Figure 4.6, B and C). No changes were observed in the other segments.

Collectively, these results suggest that Msi1 overexpression affects IEC differentiation, but not in the same way for each intestinal region. Ileum tissue at 14-dpi seemed the most dramatically altered by Msi1 overexpression, showing significant decreases in goblet cell marker RNA and increases in enterocyte marker RNAs.

Altered Notch signaling components in Msi1-overexpressing IECs

Canonical Notch signaling is a major regulator of IEC differentiation and is predicted to inhibit secretory cell differentiation and thus support an absorptive enterocyte cell fate (17). In contrast, high expression of Notch antagonist mouse atonal homolog 1 (Math1) promotes commitment of progenitor cells to the secretory cell lineage (18). I hypothesized that the status of Notch signaling would vary among the three intestinal tissue segments, with more Notch signaling in 14-dpi ileum. To test this, I assessed expression of downstream Notch effector, Hairy and enhancer of split 1 (Hes1) and its antagonistic target Math1. Though I expected *Hes1* and *Math1* expression to be inversely altered, I instead found that both antagonists were significantly upregulated (67% and 76% increase, respectively) in 14-dpi Msi1$^{O/E}$ colon compared to controls (Figure 4.7, A and B).

In contrast, 14-dpi ileum had significantly lower *Math1* expression (70% reduction) and also lower Hes1 expression (32% reduction, p=0.0547). No changes in *Hes1* and *Math1* expression were seen in any intestinal segments at 7-dpi or in jejunum at 14-dpi. Because Hes1 and Math1 act as antagonists to control IEC differentiation, we analyzed the ratio of *Hes1*-to-*Math1* RNA as a readout of Notch activity. Consistent with the reduced *Muc2*, and elevated enterocyte marker RNA levels in 14-dpi ileum of Msi1$^{O/E}$ mice, I also found a significantly higher

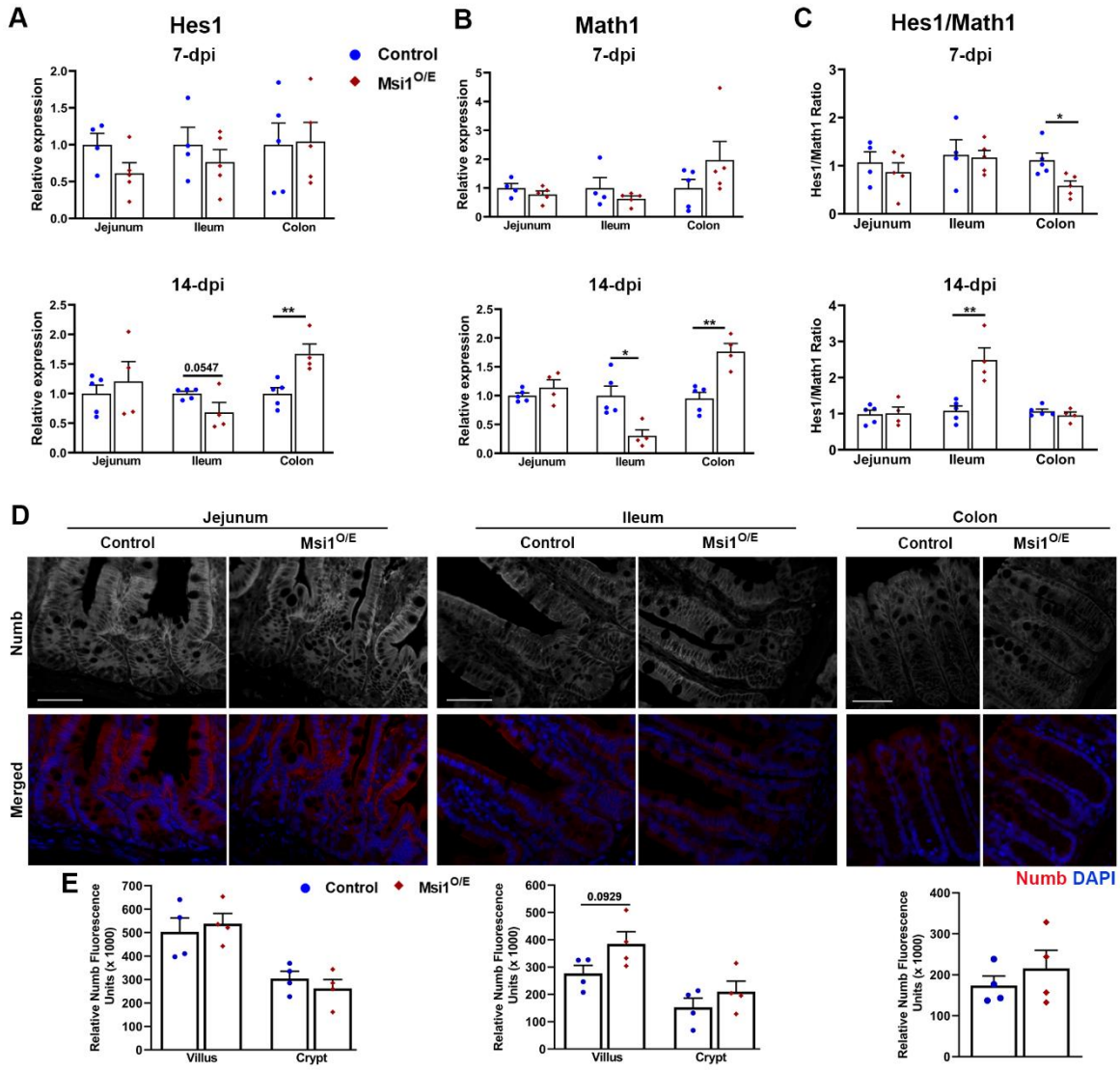

Figure 4.7: Ubiquitous Msi1 overexpression does not alter Numb immunostaining. Analyses of **(A)** *Hes1*, and **(B)** *Math1* RNAs in IECs harvested from 7- and 14-dpi mice. (7-dpi, Control jejunum, n = 4, ileum, n = 4, colon, n = 5; $Msi1^{O/E}$, n = 5; 14-dpi, Control, n = 5, $Msi1^{O/E}$, n = 4 mice). There were 3 technical replicates assayed for each mouse. Expression was normalized to *Gapdh*. **(C)** The ratios of *Hes1*-to-*Math1* RNA levels were calculated from data presented in F and G with p value determined using ΔCt values. Graphical data represent mean ± SEM for each genotype. Each mouse is shown as individual blue circle (Control) or red diamond ($Msi1^{O/E}$). Data in (A-C analyzed using an unpaired two-tailed test. **(D)** Representative immunofluorescence images for Numb (Gray, Red) and DAPI (Blue) in small intestine and colon tissue at 14-dpi. Scale bars represent 50 µm. **(E)** Quantification of Numb fluorescence intensity. Each data point represents the mean relative Numb fluorescence intensity in the villus or crypt epithelia for a single mouse (4 mice per genotype). For each mouse, 13 images were analyzed, and intensity was measured on the brightest one or two 361µm^2 epithelial sections per image. Scale bars, 50 µm. Mean ± SEM. Nested two-tailed t-test analysis. *$p < 0.05$, **$p < 0.01$.

Hes1-to-*Math1* ratio (Figure 4.7C). The only other significant change was a lower *Hes1*-to-*Math1* ratio seen in 7-dpi colons of Msi1$^{O/E}$ mice compared to their wild-type littermates. This decreased Notch readout was consistent with observed trends of decreased enterocyte and increased goblet cell marker RNAs. Taken together, my findings suggest that Msi1 regulates IEC differentiation in a temporal and region-specific manner, potentially through modulation of Notch activity in some regions.

To further investigate a potential mechanism underlying altered expression of *Hes1* and *Math1* in 14-dpi ileal and colon epithelia, I analyzed the expression of Numb, an antagonist of Notch signaling. It has been reported that Msi1 protein can bind to *Numb* mRNA and inhibit its translation, resulting in reduced Numb protein amounts and in potentiation of Notch signaling (19). I performed immunostaining for Numb (Figure 4.7D) and quantified Numb fluorescence intensity in 14-dpi intestinal epithelial tissue (Figure 4.7E). The Numb expression pattern revealed a decreasing gradient from the jejunum to the colon. In addition, I observed higher Numb protein expression in jejunum and ileum villi than in crypts. However, my analysis showed no significant differences in relative Numb protein fluorescence intensity between control and Msi1$^{O/E}$ intestinal epithelial tissue. Thus, these data suggest that altered *Hes1* and *Math1* expression in 14-dpi Msi1$^{O/E}$ epithelia is not due to modified Numb protein levels.

Decreased *Cdc20* expression in Msi1-overexpressing ileum IECs

Another possible reason for the reduced IEC proliferation observed in mice with overexpressed Msi1 is fewer intestinal stem cells (ISCs). Loss of ISCs has been correlated with diminished cell proliferative abilities and villi shortening (20). Lgr5-positive cells represent actively dividing ISCs in intestinal crypts. For ISC analysis, I focused on 14-dpi ileum because it was the most severely affected tissue in terms of differentiation. I found that the number of ISCs expressing Lgr5 RNA, as detected by in situ hybridization, did not differ between control and

Msi1$^{O/E}$ tissue in 14-dpi ileum (Figure 8, A and B). Therefore, the decrease in IEC proliferation that I observed was likely not a result of alterations in the population of Lgr5-positive ISCs.

To gain insight into the mechanism underlying the decreased proliferation observed when Msi1 is overexpressed for 14 days, I looked at expression levels for “Cancer Pathway” genes using a PCR Array. Of the 84 genes in the panel, 12 transcripts showed expression changes greater than 25% in small intestine samples from three 7-dpi Msi1$^{O/E}$ mice (Table 4.2). Of these transcripts, the only gene classified as a cell cycle regulator was *Cdc20*. Cdc20 is required for cell cycle exit and its downregulation has been shown to induce mitotic arrest (21)**.** RNA extracted from 14-dpi ileum was analyzed for *Cdc20* expression levels using independent primers for RT-qPCR. Notably, *Cdc20* expression was significantly decreased (~70%) in Msi1$^{O/E}$ IECs (Figure 4.8C), consistent with less proliferation also seen in this tissue.

Collectively my data suggest that whole-body induction of Msi1 disrupts the proliferative capacity of IECs, resulting in a considerable reduction of transit-amplifying progenitors, region-specific changes in differentiation and an overall decrease in intestinal growth and consequently, shortening of small intestines and colons.

DISCUSSION

In this study, I characterized the intestinal phenotype of ubiquitous Msi1-overexpressing mice. While investigating the molecular basis underlying intestinal shortening in Msi1-overexpressing mice, I found a significant decrease in epithelial cell proliferation in the small intestine and colon at 14-dpi. Further analysis revealed no difference in the number of Lgr5-positive stem cells. However, I found reduced *Cdc20* expression in ileum IECs at 14-dpi. Knockout of *Cdc20* in both young and adult mice has been reported to induce metaphase arrest in proliferating IECs, as well as decrease Ki-67-positive cells (22). Thus, my results suggest that

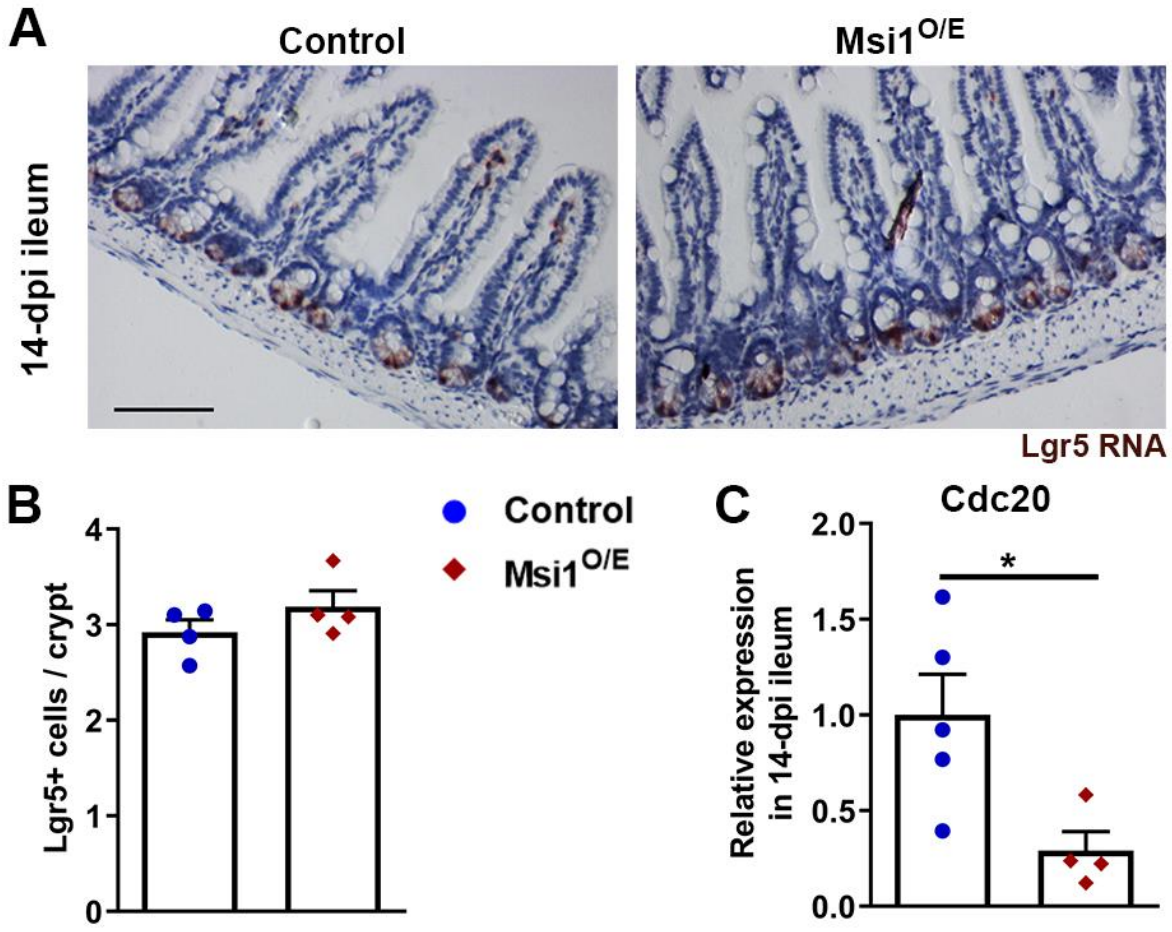

Figure 4.8: Msi1 overexpression does not alter Lgr5-positive stem cell numbers, but leads to reduced *Cdc20* expression in 14-dpi ileum tissue. (A) Representative *Lgr5* in situ hybridization staining in 14-dpi ileum tissue. Scale bar, 50 µm. (B) Quantification of *Lgr5*-positive stem cells per crypt. Each data point represents the mean number of positive stem cells per crypt. n = 20-24 crypts per mouse (4 mice per group). Data analyzed using a nested two-tailed t-test. Mean ± SEM. (C) Relative RNA expression analysis of *Cdc20* by RT-qPCR in 14-dpi IECs. (Control, n = 5, $Msi1^{O/E}$, n = 4 mice). There were 3 technical replicates assayed for each mouse. Expression was normalized to *Gapdh*. Unpaired two-tailed t-test analysis. Mean ± SEM. *$p < 0.05$

Table 4.2: Differentially expressed targets in Msi1$^{O/E}$ 7-dpi small intestinal epithelial cells. Relative target fold change expression generated by RT-qPCR analysis of 7-dpi jejunal RNA using the RT^2 Profiler^{TM} PCR Array. Target expression data was analyzed using the ΔΔCt method and normalized to the average Ct values of the five housekeeping genes provided in the array. Expression changes greater or less than 25% of the control samples were considered to be differentially expressed in Msi1$^{O/E}$ samples. N = 3 mice per group. Average fold change: Mean ± SEM.

		Relative fold change expression								
		Control			Msi1$^{O/E}$			Mean relative fold change		Expression i
Pathway	Gene	Mouse #1	Mouse #2	Mouse #3	Mouse #1	Mouse #2	Mouse #3	Control	Msi1$^{O/E}$	Msi1$^{O/E}$ vs Cont
Angiogenesis	**Vegfc**	1.122	0.928	0.951	1.224	1.536	1.187	1 ± 0.06	1.32 ± 0.11	Up
Angiogenesis	**Kdr**	0.691	0.719	1.590	0.982	2.268	1.494	1 ± 0.30	1.58 ± 0.37	Up
Apoptosis	**Casp9**	0.935	1.239	0.826	1.256	1.354	1.409	1 ± 0.12	1.34 ± 0.05	Up
Apoptosis	**Xiap**	1.362	0.780	0.857	1.349	1.434	1.462	1 ± 0.02	1.42 ± 0.34	Up
Cellular senescence	**Map2k1**	1.014	0.868	1.118	1.420	1.573	1.294	1 ± 0.07	1.43 ± 0.08	Up
DNA Damage and Repair	**Xrcc4**	1.178	0.830	0.992	1.224	1.474	1.309	1 ± 0.10	1.34 ± 0.07	Up
EMT	**Dsp**	0.870	0.996	1.134	1.343	1.844	1.396	1 ± 0.08	1.53 ± 0.16	Up
Metabolism	**Gpd2**	1.121	1.051	0.828	1.330	1.474	1.492	1 ± 0.09	1.43 ± 0.05	Up
Telomere and telemorase	**Tep1**	1.143	0.978	0.879	1.364	1.749	1.160	1 ± 0.08	1.42 ± 0.17	Up
Apoptosis	**Bcl2l11**	0.977	0.974	1.049	0.744	0.660	0.823	1 ± 0.30	0.74 ± 0.05	Down
Cell Cycle	**Cdc20**	0.515	1.171	1.314	0.615	0.676	0.685	1 ± 0.25	0.66 ± 0.02	Down
Metabolism	**Cox5a**	1.106	0.909	0.985	0.369	0.607	0.677	1 ± 0.06	0.55 ± 0.09	Down

the impaired IEC proliferation that I observed in Msi1-overexpressing mice could be due to downregulation of *Cdc20*.

The intestine increases in length and diameter during the early postnatal period, resulting in a larger digestive and absorptive epithelial surface area. These changes are driven by increased IEC proliferation, villi height and width, as well as crypt depth, density and diameter (15,23)**.** Our crypt morphology analysis revealed an overall, but marginal decrease in growth between 7- and 14-dpi. Jejunum villi height and distal colon crypt depth were substantially reduced by 14-dpi. Taken together, the shorter intestines, decreased crypt-villus growth and altered cell proliferation suggest that the intestines of Msi1-overexpressing mice have reduced luminal surface area, which may compromise their nutrient acquisition and overall health.

Here I show that Msi1 upregulation had region-specific effects on IEC differentiation; the ileum of $Msi1^{O/E}$ mice was more responsive to Msi1 upregulation than the jejunum and colon. I detected enhanced enterocyte marker expression as well as increased *Hes1*-to-*Math1* expression ratios in the ileum segments two weeks after Msi1 induction. These results indicate that ubiquitous Msi1 overexpression promoted secretory cell differentiation, potentially through modulating the activities of Math1 and Hes1. Consistent with a role for Notch in regulating IEC differentiation, I saw decreased Paneth cell numbers in the ileum a week after Msi1 induction. This finding agrees with *in vitro* studies that have shown inhibition of Paneth cell differentiation in response to Msi1 overexpression (16). Inexplicably, there were no differences in Paneth cell numbers in 14-dpi ileum tissue. Moreover, *Muc2* was downregulated in the ileum at 14-dpi, but there were no changes in *Muc2* in the other intestinal segments. Contrary to expectations, there were more goblet cells (Alcian blue) in the jejunum and ileum of $Msi1^{O/E}$ mice. It is possible that the goblet cells from Msi1-overexpressing mice were making less Muc2 as a way to compensate for the increased goblet cell numbers or as a result of the high *Hes1*-to-*Math1*

expression ratio. Additional RNA expression analysis of other goblet cell markers will be required to test this compensation model.

Msi1 protein can bind to *Numb* mRNA and inhibit its translation (19). Consequently, Msi1 overexpression has been shown to activate the Notch signaling pathway (7,19). In IEC differentiation, high Notch signaling repressed the intestinal secretory cell lineage, resulting in more enterocytes (17). Although my results from the 14-dpi ileum section were mostly consistent with Notch activation, Numb was not differentially expressed between $Msi1^{O/E}$ and control mice. In addition, I did not observe differences in Numb expression in 14-dpi jejunum and colon sections. Thus, these findings show that Msi1 upregulation did not modulate Numb expression in our $Msi1^{O/E}$ mice, in contrast to the established Msi1/Numb/Notch relationship. However, this inconsistency between Msi1 and Numb expression patterns has been reported in other mouse models. No significant changes in *Numb* translation were observed in neural stem cells that were derived from tetracycline-Msi1 mice and treated with doxycycline to induce Msi1 overexpression (3). In contrast, Msi1 deficiency in Msi1-knockout mice resulted in the downregulation of Numb protein expression and delayed gastric regeneration, indicating that Msi1 is required for translational activation of *Numb* (24). Taken together, my results show that the high *Hes1*-to-*Math1* expression ratio in 14-dpi ileum IECs was not due to altered Numb expression.

It is noteworthy that most phenotypes of our $Msi1^{O/E}$ mice differ considerably from those of other Msi1-overexpressing mouse models (5,25). Whereas my study used a ubiquitous and TAM-inducible model and focused on the early postnatal development stage, Li et al (2015), utilized a doxycycline-inducible collagen promoter to drive Msi1 expression in adult mice (5). In the Cambuli et al. (2015) study, Msi1 overexpression was intestine epithelial cell-specific, driven by a non-inducible villin promoter from embryonic day 11 (25). In contrast to my findings, both the inducible collagen promotor-driven adult mouse model and the villin-promoter driven model

reported increased IEC proliferation in the small intestine, which correlated with enhanced stem cell marker expression and numbers. However, similar to my 7-dpi findings, Cambuli et al. showed no differences in colon IEC proliferation. In terms of IEC differentiation, Li et al. reported a decrease in the overall number of differentiated cells, whereas, Cambuli et al., observed no differences. Although Msi1 overexpression was lethal in our mice around two weeks after induction, Msi1 driven by a collagen promoter resulted in lethality within three days (5). Discrepancies between these three mouse models could be due to the age at which Msi1 transgene expression was initiated and the tissue and cell type-specificity of the expression. Another consideration is that our $Msi1^{O/E}$ mice overexpress Msi1 in all cells and tissues. This might be the reason that my study is the first to report differences in mouse body and organ weights.

In summary, we have successfully developed a conditional and Cre-inducible Msi1 knock-in line by targeting the *Rosa26* locus. Msi1 overexpression appears to have a global inhibitory effect on mouse postnatal development, with prominent phenotypes observed in intestines, liver, spleen, lung and brain. My detailed analysis of intestinal tissue revealed roles for Msi1 in maintenance of intestinal homeostasis which might be important for future therapies that manipulate Msi1 activity. Msi1 upregulation for 14 days promoted enterocyte and inhibited goblet cell differentiation marker expression in the ileum, consistent with a measured elevated readout of Notch signaling. At earlier stages, the ileum showed depressed Paneth cell numbers, also consistent with elevated Notch signaling. In addition to this analysis of intestinal phenotypes, the Cre-inducible Msi1 model will be a useful tool for future investigations of the regulatory functions of Msi1 in other tissues and cell types at different developmental stages.

METHODS AND MATERIALS

Tissue sample preparation and Immunofluorescence

The small intestine was divided into three sections: duodenum, ileum and jejunum. The duodenum was the most proximal 5cm and was not further analyzed. Jejunum and ileum sections were the proximal two-thirds and distal third of the remaining small intestinal tissue, respectively. The jejunum, ileum and colon tissues were flushed with 10% saline-buffered formalin, cut lengthwise, individually rolled into “Swiss rolls”, and fixed in 10% saline-buffered formalin for 24 hr.

In brief, for immunofluorescence staining, 4µm tissue sections were deparaffinized 3x in xylene-substitute for a total of 30 min, rehydrated in a graded ethanol series (100, 95, 80, 70, 50%) for 5 min each, and permeabilized in methanol (0.1% Tween20) for 15 min on a shaker. Slides were washed 2x in absolute methanol for 5 min each, followed by a PBS wash. Antigen-retrieval was achieved by incubating slides in 0.01M citrate buffer (0.05% Tween20, pH 6.2) in a 90-95^{o}C water bath for 40 min. Slides were incubated for 2 hr in a PBS-blocking buffer containing 2% normal goat serum, 0.1% Triton X-100, 0.05% Tween20, 5% cold-fish skin gelatin, and 10% BSA (w/v). Sections were then incubated with primary antibodies overnight at 4^{o}C. Primary antibodies used were Msi1 (1:1000 Millipore, #MABE268 clone 7B11.1), Jag1 (1:50 Cell Signaling Tech (D4Y1R), #70109), Ki-67 (1:400 Cell Signaling Tech, #D3B5), lysozyme (1:500 DakoCytomation, #EC 3.2.17), β-catenin (1:500 BD Transduction, #610154), and Numb (1:500 Cell Signaling Tech (C29G11), #2756) . Slides were rinsed 3x in PBS for 15 min total, incubated with Alexa Fluor secondary antibodies (1:1000 Invitrogen) for 1 hr at room temperature, and rinsed 3x in PBS before counterstaining with DAPI (Invitrogen, #P36962).

Immunoperoxidase staining

After deparaffinization, rehydration, permeabilization, and methanol washes; slides were incubated in 3% H_2O_2 methanol (100%) for 20 min. Antigen retrieval, blocking, and primary

antibody (SP-1 Chromogranin A, ImmunoStar, #20085), incubation steps were similar to those for immunofluorescence staining. Goat anti-rabbit HRP-conjugated secondary antibody (1:1000 Bio-Rad, #172-1019) and 3,3'-diaminobenzidine tetrahydrochloride substrate (Invitrogen, #00-2020) were used. Tissue sections were counterstained with Gill's Hematoxylin (American MasterTech, HXGHE1LT) for 5 min followed by a 2 min water rinse. Bluing was achieved by dipping slides in 0.2% ammonia water for 30 sec. Slides were then rinsed in water for 2 min, dehydrated in ethanol (50, 70, 80, 95, 100%) for a min each, and washed 2x in xylene-substitute for 10 min total before application of mounting solution (Biocare Medical, EM897L).

Hematoxylin and eosin staining

Deparaffinized slides were rehydrated in ethanol (5 min in 100%, 2 min in 90%, 2 min in 70%) 2x for each concentration. Then slides were washed 2x in water for 2 min, stained with Gill's Hematoxylin for 8 min, washed in water for 2 min, and then blued as above. This was followed by two rinses in water for a minute each, incubation in 95% ethanol for a minute, and staining with Eosin Y (Fisher Scientific, 314-630) for a minute. After dehydration in ethanol (95%, 100%) for 2 min with two changes for each concentration, slides were briefly washed in xylene-substitute and then mounting solution (Biocare Medical, EM897L) was applied.

Alcian blue staining

For goblet cell staining, deparaffinized slides were rehydrated in ethanol (100, 95, 80, 70, 50%) for 5 min each and then washed 2x in water for 5 min. Slides were stained in 1% (w/v) Alcian blue solution (Sigma Aldrich, dissolved in 3% acetic acid, pH 2.5) for 30 min followed by two washes in water for 5 min each. Counterstaining was achieved by incubating slides with Nuclear Fast Read (Newcomer Supply, 1255A) for 5 min. Slides were then washed 2x in water for a total of 4 min. This was followed by dehydration in ethanol (50, 70, 80, 95, 100%) for a min each, three xylene washes for 5 min each, and application of mounting solution.

RNA in situ hybridization

RNA in situ hybridization was performed using the RNAscope® 2.5 HD Detection Kit (ACD) according to manufacturer's protocol. Briefly, after deparaffinization and hydrogen peroxide treatment (ACD, #322335), antigen retrieval on 4µm tissue sections was achieved by boiling slides in 1X Target Retrieval Reagent (ACD, #322000) in a 99-102^{o}C water bath for 15 minutes. Slides were dipped in 100% ethanol and air dried at room temperature. Then protease (ACD, #322331) was performed at 40^{o}C for 30 minutes. This was followed by hybridization using target probes for Lgr5 (ACD, #312171) at 40^{o}C for 2 hours. Mm-Polr2a (ACD, #312471) and dapB (ACD, #310043) probes were used for the positive and negative control sections, respectively. The signal was amplified and detected using the Red Detection Reagent (ACD, #322360). Counterstaining was achieved by incubating slides in 50% Gill's Hematoxylin for 2 min at room temperature and then blued in 0.02% ammonia water for 10 sec. After dehydration at 60^{o}C for 15 minutes, slides were dipped in xylene before application of mounting solution (Biocare Medical, EM897L).

Microscope image acquisition and analysis

Immunofluorescence images were acquired using a Zeiss (Axiovert 135) microscope and Hamamatsu (C10600) digital camera. A Nikon (Eclipse 80i) microscope equipped with a ProgRes C3 (Jenoptik) digital camera was used to capture immunohistochemistry, H&E and Alcian blue images. RNA in situ hybridization images were acquired using a Leica (MZFLIII) dissecting microscope and a Leica DFC 320 camera. Slides were assigned coded IDs and images were taken by an investigator who was blinded to sample genotype. An additional blinding step was performed, before image analysis, by renaming each acquired image with a random 4-letter code (generated using Excel). Images and slides were decoded after completion of measurements and/or counting analysis. Image brightness and levels were adjusted in Photoshop (Adobe), using identical settings for matched experiments.

Jag1 and Numb immunofluorescence signal intensities were measured using ImageJ software. For Jag1, signal intensities were measured on the brightest four 150 μm^2 regions per image, and for consistency purposes, these four regions were within the bottom two-thirds of crypts. For Numb, measurements were taken on the brightest one or two 361 μm^2 regions per image, in the villus and/or crypt epithelium. Intensity data were analyzed using the corrected total cellular fluorescence method (CTCF). CTCF = Integrated fluorescence density – (Area of selected tissue region X Mean fluorescence of background readings). The background readings were measured from negative control (no primary antibody, secondary only) slides.

Isolation of mouse intestinal epithelial cells and RNA preparation

Jejunum, ileum and colon epithelial cells were isolated as previously described with minor modifications (26,27). Intestinal tissue pieces were incubated in 0.04% sodium hypochlorite solution for 5 min on ice, and then incubated in Solution B (2.7 mM KCl, 150 mM NaCl, 1.2 mM KH_2PO_4, 68 mM Na_2HPO_4, 1.5 mM EDTA, 0.5 mM DTT) for 10 min on ice. The isolated cell suspension was centrifuged at 1,000 rpm for 10 min at 4^oC. Cell pellets were resuspended in Trizol (Life Technologies, #15596-026), 4ml for Jejunum, 2ml for ileum, and 1ml for colon, for total RNA extraction using the manufacturer's protocol; with the isopropanol incubation step at 20^oC overnight to optimize RNA precipitation. DNase I (NEB, #M0303S) digestion was performed to remove genomic DNA contaminants from the resuspended RNA, followed by further purification on RNeasy columns (Qiagen, #74104).

Differential target expression analysis using RT^2 Profiler^{TM} PCR Array

Jejunum intestinal epithelium cells were isolated from mice 7 days after TAM administration. Total RNA was extracted using Trizol (Life Technologies, #15596-026) and purified on RNeasy columns (Qiagen, #74104). Then complementary DNA (cDNA) synthesis was performed using 1µg purified total RNA and the RT^2 First Strand Kit (Qiagen, #330401) following the

manufacturer's protocol. This kit included a gDNA elimination step. Prepared cDNA was mixed with the RT^2 SYBR green (Qiagen, #330502) and dispensed in a 96-well RT^2 Profiler PCR Array for the Mouse Cancer PathwayFinder™ (Qiagen, #330231 PAMM-033ZA) according to manufacturer's recommendations. A single array was used for each individual mouse (3 mice per genotype) and assayed in a DNA Engine Opticon 2 System (MJ Research). Target expression was analyzed using the ΔΔCt method and normalized to the average Ct values of the five housekeeping genes provided in the array. For the initial analysis, targets with an expression change greater or less than 25% of the control samples were considered to be differentially expressed in Msi1-overexpressing samples.

Complementary DNA generation and Gene expression analysis

1µg purified total RNA was used to generate complementary DNA (cDNA). A 17µl reaction mixture containing RNA, Random Primer 6 (NEB, #S1230S), dNTPs (NEB, #N0447S) and nuclease-free water was incubated at 65^{o}C for 5 min, and quickly put on ice. M-MLUV Reverse Transcriptase (1µl NEB, #M0253S) and 2µl of enzyme buffer were added to the reaction mixture. For negative controls, nuclease-free water was used instead of reverse transcriptase. The final concentration was 6µM for Random Primer 6, and 0.75mM for dNTPs. PCR conditions for cDNA generation were 25^{o}C for 5 min, 42^{o}C for 1hr, and inactivation at 65^{o}C for 20 min. The cDNA product was diluted 1:5 with nuclease-free water and stored at -20^{o}C in aliquots to avoid repeated freeze-thaw cycles. For RT-qPCR, 1.6 µl of 1:10 further diluted cDNA was mixed with 300nM of each target primer, and 1X SYBR Green (DyNAmo HS, ThermoFischer, # F-140; or PowerUp, ThermoFischer, #A25742) in a 20 µl reaction mix and assayed in a DNA Engine Opticon 2 System (MJ Research) according to manufacturer's recommendations. 4-5 independent RNA samples were used for each genotype and 3 technical replicates were assayed for each mouse. Targets analyzed were *Cdc20*, *Hes1*, *Lactase*, *Math1*, *Msi1*, *Muc2,* and *Sucrase-isomaltase (Sis)*. Cycle threshold (Ct) values for the housekeeping gene *Gapdh*

were used as an internal control and for normalizing target Ct values. Primer sequences for targets are shown in Table 4.3.

The PCR efficiency of each primer pair was determined by performing a standard curve using 1:5 or 1:10 serial-diluted cDNA. To enhance precision, only raw Ct values of the triplicate reactions that varied by < 0.6 were used to calculate the mean Ct value for each biological sample. The ΔΔCt method was used to analyze expression levels for targets with primer efficiencies that differed by less than ±5% from the Gapdh primer efficiency. For those targets, an unpaired two-tailed t-test was performed on grouped non-averaged ΔΔCt values to determine statistical significance in expression levels between control and mutant samples. In contrast, *Cdc20* and *Math1* efficiencies differed from *Gapdh* by > 5%; therefore, expression levels were calculated according to the method described by (28) and data was analyzed using an unpaired two-tailed t-test on grouped non-averaged fold change values.

Table 4.3: **RT-qPCR Primer sequences and efficiencies**. Primer efficiencies and expression levels assayed using DyNAmo HS SYBR Green indicated by [a]; whereas [b] indicates assays that were performed using PowerUp SYBR Green.

Gene	Forward Primer (5' - 3')	Reverse Primer (5' - 3')	Efficiency
Cdc20	TTCGTGTTCGAGAGCGATTTG	ACCTTGGAACTAGATTTGCCA	101.31% [b]
Gapdh	TGGCCTTCCGTGTTCCTAC	GAGTTGCTGTTGAAGTCGCA	96.61% [a], 91.54% [b]
Hes1	CCAGCCAGTGTCAACACGA	AATGCCGGGAGCTATCTTTCT	90.6% [b]
Lac	CTCTTCTCAGGGAGGAAAGC	AGGAAATCCACGGAGCCCTT	90.29% [b]
Math1	ATCCCGTCCTTCAACAACGAC	CTCTCCGACATTGGGAGTCTG	100.08% [b]
Msi1	ATGCTGGGTATTGGGATGCT	CGGGGAACTGGTAGGTGTAA	92.03% [b]
Muc2	GATGCACTCATGGTGGAGCT	TCAGGCTTGTTGATCTTCTGCA	99.58% [a]
Sis	TGACTACCATACAGGGGAAGA	TCATATGTGTCTATCGACTCTC	92.31% [a]

Statistical analysis

All data analysis was performed using GraphPad Prism 8 software. Data for body and organ weights, lengths or proportions, and RT-qPCR data were analyzed using an unpaired two-tailed

t-test. Nested t-tests were used to analyze data for experiments where multiple technical measurements were taken from each mouse. These experiments included analysis of cell proliferation, morphological measurements and cell differentiation staining. Sample sizes for mice, crypts and villi analyzed are given in figure legends.

ACKNOWLEDGEMENTS

We thank William McGuinness for providing assistance with mouse husbandry and Vinamratha Rao for assistance with the crypt-villi architecture measurements. We extend our gratitude to TaconicArtemis GmbH for help with mouse design and generation, the KUMC histology core for use of tissue embedding equipment and the University of Kansas Animal Care Unit for mouse husbandry.

FUNDING

This work was supported by National Institutes of Health (R01 CA178831 and P30CA168524) and the Provost's Strategic Initiative Grant, Research Investment Council (University of Kansas).

REFERENCES

1. Kayahara T, Sawada M, Takaishi S, Fukui H, Seno H, Fukuzawa H, et al. Candidate markers for stem and early progenitor cells, Musashi-1 and Hes1, are expressed in crypt base columnar cells of mouse small intestine. FEBS Letters. 2003 Jan 30;535(1–3):131–5.
2. Cambuli FM, Rezza A, Nadjar J, Plateroti M. Brief report: Musashi1-eGFP mice, a new tool for differential isolation of the intestinal stem cell populations: Musashi1 and the Intestinal Crypt Stem Cells. Stem Cells. 2013 Oct;31(10):2273–8.
3. Katz Y, Li F, Lambert NJ, Sokol ES, Tam W-L, Cheng AW, et al. Musashi proteins are post-transcriptional regulators of the epithelial-luminal cell state. eLife. 2014;3:e03915.
4. Sureban SM, May R, George RJ, Dieckgraefe BK, McLeod HL, Ramalingam S, et al. Knockdown of RNA binding protein Musashi-1 leads to tumor regression in vivo. Gastroenterology. 2008 May;134(5):1448-1458.e2.

5. Li N, Yousefi M, Nakauka-Ddamba A, Li F, Vandivier L, Parada K, et al. The Msi family of RNA-binding proteins function redundantly as intestinal oncoproteins. Cell Rep. 2015 Dec;13(11):2440–55.

6. Spears E, Neufeld KL. Novel double-negative feedback loop between Adenomatous Polyposis Coli and Musashi1 in colon epithelia. J Biol Chem. 2011 Feb 18;286(7):4946–50.

7. Rezza A, Skah S, Roche C, Nadjar J, Samarut J, Plateroti M. The overexpression of the putative gut stem cell marker Musashi-1 induces tumorigenesis through Wnt and Notch activation. J Cell Sci. 2010 Oct 1;123(19):3256–65.

8. Jahn HM, Kasakow CV, Helfer A, Michely J, Verkhratsky A, Maurer HH, et al. Refined protocols of tamoxifen injection for inducible DNA recombination in mouse astroglia. Sci Rep. 2018 Dec;8(1):5913.

9. Valny M, Honsa P, Kirdajova D, Kamenik Z, Anderova M. Tamoxifen in the mouse brain: implications for fate-mapping studies using the tamoxifen-inducible Cre-loxP system. Front Cell Neurosci. 2016 Oct;10:243

10. Bohin N, Carlson EA, Samuelson LC. Genome toxicity and impaired stem cell function after conditional activation of CreERT2 in the intestine. Stem Cell Rep. 2018 Dec;11(6):1337–46.

11. Gue M, Bonbonne C, Fioramonti J, More J, Del Rio-Lacheze C, Comera C, et al. Stress-induced enhancement of colitis in rats: CRF and arginine vasopressin are not involved. Am J Physiol Gastrointest Liver Physiol. 1997 Jan 1;272(1):G84–91.

12. Tache Y, Perdue MH. Role of peripheral CRF signalling pathways in stress-related alterations of gut motility and mucosal function. Neurogastroenterol Motil. 2004 Apr;16(s1):137–42.

13. Sakakibara S, Okano H. Expression of neural RNA-binding proteins in the postnatal CNS: implications of their roles in neuronal and glial cell development. J Neurosci. 1997 Nov 1;17(21):8300–12.

14. Ruzankina Y, Pinzon-Guzman C, Asare A, Ong T, Pontano L, Cotsarelis G, et al. Deletion of the developmentally essential gene ATR in adult mice leads to age-related phenotypes and stem cell loss. Cell Stem Cell. 2007 Jun;1(1):113–26.

15. Dehmer JJ, Garrison AP, Speck KE, Dekaney CM, Van Landeghem L, Sun X, et al. Expansion of intestinal epithelial stem cells during murine development. PLoS ONE. 2011 Nov 10;6(11):e27070.

16. Murayama M, Okamoto R, Tsuchiya K, Akiyama J, Nakamura T, Sakamoto N, et al. Musashi-1 suppresses expression of Paneth cell-specific genes in human intestinal epithelial cells. J Gastroenterol. 2009 Mar;44(3):173–82.

17. Fre S, Huyghe M, Mourikis P, Robine S, Louvard D, Artavanis-Tsakonas S. Notch signals control the fate of immature progenitor cells in the intestine. Nature. 2005 Jun;435(7044):964–8.

18. VanDussen KL, Samuelson LC. Mouse atonal homolog 1 directs intestinal progenitors to secretory cell rather than absorptive cell fate. Developmental Biology. 2010 Oct;346(2):215–23.

19. Imai T, Tokunaga A, Yoshida T, Hashimoto M, Mikoshiba K, Weinmaster G, et al. The neural RNA-binding protein Musashi1 translationally regulates mammalian numb gene expression by interacting with its mRNA. Mol Cell Biol. 2001 Jun 15;21(12):3888–900.

20. Zhou W-J, Geng ZH, Spence JR, Geng J-G. Induction of intestinal stem cells by R-spondin 1 and Slit2 augments chemoradioprotection. Nature. 2013 Sep;501(7465):107–11.

21. Eichhorn JM, Sakurikar N, Alford SE, Chu R, Chambers TC. Critical role of anti-apoptotic Bcl-2 protein phosphorylation in mitotic death. Cell Death Dis. 2013 Oct;4(10):e834–e834.

22. Manchado E, Guillamot M, de Cárcer G, Eguren M, Trickey M, García-Higuera I, et al. Targeting mitotic exit leads to tumor regression in vivo: modulation by Cdk1, Mastl, and the PP2A/B55α,δ Phosphatase. Cancer Cell. 2010 Dec;18(6):641–54.

23. Cheng H, Bjerknes M. Whole population cell kinetics and postnatal development of the mouse intestinal epithelium. Anat Rec. 1985 Apr;211(4):420–6.

24. Takahashi T, Suzuki H, Imai T, Shibata S, Tabuchi Y, Tsuchimoto K, et al. Musashi-1 post-transcriptionally enhances phosphotyrosine-binding domain-containing m-Numb protein expression in regenerating gastric mucosa. PLoS ONE. 2013 Jan 4;8(1):e53540.

25. Cambuli FM, Correa BR, Rezza A, Burns SC, Qiao M, Uren PJ, et al. A mouse model of targeted Musashi1 expression in whole intestinal epithelium suggests regulatory roles in cell cycle and stemness. Stem Cells. 2015 Dec;33(12):3621–34.

26. Zeineldin M, Neufeld K. Isolation of epithelial cells from mouse gastrointestinal tract for western blot or RNA analysis. Bio-Protocol. [Internet]. 2012 [cited 2019 Sep 3];2(22). Available from: https://bio-protocol.org/e292

27. Zeineldin M, Cunningham J, McGuinness W, Alltizer P, Cowley B, Blanchat B, et al. A knock-in mouse model reveals roles for nuclear Apc in cell proliferation, Wnt signal inhibition and tumor suppression. Oncogene. 2012 May;31(19):2423–37.

28. Pfaffl MW. A new mathematical model for relative quantification in real-time RT-PCR. Nucleic Acid Res. 2001 May 1;29(9):45e–45.

29. Chiremba TT, Neufeld KL. Constitutive Musashi1 expression impairs mouse postnatal development and intestinal homeostasis. Mol Biol Cell. 2020 Nov 11. Ahead of print. Available: https://www.molbiolcell.org/doi/abs/10.1091/mbc.E20-03-0206#

CHAPTER 5: MUSASHI1 AND INTESTINAL ION TRANSPORTERS

ABSTRACT

Normal transport of ions across the intestinal epithelium tissue is essential for maintenance of electrolyte balance. Aberrant ion transporter function in the intestinal epithelium can result in diarrhea and dehydration, which can be fatal if left untreated. Ubiquitous Msi1-overexpressing ($Msi1^{O/E}$) mice exhibited similar phenotypes to mouse models with abnormal expression of ion transporters. These phenotypes included drastic weight loss, failure to thrive, and bloated intestines. I hypothesized that altered expression of intestinal ion transporters and dehydration could underlie the impaired growth and premature death of $Msi1^{O/E}$ mice. Therefore, I analyzed expression of intestinal ion transporters and performed dehydration studies in order to determine whether the $Msi1^{O/E}$ mice were dying from dehydration. Here I show that $Msi1^{O/E}$ intestinal tissue had enhanced expression of the ion transporters *Slc26a3*, *Slc9a3*, and *Atp12a*. However, I did not find evidence of excessive water loss in these $Msi1^{O/E}$ mice. This result suggests that $Msi1^{O/E}$ mice were not dying from dehydration.

INTRODUCTION

The small intestine absorbs nutrients and water from the food and drink that we ingest. While the colon mainly absorbs water from the remaining food material and generates stool. In addition to food and water absorption, the intestines are involved in the secretion and absorption of ions, also known as electrolytes. These ions include sodium (Na^+), chloride (Cl^-), hydrogen (H^+), potassium (K^+), calcium (Ca^{2+}), and bicarbonate (HCO_3^-). The transport of ions across the intestinal tissue is achieved by ion transporters and channels that are embedded within the apical brush border and basolateral membranes of intestinal epithelial cells. Malfunctions of ion transporters can cause gastrointestinal diseases with symptomatic diarrhea, which results in

electrolyte imbalance (1). If left untreated, diarrhea can be life-threatening because it causes excessive water loss and dehydration-related complications, such as low blood volume, fatigue, and kidney failure (2). Thus, it is essential to identify molecular factors that control the expression and functioning of intestinal ion transporters and channels.

The transmembrane protein DRA (Down-regulated in adenoma), also known as SLC26A3 (Solute carrier family 26 member 3), is expressed on the apical membrane of intestinal enterocytes. DRA was first isolated from normal human colon tissue (3). The duodenum and colon tissues have higher DRA expression than jejunum and ileum sections (4). DRA was initially predicted to be a tumor suppressor because its expression decreases in colon adenocarcinomas (3,5). However, subsequent studies showed that the primary role of DRA is as an anion exchanger which absorbs Cl^- into enterocytes and secretes HCO_3^- into the intestinal lumen (6,7). DRA expression in the intestinal epithelium is positively regulated by Caudal-type homeobox 2 (CDX2), and Hepatocyte nuclear factors 1α and β (HNF1A and HNF1B) (8,9). CDX2, HNF1A, and HNF1B are transcription factors that are involved in intestinal cell differentiation and cell fate commitment (9–11).

DRA is an essential transporter because its loss or reduced activity causes chloride-losing diarrhea (CLD). Several genetic mutations in *DRA* have been linked to congenital CLD (OMIM 2147000), a rare inherited autosomal disease (12,13). CLD is characterized by a high fecal chloride concentration and increased water loss. Mice with reduced or complete loss of *Dra* expression exhibit CLD symptoms, in addition to drastic weight loss, stunted growth, and bloated intestines with watery contents (9,14). While analyzing ubiquitous Msi1-overexpressing ($Msi1^{O/E}$) mice 14-days post-tamoxifen injection (14-dpi), I observed that the intestinal tissue was pinkish, bloated, and had watery contents. In addition, phenotypes including fatality by 14-dpi, enhanced goblet cell numbers, and decreased *Muc2*, *Hes1*, and *Math1* expression in 14-dpi ileum tissue (Chapter 4) were identical to those reported in *Dra-knockout* and *Hnf1a;Hnf1b* double-knockout mice (9,14). Given the similarities between these mice and our $Msi1^{O/E}$ model,

I hypothesized that the Msi1$^{O/E}$ mice had compromised *Dra* expression which would likely cause dehydration, stunted growth, and possibly the early death that I observed. Here I report preliminary findings from my analysis of ion transporter expression in Msi1$^{O/E}$ mice.

RESULTS

Ubiquitous Msi1-overexpression results in enhanced Nhe3 and Atp12a expression

Fig 5.1A shows the distention and watery contents in Msi1$^{O/E}$ intestinal tissue. Absorption of sodium chloride (NaCl) into enterocytes is achieved by coupling Dra anion exchanger activity to the Na^+/H^+ cation exchange activity of Nhe3 (Sodium-hydrogen antiporter 3) (15). Nhe3, also known as Slc9a3 (Solute carrier family 9 member 3), is expressed at the apical brush border of enterocytes (Fig. 5.1B). It has been shown that dehydration and loss of chloride due to low Dra expression and function can promote expression of Nhe3, possibly as a way to compensate for the loss of the coupling between Nhe3 and Dra, and to increase Na^+ absorption (14). In addition to Nhe3, compromised Dra activity also increases expression of Atp12a (H^+/K^+ transporting, non-gastric, alpha polypeptide), and ENaC (Epithelial sodium channel) transporters (14).

To investigate potential alterations in expression patterns of ion transporters in Msi1$^{O/E}$ mice, I analyzed expression of *Nhe3* and *Atp12a* in isolated intestinal epithelial cells (IECs) by RT-qPCR. *Atp12a* mRNA levels were significantly higher ($p = 0.0218$) in 14-dpi Msi1$^{O/E}$ colon IECs than in control samples (Fig. 5.1C). Negligible or no *Atp12a* expression was observed in ileum IECs (data not shown). Although *Nhe3* expression trended to be higher in Msi1$^{O/E}$ jejunum and colon samples from 7-dpi mice, it was not significantly different from control levels (Fig. 5.1D). In contrast, there was significantly more *Nhe3* in Msi1$^{O/E}$ ileum ($p = 0.0003$) and colon ($p = 0.0260$) IECs when compared to controls at 14-dpi (Fig. 5.1E). Taken together, my results show that Msi1 overexpression correlates with increased intestinal expression of *Nhe3* and *Atp12a* by 14-dpi.

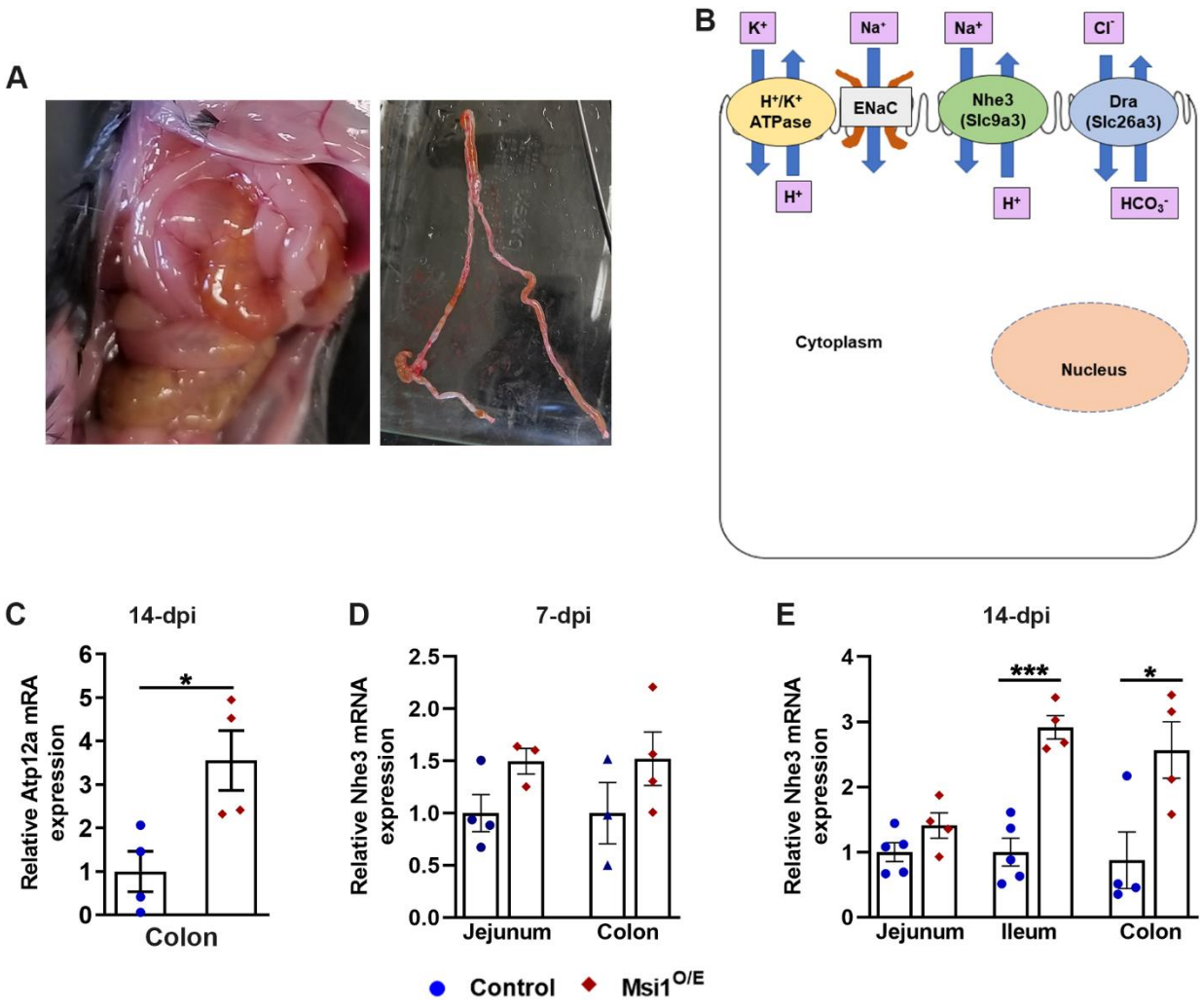

Figure 5.1: Enhanced expression of intestinal ion transporters in Msi1-overexpressing mice. (A) Preliminary intestinal images from a Msi1$^{O/E}$ mouse showing bloated and reddish-pink colored intestines **(B)** Ion transporters involved in the absorption and export of various ions in the intestinal epithelial. Analyses of **(C)** *Atp12a* and **(D, E)** *Nhe3* mRNAs in IECs harvested from 7- and 14-dpi mice (7-dpi, Control jejunum n = 4, colon n= 3; Msi1$^{O/E}$, jejunum n = 3, colon n = 4; 14-dpi, Control n = 5, Msi1$^{O/E}$, n = 4). There were 3 technical replicates assayed for each mouse. Expression was normalized to *Gapdh*. Graphical data represent mean ± SEM for each genotype. Each mouse is shown as individual blue circle (Control) or red diamond (Msi1$^{O/E}$). Data analyzed using an unpaired two-tailed test. *p < 0.05, ***p < 0.001.

Upregulation of Dra in Msi1$^{O/E}$ colon

To investigate whether the elevated *Nhe3* and *Atp12a* expression in 14-dpi Msi1$^{O/E}$ IECs was due to decreased Dra expression, we performed immunofluorescence and RT-qPCR assays. Representative images of Dra immunofluorescence in 14-dpi distal colon tissues at low and high magnification are shown in Figures 5.2 A and B, respectively. Unexpectedly, enhanced Dra protein levels were observed in images from Msi1$^{O/E}$ tissue. When quantified, the signal intensity for Dra fluorescence was significantly higher (p-0.0193) in distal colons from Msi1$^{O/E}$ mice than control mice (Fig. 5.2C). Furthermore, there was significantly (p = 0.0489) more *Dra* mRNA in Msi1$^{O/E}$ colon IECs. Therefore, my results suggest that ubiquitous Msi1 overexpression results in enhanced Dra expression at both the mRNA and protein levels.

Msi1-overexpressing mice are not dehydrated

To determine whether dehydration in Msi1 overexpressing mice could underlie the increased expression of intestinal ion transporters, I analyzed water content of mouse fecal pellets. When mice are dehydrated and losing water due to diarrhea they have fluid-filled intestines and watery fecal pellets. This results in increased fecal water content. Mice were injected with a single tamoxifen dose at ~5 weeks, and weighed daily to ensure that their growth phenotype was similar to that of previous litters (Chapter 3). As expected, the Msi1$^{O/E}$ mice had stunted growth and lagged behind their littermate controls (Fig. 5.3A). However, the Msi1$^{O/E}$ mice in this group started losing weight on 12-dpi; that is, 2-days later than the initial litters (Chapter 3). The percentage water content of the fecal pellets was relatively the same between Msi1$^{O/E}$ and control mice for most of the experiment, and it ranged between 48 % and 56 % (Fig. 5.3B).

However, the mutant mice had significantly more water in their pellets than mutant mice (54.31% vs. 50.74%, p = 0.0409) at 13-dpi. Although Msi1$^{O/E}$ intestines was more transparent and had yellowish fluid contents, they were not bloated and did not contain more fluid when

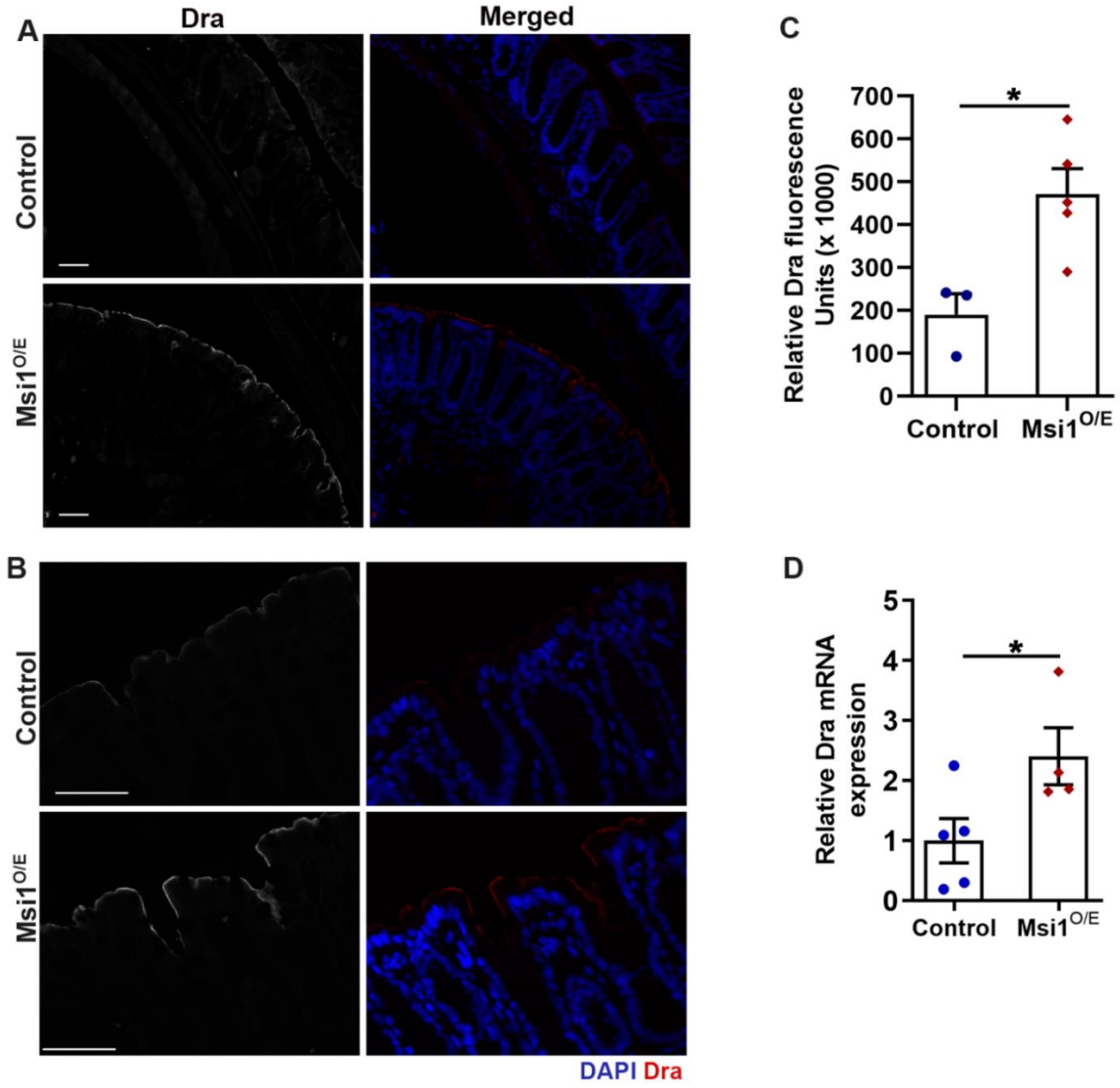

Figure 5.2: Increased Dra expression in 14-dpi distal colon epithelial tissue of Msi1-overexpressing mice. Representative immunofluorescence staining images for Dra (Gray, Red) and DAPI (Blue) in 14-dpi colon tissue at **(A)** low and **(B)** high magnification . Scale bars represent 50 µm. **(C)** Quantification of Dra immunofluorescence intensity. Each data point represent the mean relative Dra intensity in the crypt epithelial for a single mouse (Control n = 3, $Msi1^{O/E}$ n = 5). 4-6 images were analyzed for each mouse, and intensity was measured on the apical membrane. mean ± SEM. Nested two-tailed analysis. *$p < 0.05$. **(D)** Evaluation of Dra expression in isolated IECs by RT-qPCR. Expression was normalized to *Gapdh*. Each mouse is shown as individual blue circle (Control) or red diamond ($Msi1^{O/E}$). There were 3 technical replicates assayed for each mouse (14-dpi, Control, n = 5, $Msi1^{O/E}$, n = 4 mice). Data analyzed using an unpaired two-tailed test. ***$p < 0.001$, ****$p < 0.0001$. mean ± SEM.

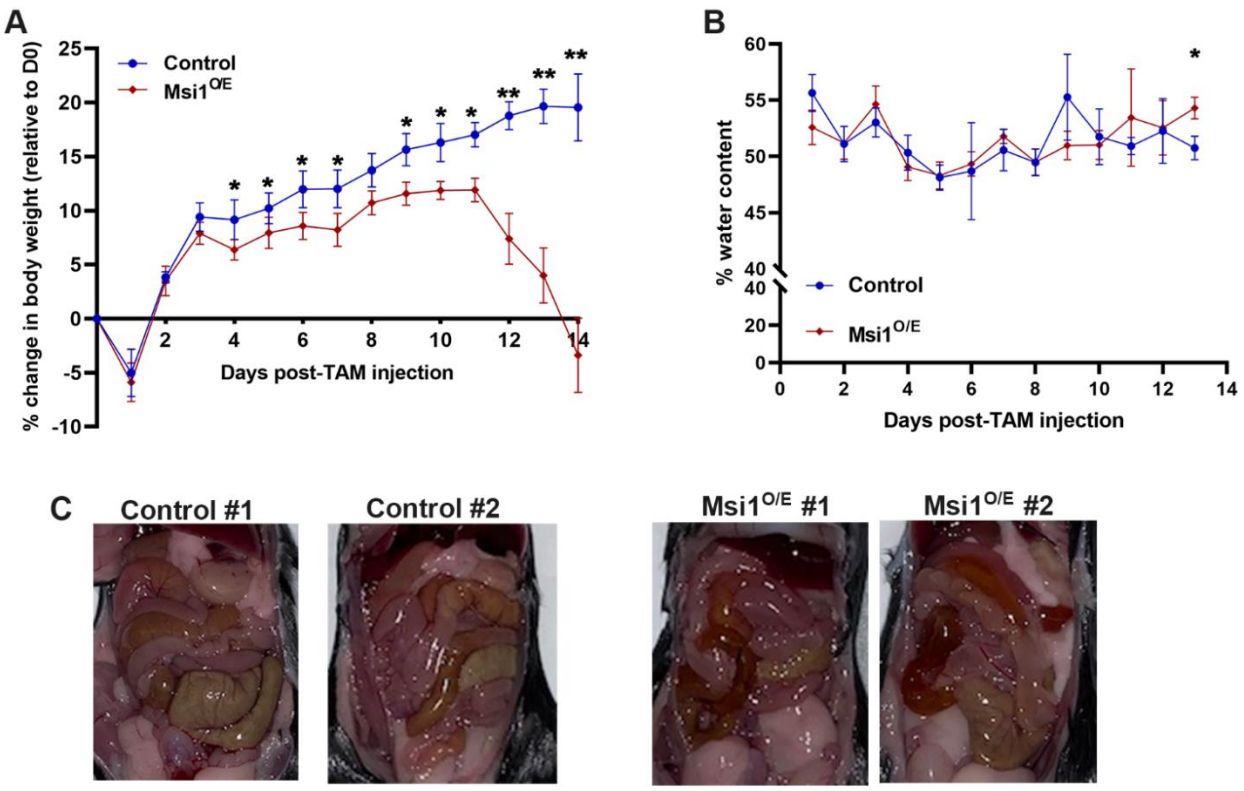

Figure 5.3: Analysis of dehydration in Msi1-overexpressing mice. (A) Daily growth curve, and **(B)** Stool water content of control and Msi1$^{O/E}$ mice from 0 to 14-dpi. Control (0- to 7-dpi n = 7, 8- to 14-dpi n = 4), Msi1$^{O/E}$ (0- to 7-dpi n = 10, 8- to 14-dpi n = 7). Graphical data represent mean ± SEM. Data analyzed using an unpaired two-tailed t-test *p < 0.05, **p < 0.01. **(C)** Morphological analyses of intestinal tissues from control and Msi1$^{O/E}$ mice (n = 2 for each genotype).

compared to control samples. Taken together, our results suggest that the Msi1$^{O/E}$ mice are not dehydrated during the majority of the experiment and their intestines do not show signs of diarrhea that is associated with loss of Dra expression and function.

DISCUSSION

Based on phenotype similarities between *Dra-knockout* (9,14) and our Msi1$^{O/E}$ mice, I hypothesized that there was decreased Dra expression in Msi1$^{O/E}$ intestinal epithelial tissue. I also predicted that *Nhe3* and *Atp12a* expression would be upregulated in order to compensate for the loss of Dra expression and activity. As expected, I observed enhanced *Nhe3* and *Atp12a* expression in Msi1$^{O/E}$ colon tissue. In contrast, there was more *Dra* mRNA colon IECs and elevated DRA protein in distal colon tissue of Msi1$^{O/E}$ mice at 14-dpi. These findings contradict our hypothesis.

Furthermore, my experiments failed to demonstrate prolonged dehydration in the Msi1$^{O/E}$ mice as I had predicted. The fecal pellets of Msi1$^{O/E}$ mice had more water content than those of control mice on 13-dpi, suggesting the onset of possible dehydration in these mice. In addition, the yellowish watery-contents and increased transparency of the Msi1$^{O/E}$ intestines implied absorption differences between mutant and control mice. However, the limited duration of my experiment due to low survival of Msi1$^{O/E}$ mice makes it difficult to extend the experiment and study dehydration past 13-dpi.

Although the results did not support my hypothesis, it is interesting that Msi1 overexpression resulted in elevated expression of the three ion transporters that were analyzed. Enhanced *Nhe3* was observed in an intestinal-specific gain-of-function mouse model for Msi1 (16). However, upregulation of Dra and *Atp12* following Msi1 overexpression has not been reported before. It is possible that Msi1 binds to the mRNAs encoding these transporters and positively regulates their translation. *Dra* and *Nhe3* transcripts were bound to Msi1 in a doxycycline-inducible mouse model that overexpressed Msi1 under the control of a *collagen1*

promoter (17). However, the effect of Msi1 binding to these mRNAs is yet to be fully determined. Another possible mechanism is that Msi1 influences expression of these targets indirectly by controlling expression of transcription factors that regulate expression of genes encoding these ion transporters. For example, *Cdx2* and *Hnf1b* transcripts were also identified as direct targets of Msi1 in the doxycycline-inducible Msi1 mice. Given the essential role of Dra in chloride absorption, it will be interesting to investigate the mechanism by which Msi1 regulates *Dra* expression.

MATERIALS AND METHODS

Dra (Slc26a3) immunofluorescence

Colon tissues were flushed with 10% saline-buffered formalin, cut lengthwise, individually rolled into “Swiss rolls”, and fixed in 10% saline-buffered formalin for 24 hr. The tissue was then stored in 70% ethanol before paraffin embedding. In brief, 4µm tissue sections were deparaffinized 3x in xylene-substitute for a total of 30 min, rehydrated in a graded ethanol series (100, 95, 80, 70, 50%) for 5 min each, and slides were washed in PBS. Antigen-retrieval was achieved by incubating slides in 0.01M citrate buffer (0.05% Saponin, pH 6.2) in a 90-95^{o}C water bath for 20 min. Slides were cooled at room temperature for 20 min, washed 2 times in PBS for 3 min each, and then incubated for 2 hr in a PBS-blocking buffer containing 2% normal goat serum, 0.05% Saponin, 5% cold-fish skin gelatin, and 10% BSA (w/v). Sections were then incubated with Dra/Slc26a3 (1:200 Invitrogen, #PA5-57508) primary antibody overnight at 4^{o}C. Slides were rinsed 3x in PBS for 15 min total, incubated with Alexa Fluor 568 secondary antibody (1:1000 Invitrogen) for 1 hr at room temperature, and rinsed 3x in PBS before counterstaining with DAPI (Invitrogen, #P36962).

Microscope image acquisition and analysis

Immunofluorescence images were acquired using a Zeiss (Axiovert 135) microscope and Hamamatsu (C10600) digital camera. Slides were assigned coded IDs and images were taken by an investigator who was blinded to sample genotype. An additional blinding step was performed, before image analysis, by renaming each acquired image with a random 4-letter code (generated using Excel). Images and slides were decoded after completion of measurements and/or counting analysis. Image brightness and levels were adjusted in Photoshop (Adobe), using identical settings for matched experiments. Dra immunofluorescence signal intensities were measured using ImageJ software. Signal intensities were measured on the apical membrane of the crypts. Intensity data were analyzed using the corrected total cellular fluorescence method (CTCF). CTCF = Integrated fluorescence density – (Area of selected tissue region X Mean fluorescence of background readings). The background readings were measured from negative control (no primary antibody, secondary only) slides.

Gene expression analysis by RT-qPCR

Isolation of mouse intestinal epithelial cells, RNA preparation, generation of complementary DNA, and gene expression analysis by RT-qPCR were performed as described in Chapter 3.

Table 5.1: **RT-qPCR Primer sequences and efficiencies**. Primer efficiencies and expression levels assayed using PowerUp SYBR Green.

Gene	Forward Primer (5' - 3')	Reverse Primer (5' - 3')	Efficiency
Atp12a	ATGCGCCGGAAAACAGAAATC	CTCCTCCTGACTCTTGTTGG	100 %
Dra	CCATCGAACTCATCATGACTG	GGGTTGAAATCCAAGACTCAT	99.42 %
Gapdh	TGGCCTTCCGTGTTCCTAC	GAGTTGCTGTTGAAGTCGCA	90.66 %
Nhe3	ATGTCAGTGCTGTATGCCTGGA	CGTGCCGACTATAGAGATGCTTG	99.09 %

Measurement of water content in fecal pellets

1.5 mL microcentrifuge tubes were labelled and pre-weighed. Mouse fecal pellets were collected at the same time that mice were being weighed. Mice usually produced a fecal pellet when they were removed from the housing cages into an empty tip box that was used for their weighing. The number of fecal pellets was recorded and pellets were transferred to a pre-weighed and labelled tube. Then the wet pellets were measured and dried in an oven at 50^{o} C for 20 hours with the tube lid open. The dry pellets were measured and the percentage of water content was calculated as: *% Water content = ((Wet weight - Dry weight)/ Wet weight) * 100*.

Statistical analysis

All data was analyzed using GraphPad Prism 8 software. RT-qPCR, mouse daily weights, and fecal water content were analyzed using an unpaired two-tailed t-test. Immunofluorescence signal intensities for Dra were analyzed using a nested two-tailed t-test.

ACKNOWLEDGEMENTS

We would like to thank William McGuinness for assistance with mouse tamoxifen injections, and Kayla Castillo for assistance with mouse tissues harvesting.

REFERENCES

1. Moe AE. Electrolyte balance in gastrointestinal disease. Calif Med 1955;83(5):339–42.
2. Watso JC, Farquhar WB. Hydration status and cardiovascular function. Nutrients. 2019 Aug 11;11(8):1866.
3. Schweinfest CW, Henderson KW, Suster S, Kondoh N, Papas TS. Identification of a colon mucosa gene that is down-regulated in colon adenomas and adenocarcinomas. PNAS. 1993 May 1;90(9):4166–70.
4. Silberg DG, Wang W, Moseley RH, Traber PG. Silberg et al 1995 DRA is a transmembrane protein. JBC. 1995 May 19;270(20):11897–902.
5. Antalis TM, Reeder JA, Gotley DC, Byeon MK, Walsh MD, Henderson KW, et al. Down-regulation of DRA correlates with colon tumor progression. 1998 Aug;4(8):1857-63.

6. Melvin JE, Park K, Richardson L, Schultheis PJ, Shull GE. Mouse Down-regulated in Adenoma (DRA) is an intestinal Cl^-/HCO_3^- Exchanger and is up-regulated in colon of mice lacking the NHE3 Na^+/H^+ Exchanger. J Biol Chem. 1999 Aug 6;274(32):22855–61.

7. Chernova MN, Jiang L, Shmukler BE, Schweinfest CW, Blanco P, Freedman SD, et al. Acute regulation of the SLC26A3 congenital chloride diarrhoea anion exchanger (DRA) expressed in *Xenopus* oocytes. J Physiol. 2003 May;549(1):3–19.

8. Chatterjee I, Kumar A, Castilla-Madrigal RM, Pellon-Cardenas O, Gill RK, Alrefai WA, et al. CDX2 upregulates SLC26A3 gene expression in intestinal epithelial cells. Am J Physiol Gastrointest Liver Physiol. 2017 Sep 1;313(3):G256–64.

9. D'Angelo A, Bluteau O, Garcia-Gonzalez MA, Gresh L, Doyen A, Garbay S, et al. Hepatocyte nuclear factor 1 and control terminal differentiation and cell fate commitment in the gut epithelium. Development. 2010 May 1;137(9):1573–82.

10. Verzi MP, Shin H, San Roman AK, Liu XS, Shivdasani RA. Intestinal master transcription factor CDX2 controls chromatin access for partner transcription factor binding. Mol Cell Biol. 2013 Jan 15;33(2):281–92.

11. Yamamoto H, Bai Y-Q, Yuasa Y. Homeodomain protein CDX2 regulates goblet-specific MUC2 gene expression. Biochem Biophys Res Comm. 2003 Jan;300(4):813–8.

12. Hoglund P, Haila S, Socha J, Tomaszewski L, Saarialho-Kere U, Karjalainen-Lindsberg M-L, et al. Mutations of the Downregulated in adenoma DRA gene cause congenital chloride diarrhea. Nat Genet. 1996 Nov;14:316–9.

13. Hoglund P, Sormaala M, Haila S, Socha J, Rajaram U, Scheurlen W, et al. Identification of seven novel mutations including the first two genomic rearrangements in SLC26A3 mutated in congenital chloride diarrhea. Hum Mutat. 2001 Sep;18(3):233–42.

14. Schweinfest CW, Spyropoulos DD, Henderson KW, Kim J-H, Chapman JM, Barone S, et al. Slc26a3-deficient mice display chloride-losing diarrhea, enhanced colonic proliferation, and distinct up-regulation of ion transporters in the colon. J Biol Chem. 2006 Dec 8;281(49):37962–71.

15. Walker NM, Simpson JE, Yen P, Gill RK, Rigsby EV, Brazill JM, et al. Down-regulated in Adenoma Cl/HCO3 Exchanger couples with Na/H Exchanger 3 for NaCl Absorption in murine small intestine. Gastroenterology. 2008 Nov;135(5):1645-1653.e3.

16. Cambuli FM, Correa BR, Rezza A, Burns SC, Qiao M, Uren PJ, et al. A mouse model of targeted Musashi1 expression in whole intestinal epithelium suggests regulatory roles in cell cycle and stemness. Stem Cells. 2015 Dec;33(12):3621–34.

17. Li N, Yousefi M, Nakauka-Ddamba A, Li F, Vandivier L, Parada K, et al. The Msi family of RNA-binding proteins function redundantly as intestinal oncoproteins. Cell Rep. 2015 Dec;13(11):2440–55.

CHAPTER 6: AN INTESTINE-SPECIFIC MSI1-OVEREXPRESSING MOUSE

ABSTRACT

Previous work from our lab identified a mutual-inhibitory relationship between Musashi (Msi1) and the tumor suppressor Adenomatous polyposis coli (Apc) in human colonocytes. We predicted that this relationship is essential for maintenance of homeostasis in the intestinal epithelium. Moreover, my results from ubiquitous Msi1 overexpressing mice (Chapters 3-5) suggested a role for Msi1 in regulating homeostasis of the intestinal epithelial tissue. Therefore, I utilized an intestine-specific mouse model to further my analysis of the potential functions of Msi1 in vivo. Here I report that intestine-specific overexpression of Msi1 results in shorter colons, but is not enough to disrupt mouse postnatal growth. Unexpectedly, I observed unilateral kidney enlargement in these intestine-specific Msi1-overexpressing mice.

INTRODUCTION

In this chapter I describe preliminary results from experiments which were performed using mice that overexpress Msi1 specifically in the intestinal epithelium. Given that our ubiquitous Msi1-overexpressing mice had a strong intestinal phenotype, we aimed to investigate potential roles of Msi1 in early postnatal development using an intestine-specific inducible mouse strain. Our long-term goal for this intestine-specific model will be to determine whether overexpression of Msi1 is enough to induce formation of intestinal polyps.

RESULTS

Intestinal-specific Msi1-overexpression does not impair early postnatal development

To generate intestine-specific inducible Msi1 mice, *Rosa26*$^{Msi1/Msi1}$ (Figure 3.1A) mice were bred with hemizygous *Villin1-CreER*^{T2} mice (1). Our breeding scheme produced single-

transgenic *Rosa26*$^{Msi1/+}$, and double-transgenic *Vil-CreER*^{T2}*; Rosa26*$^{Msi1/+}$ pups. Expression of the tamoxifen-inducible Cre recombinase in *Vil-CreER*^{T2} mice was controlled by the intestinal *Villin1* (*Vil1*) promoter. For this study, 5-weeks old mice were given TAM injections for 5 consecutive days to induce *Msi1* transgene expression in the intestinal epithelial of *Vil-CreER*^{T2}*; Rosa26*$^{Msi1/+}$ mice. Single transgenic *Rosa26*$^{Msi1/+}$ littermates also received TAM injections, but they continued expressing endogenous levels of Msi1 due to the absence of the *Vil-CreER*^{T2} transgene. For simplicity purposes, I will refer to TAM-injected *Rosa26*$^{Msi1/+}$, and *Vil-CreER*^{T2}*; Rosa26*$^{Msi1/+}$ mice as control and Vil-Msi1$^{O/E}$ mice, respectively.

First, I analyzed the postnatal development of Vil-Msi1$^{O/E}$ mice by measuring their daily body weights up to 14-days post-TAM injections (dpi) (Figure 6.1A). Both control and Vil-Msi1$^{O/E}$ mice gained weight steadily during the 14-day period and there were no significant differences in their daily growth. Unlike the ubiquitous Msi1$^{O/E}$ mice (Figure 3.3A), Vil-Msi1$^{O/E}$ survived past the 14-dpi time point.

No significant alterations in organ sizes at 15-weeks post-TAM injections

To investigate whether Msi1 could act as a proto-oncogene in the intestinal epithelial tissue, I set up a 15-week long experiment after which TAM-injected mice were euthanized and analyzed. Mice were weighed once a week after the 14-dpi time point and both groups showed a gradual growth pattern up to 9-weeks post-TAM injections (wpi) (Figure 6.1B). There was a sharp, but insignificant decrease in the growth pattern of Vil-Msi1$^{O/E}$ mice at 10-wpi. Although the Vil-Msi1$^{O/E}$ mice resumed growth recovered by 11-wpi, their growth lagged behind that of control mice for the rest of the experiment (Figures 6.1B and 6.2A).

To further determine effects of intestinal-specific Msi1 overexpression on tissue growth, I measured body length, intestinal length, and organ sizes at 15-wpi. The colons of Vil-Msi1$^{O/E}$ mice were significantly shorter than those of control mice (Figure 6.2D).Vil-Msi1$^{O/E}$ mice also were shorter than controls, but the difference was not significant ($p = 0.0630$) (Figure 6.2B).

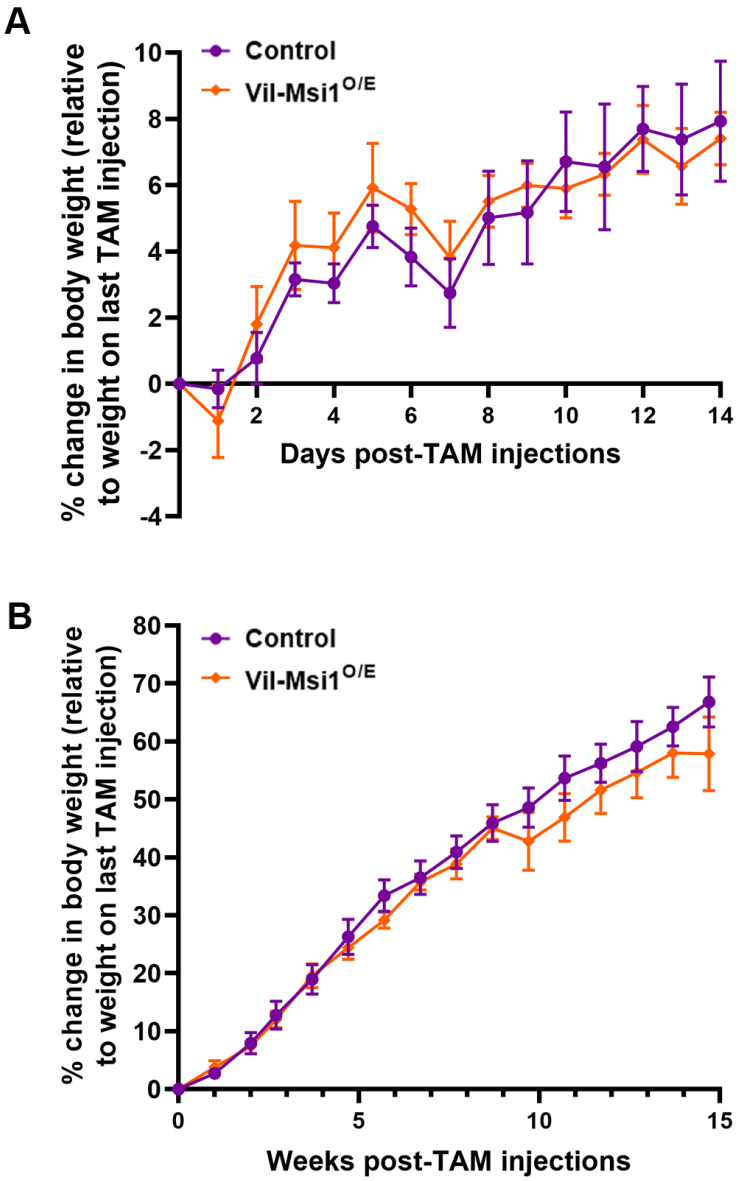

Figure 6.1: No significant difference in body weight between control and Vil-Msi1$^{O/E}$ mice. (A) Daily body weight analysis relative to weight on last TAM injection (total of 5X daily injections). (B) Body weight analysis up to ~15 weeks post-TAM injections. N =5 mice per group. Data analyzed using an unpaired student's t-test. Error bars represent SEM.

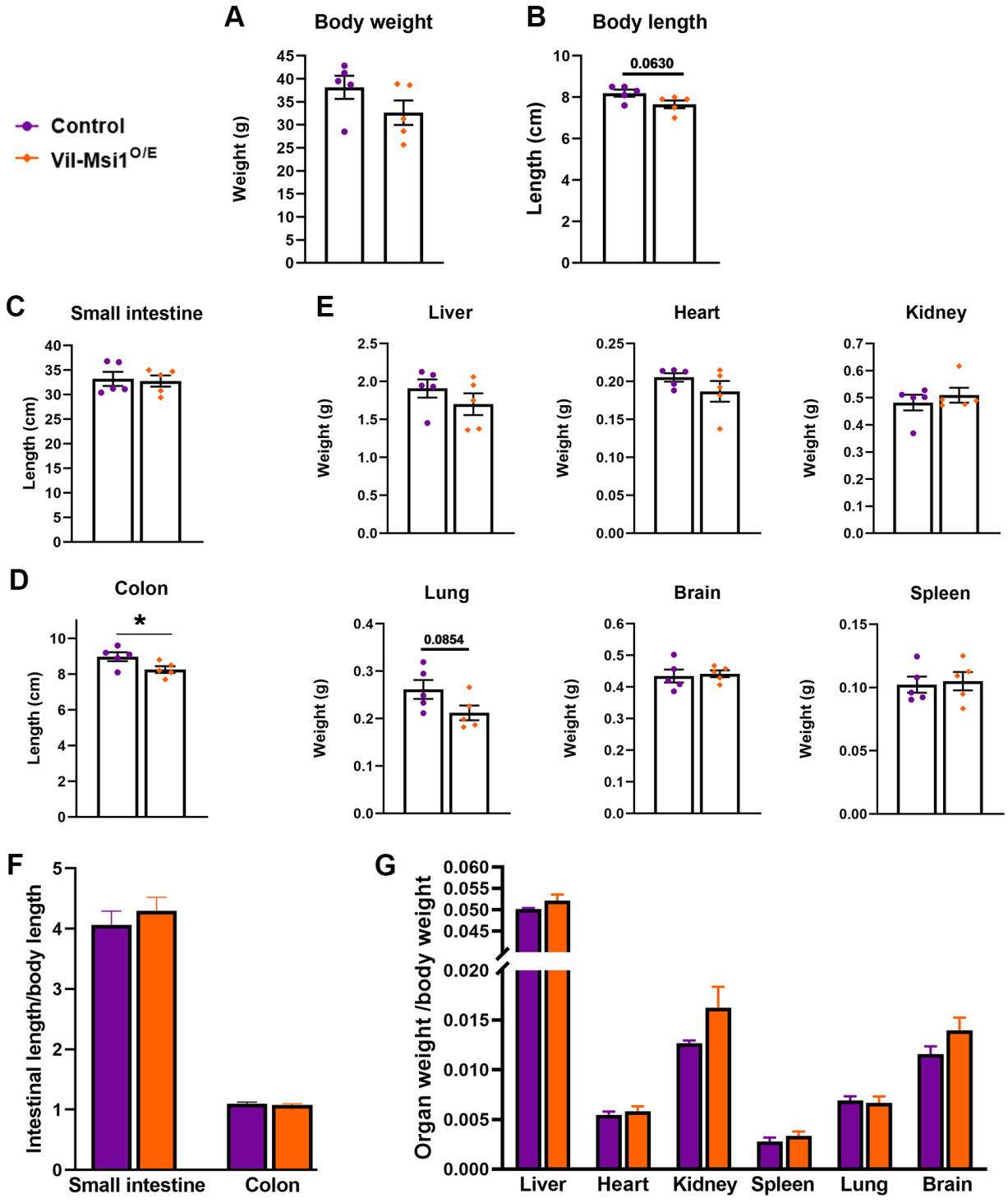

Figure 6.2: Body and organ size analysis in Vil-Msi1$^{O/E}$ mice at 15 weeks post-TAM injections. (A) Body weight, (B) Body length, (C-D) Intestinal length, (E) Organ weights, (F) Intestinal length to body length proportions, (G) Organ weight to body weight proportions. N = 5 mice per group. Data analyzed using an unpaired student's t-test. *p < 0.05. Error bars represent SEM.

Furthermore, the length of the small intestinal tissue and weights of the liver, heart, kidney, lung, brain, and spleen of Vil-Msi1$^{O/E}$ mice did not differ significantly from those of control mice (Figures 6.2C and E). Lastly, I observed no overt differences in intestinal-to-body length or organ-to-body weight proportions between control and Vil-Msi1$^{O/E}$ mice.

Increased kidney size in Vil-Msi1$^{O/E}$ mice

Unexpectedly, I observed unilateral kidney enlargement in 2 Vil-Msi1$^{O/E}$ female mice (Figure 6.3). The right kidney in these two mice was bigger than the left kidney. Part of the right kidney of Mouse #2 is missing in the image in Figure 6.3 because one-third of the kidney was filled with fluid and accidentally burst during dissection. Kidneys were of normal size in the 3 male Vil-Msi1$^{O/E}$ mice.

DISCUSSION

In this preliminary study, I showed that overexpressing Msi1 specifically in the intestinal epithelial tissue of 5-week old mice does not disrupt their postnatal growth or viability. Unlike the ubiquitous Msi1$^{O/E}$ mice that started dying at 14-dpi, the Vil-Msi1$^{O/E}$ mice can be utilized in long-term experiments to investigate potential proto-oncogenic effects of Msi1.

A remarkable phenotype of Vil-Msi1$^{O/E}$ mice which is similar to that of the ubiquitous Msi$^{O/E}$ mice is that they both have significantly shorter colons when compared to controls (Figures 3.3E and 6.2D). In addition, their colon-to-body length proportions are not differently from those of controls (Figures 3.4 and 6.2F). These results suggest that the colon tissue of these two models is possibly responding to Msi1 upregulation in a similar manner even though the total populations of cells overexpressing Msi1 are different between the two models. Future experiments will focus on analyzing and comparing the colon tissue response to Msi1 upregulation in Vil-Msi1$^{O/E}$ and ubiquitous Msi1$^{O/E}$ mice.

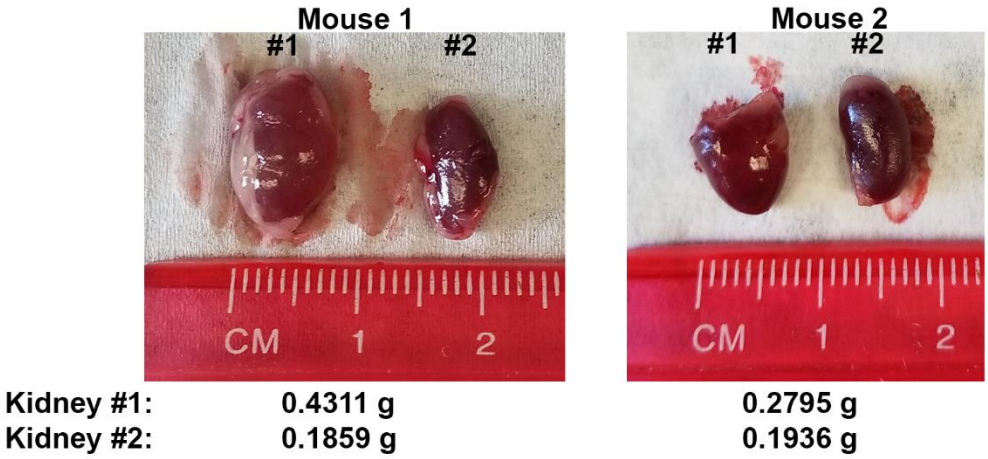

Figure 6.3: Abnormal kidney size in Vil-Msi1$^{O/E}$ mice at 15-weeks post-TAM injections. Enlarged right kidneys in 2 female Vil-Msi1$^{O/E}$ mice.

Lastly, the enlarged kidney phenotype in female Vil-Msi1$^{O/E}$ mice suggest that Msi1 overexpression has growth effects in the kidney tissue. Even though the Vil1 promoter was used to drive intestine-specific transgene expression (1–5), patchy expression of reporter transgenes was observed in non-intestinal tissues including the kidney (1,6). It is possible that our Vil-Msi1$^{O/E}$ mice have upregulated Msi1 expression in the kidneys. However, a recent study showed that *Cre-ER^{T2}* reporter expression in the same *Vil-CreER^{T2}* strain that we utilized is restricted to the small intestine, colon and seminiferous tubules in the testis (6). Therefore, other factors might underlie the enlarged kidney phenotype in our female Vil-Msi1$^{O/E}$ mice. These other unknown factors could explain why the male Vil-CreER^{T2} mice did not have enlarged kidneys.

MATERIALS AND METHODS

Mouse husbandry

Mouse use was approved by the Institutional Animal Care and Use Committee at the University of Kansas. All mouse experiments adhered to federal regulations and institutional guidelines. Mice were maintained in the Animal Care Unit at the University of Kansas under the animal use statement 137-02 and were housed in cages with sex-matched littermates, except for breeding purposes, and fed *ad libitum* water and chow (ENVIGO, Teklad global #2918).

Mice breeding and genotyping

A hemizygous B6.Cg-Tg(Vil1-cre/ERT223Syr/J) (1) male breeder was purchased from The Jackson Laboratory (# 020282). *Rosa26$^{Msi1/Msi1}$* females were crossed with the *Vil-CreER^{T2}* males to produce pups that were single transgenic *Rosa$^{Msi1/+}$*, or double transgenic *Rosa$^{Msi1/+}$;Vil1-CreER^{T2}*. Tail-snips from 3-weeks old pups were digested in 0.2mg/ml Proteinase K (ThermoFischer, #EO0491) at 55^{o}C overnight and heat-inactivated at 95^{o}C for 10 min to

extract genomic DNA. Primers used to genotype for Msi1 were: Msi1 WT Forward (WT_F) 5'-CTCTTCCCTCGTATCTGCAACTCC-3'; Msi1 WT Reverse (WT_R) 5'-CATGTCTTTAATCTACCT CGATGG-3'; Msi1 knock-in Forward (KI_F) 5'-TGGCAGGCTTGAGATCTGG-3'; Msi1 knock-in Reverse (KI_R) 5'-CCCAAGGCACACAAAAAACC-3'. PCR conditions, using OneTaq DNA polymerase (NEB, #M0482S), were 95^{o}C for 5 min, 35 cycles (95^{o}C for 30 sec, 60^{o}C for 30 sec, 72^{o}C for 1 min) and 72^{o}C for 10 min. Msi1 WT primers amplified a 299 bp sequence of the endogenous *Rosa26* locus. The binding sites for WT primers were also in the *Rosa26* knock-in allele, but there was no amplification due to the large transgenic vector inserted between the primer binding sites. The Msi1 knock-in primers amplified a 492 bp fragment. Primers used to identify Cre were: VilCreT2-FW 5'- CCAGTTTCCCTTCTTCCTCTG-3' and VilCreT2-RV 5'-CGGTTATTCAACTTGCACCA-3'. PCR conditions were 94^{o}C for 3 min, 35 cycles (94^{o}C for 30 sec, 53^{o}C for 1 min, 68^{o}C for 30 sec) and 68^{o}C for 5 min and the Cre fragment size was 225 bp. To confirm the DNA quality of *Rosa26*$^{Msi1/+}$ mouse samples analyzed for Vil-CreER^{T2}, an internal control fragment (492 bp) was amplified using the Msi1 knock-in primers.

Administration of Tamoxifen

5-week old mice, both sexes, were administered intraperitoneal injections of 50 mg/kg body weight tamoxifen (TAM) (MP Biomedicals, #156738) solution for five consecutive days. TAM was prepared under sterile conditions by dissolving in 10:1 sunflower oil/ethanol mixture. 10% of the mixture was evaporated before administration into mice. Both control and experimental mice were injected with TAM. Mice were euthanized by CO_2 asphyxiation followed by cervical dislocation at 15-weeks post-tamoxifen injections. Age-matched littermates were used for all experiments.

B**ody weight, organ weights and length measurements**

Mice were weighed daily for the first 2 weeks after the TAM injections and then weekly up to 15 weeks. Final body weights were measured immediately after mouse sacrifice. To obtain total body lengths, mice were laid face-down on a flat surface and body length was measured from the base of the skull to the anus. Organs were promptly excised and weighed, or their lengths measured. Organ to body weight proportions for liver, kidneys, thymus, spleen, lungs and brain were calculated by dividing the weight of the organ by the body weight of the mouse. Intestinal length to body length proportions were also determined for the small intestine and colon.

Statistical analysis

All data analysis was performed using GraphPad Prism 8 software. Data for body and organ weights, lengths and proportions were analyzed using an unpaired two-tailed t-test.

ACKNOWLEDGEMENTS

We thank William McGuinness for providing assistance with tamoxifen injections and the University of Kansas Animal Care Unit for mouse husbandry.

FUNDING

This work was supported by the University of Kansas Cancer Center Pilot Award.

REFERENCES

1. El Marjou F, Janssen K-P, Hung-Junn Chang B, Li M, Hindie V, Chan L, et al. Tissue-specific and inducible Cre-mediated recombination in the gut epithelium. Genesis. 2004 Jul;39(3):186–93.

2. Bohin N, Carlson EA, Samuelson LC. Genome toxicity and impaired stem cell function after conditional activation of CreERT2 in the intestine. Stem Cell Rep. 2018 Dec;11(6):1337–46.

3. Yousefi M, Li N, Nakauka-Ddamba A, Wang S, Davidow K, Schoenberger J, et al. Msi RNA-binding proteins control reserve intestinal stem cell quiescence. J Cell Biol. 2016 Nov 7;215(3):401–13.

4. Li N, Yousefi M, Nakauka-Ddamba A, Li F, Vandivier L, Parada K, et al. The Msi family of RNA-binding proteins function redundantly as intestinal oncoproteins. Cell Rep. 2015 Dec;13(11):2440–55.

5. Cambuli FM, Correa BR, Rezza A, Burns SC, Qiao M, Uren PJ, et al. A mouse model of targeted Musashi1 expression in whole intestinal epithelium suggests regulatory roles in cell cycle and stemness. Stem Cells. 2015 Dec;33(12):3621–34.

6. Rutlin M, Rastelli D, Kuo WT, Estep JA, Louis A, Riccomagno MM, et al. The Villin1 gene promoter drives Cre recombinase expression in extraintestinal tissues. Cell Mol Gastroenterol Hepatol. 2020;10(4):864-867.e5.

CHAPTER 7: MUSASHI1 AS A POTENTIAL THERAPEUTIC TARGET FOR CANCER

ABSTRACT

Musashi1 (Msi1) is upregulated in several cancer types, and has been implicated in tumor growth and survival. The knockdown of Msi1 in cancer cells can result in tumor regression. As such, we proposed that Msi1 is a potential therapeutic target for cancers that exhibit elevated Msi1 expression. Here I describe results from a collaborative study which focused on designing and testing small molecule inhibitors of Msi1. I screened small molecule inhibitors using an in vitro assay and identified three promising compounds that disrupted Msi1 activity at low doses.

INTRODUCTION

Cancer is characterized by uncontrolled proliferation of cells that have acquired growth- and survival-promoting mutations. Traditional chemotherapy involves the intravenous administration of cytotoxic agents that target these rapidly dividing cells. Chemotherapy agents can halt division of cancer cells in any phase of the cell cycle and also induce DNA damage which can cause cell death (1). Consequently, the removal of cancer cells results in shrinking of tumors. However due to the non-selective nature of cytotoxic agents, normal cells that are constantly dividing, such as hair, blood, immune, and intestinal epithelial cells, are also targeted and destroyed. This non-selectivity underlies side effects including hair loss, anemia, nausea, and appetite changes that are usually experienced by patients undergoing chemotherapy (2). As such, intensive research has focused on the development of more targeted therapies with lower toxicity.

Targeted therapy for cancer involves the identification of molecular factors that underlie the abnormal growth and survival of cancer cells. These molecular factors belong to signaling

pathways that drive the hallmarks of cancer including the ability of cancer cells to generate their own growth signals, evade programmed cell death, resist exogenous anti-growth signals, proliferate limitlessly, undergo angiogenesis, invade and metastasize, and evade immune system surveillance (3). The goal of targeted therapy is to develop drugs or molecules that can interfere with one or more of these hallmarks and eliminate the self-sufficient growth of cancer cells (4). Small molecule inhibitors are one of the main classes of targeted therapy for cancer, and they are small compounds (≤ 500 Da) that can easily enter the cell (4,5). Due to their size, small molecule inhibitors can be used to target extracellular and intracellular molecular factors, as well as be administered orally (4,6).

Small molecule inhibitors interfere with binding or interaction of proteins with their normal ligands. For example, the small molecule Gleevec (also known as Imatinib) competitively inhibits the interaction of ATP with tyrosine kinases (7,8). This interaction is necessary for phosphorylation of the kinase and the subsequent phosphorylation of downstream proteins that promote cell growth, proliferation and survival (7,8). One of these tyrosine kinases is BCR-ABL, a fusion protein that results from a translocation mutation between *Breakpoint cluster region* (*BCR*) and *Abelson tyrosine kinase* (*ABL*) genes. The *BCR-ABL* mutation underlies the pathogenesis of chronic myeloid leukemia (CML) (9–12). Gleevec is one of the successful small molecule inhibitors approved for CML treatment by the Food and Drug Administration (FDA). Given the success of Gleevec and other targeted therapies for cancer treatment, many studies have been focused on identifying additional therapeutic targets and designing small molecule inhibitors.

The RNA-binding protein Musashi1 (Msi1) is overexpressed in several cancer types including glioblastoma, colorectal, breast, lung and prostate cancers (13–21). Enhanced Msi1 expression has been shown to promote proliferation, migration, and chemoresistance in cancer cells (15,16,18,22–24). Inversely, the knockdown of Msi1 in tumors or cancer cell lines results in

growth inhibition and tumor regression (13,14,17–19). Msi1 binds to sequence-specific motifs in the coding sequences, introns, and untranslated regions of target RNAs (15,18,21,25–27). Binding of Msi1 to targets can result in translational inhibition (18,21,25,28,29), stabilization (23,30), increased translation (15,31–33) or alternative splicing (15,18,33) of specific mRNA targets. One way to target Msi1 in cancers that express elevated Msi1 would be to utilize small molecule inhibitors that can compete and interfere with target RNA binding to Msi1.

As such, Dr. Neufeld, Dr. Liang Xu and Dr. John Karanicolas collaborated on a project that focused on designing and testing small molecule inhibitors for Msi. Here I describe results from cell-based luciferase assays that were performed to test the effectiveness of these small molecules in inhibiting Msi1.

RESULTS

A cell-based bioluminescence assay for screening Msi1 small molecule inhibitors

To identify small molecule inhibitors that could effectively target and disrupt Msi1 activity, I utilized a Firefly luciferase cell-based assay to test the inhibitors. Msi1 represses *Numb* translation by binding to the *Numb* 3'UTR (25) and interfering with translation initiation (34). For the cell culture assays, a plasmid vector expressing *Firefly Luciferase* coding sequence (CDS) and *Numb* 3'-UTR under the control of a strong SV40 (Simian Virus 40) promoter was transfected into human colon cancer-derived HCT116βW cells (Fig. 7.1A, B). Another set of cells was transfected with a plasmid vector expressing only the *Firefly Luciferase* reporter gene. Then the cells were treated with either dimethyl sulfoxide (DMSO) or with potential small molecule inhibitors for 24 hours, after which time the cells were harvested and lysed. I then measured the luciferase activity of the cell lysates (Fig. 7.1C).

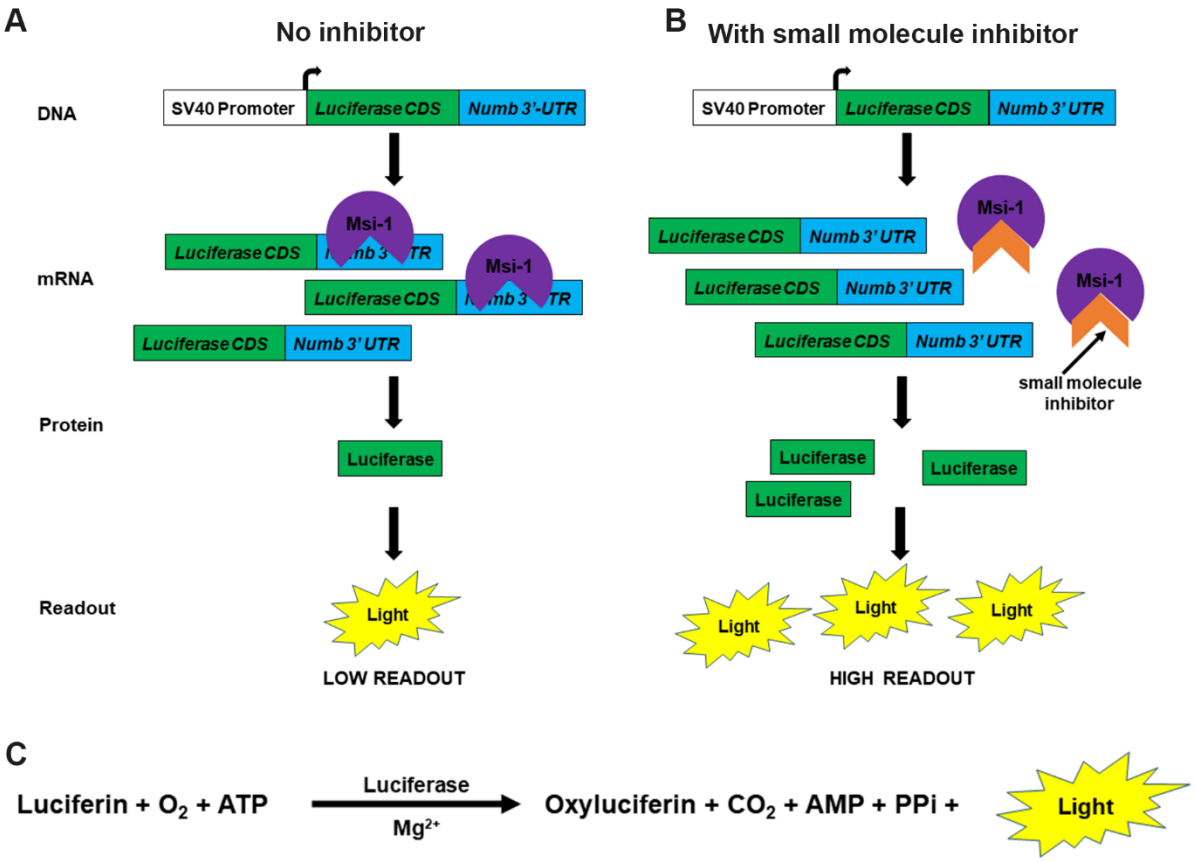

Figure 7.1: **Schematic representation of the Firefly luciferase reporter assay for testing small molecule inhibitors**. HCT116βW cells are transfected with a luciferase reporter construct fused to the *Numb*-3'-UTR (shown in B) or lacking a *Numb*-3'UTR insert (not shown in schematic). The transfected cells are then treated with a potential inhibitor. **(A)** In the absence of a small molecule inhibitor (cells treated with DMSO only), Msi1 binds to the 3'UTR of *Numb* and inhibits translation of the *Luciferase* mRNA. This results in diminished luciferase protein levels, and consequently in low luciferase readout. **(B)** Potent Msi1 inhibitors are expected to interfere with Msi1 binding to the *Numb* 3'-UTR and thus allow translation of the *Luciferase-Numb*-3'-UTR mRNA. This results in increase luciferase activity readout. **(C)** Reaction equation for the Firefly luciferase bioluminescence assay.

The majority of small molecules tested are ineffective against Msi1

Results of small molecule inhibitor testing are shown in Fig. 7.2. The black and gray bars represent relative luciferase activity for samples transfected with the control (no *Numb* 3'UTR) vector and the *Luciferase-Numb-3'-UTR* vector, respectively. The luciferase assay had two controls (1) control-transfected cells (plasmid vector expressing only the *Firefly Luciferase* reporter without the *Numb 3'UTR*), and (2) DMSO-treated cells that were transfected with either the control vector or the *Firefly Luciferase-Numb-3'UTR* fusion vector. All compounds were resuspended in DMSO; thus, the DMSO-controls served as negative controls. Another negative control was the small molecule R4 which had previously been shown to have no antagonistic effect on Msi1.

The positive control was (-)-gossypol, a natural phenolic compound that is derived from cotton plant. It has been shown that -(-)gossypol binds to and inhibits Msi1 activity in colon cancer cell lines (35). My experiments confirmed this inhibitory activity of -(-)gossypol on Msi1. There was higher relative luciferase activity in the -(-)gossypol-treated *Numb-3'-UTR*-transfected lysates (Fig. 7.2A). If a small molecule effectively inhibited Msi1, I expected the luciferase activity of the *Firefly Luciferase-Numb-3'UTR* cell lysate to be higher than the activities of the DMSO and control-vector lysates.

Of the 44 inhibitors tested at a final concentration of 20 µM, only 9 had a higher relative luciferase activity for the Numb 3'-UTR samples than controls. These inhibitors were TC1, TC4, TC22, R13 (newly synthesized in Fig. 7.2B), CB3, CB4, CB5, CB6, and YA81. Out of these 9 small molecules, 4 (TC1, TC4, TC22, CB4) met the threshold (>0.8 units) above the control sample activity. In addition to analyzing the luciferase activity of samples, I also examined the morphology of cells before harvesting and lysing them. There were more detached, rounded, and floating cells in the samples that were treated with TC1, TC4 and TC22.

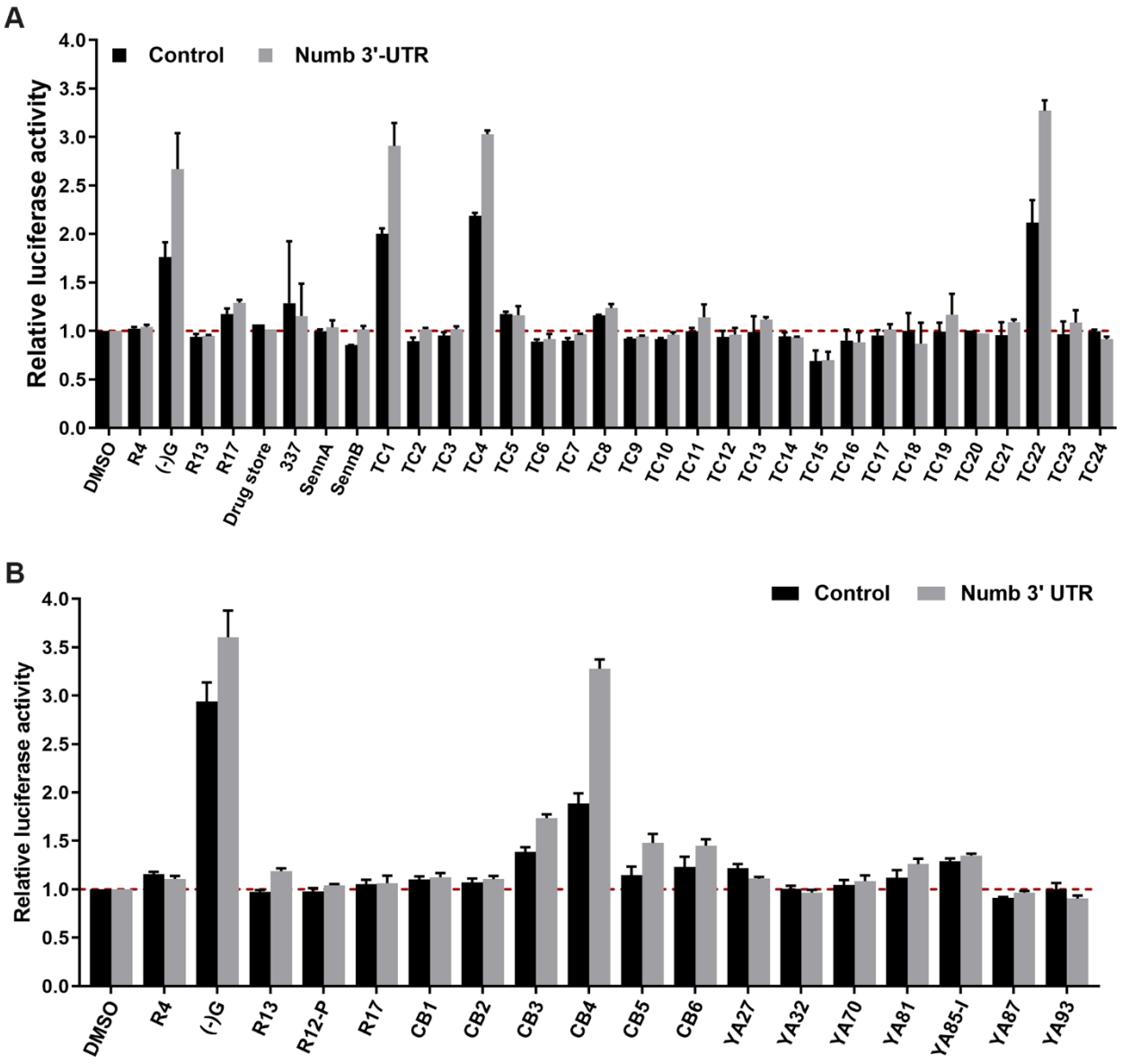

Figure 7.2: **Luciferase reporter assay for small molecule Msi1 inhibitors. (A)** First set of small molecules tested. **(B)** Second set of inhibitors tested. R13 and R17 were freshly synthesized samples. Positive control (-)-gossypol [(-)G] was tested at 5 μM, while the negative control R4 and the remaining inhibitors were tested at 20 μM final concentration. Firefly luciferase activity was normalized to Renilla luciferase activity in order to control for differences in transfection efficiencies between samples. Then to calculate the relative luciferase activity, the average Firefly/Renilla value of each sample was normalized to that of the DMSO sample. The DMSO-treated sample was the solvent control; all compounds were resuspended in DMSO. Control (black bars) are samples that were transfected with the pGL3-promoter plasmid that lacked the Num 3'-UTR. This control was for testing the specificity of the small molecule inhibitors. Error bars represent SEM. Assays were performed two independent times for the non-control small molecules in (A), except for the Drug store and TC20 molecules which were tested only once. For (B), each compound was tested at least 3 independent times.

Potential hits are effective at lower concentrations

To further investigate potential hits and determine whether they were effective at concentrations below the initial screening concentration (20 µM), I performed dose-response assays for TC1, TC4, and TC22. It is recommended that small molecules be used at concentrations less than or equal to 10 µM in order to increase their specificity (36). Therefore, I tested TC1, TC4, and TC22 at 0.5, 1, 2.5, 5, and 10 µM (Fig 7.3 A-C).

The relative luciferase activity of samples treated with TC1 increased steadily from to 2.5 to 10 µM (Fig. 7.3A). In contrast, TC4-treated samples did not show a continuously upwards trend (Fig. 7.3B). Only the 0.5, 2.5, and 5µM treatments had more luciferase activity than the control-transfected samples. Unexpectedly, both the control and *Numb* 3-UTR samples that were treated with 10 µM TC4 had lower luciferase activity than the 2.5, and 5µM samples. Lastly, TC22 gave similar luciferase activities for the 2.5, and 5µM samples and these were lower than that of the 10 µM-treated cell lysates (Fig. 7.3C). Molecular structures for TC1, TC4, TC22, and -(-)gossypol are shown in Fig. 7.3 D-G. Taken together, these results suggest that TC1, TC4, and TC22 could potentially be effective at inhibiting Msi1 protein activity.

DISCUSSION

Using a cell-based luciferase assay, I identified 4 small molecules (TC1, TC4, TC22, and CB4) that show potential effectiveness at inhibiting Msi1 activity. In addition, dose-response analysis revealed that TC1, TC4, and TC22 were effective at low concentrations (≤ 10 µM). This is an essential requirement when designing specific small molecules because the low concentration reduces the probability of targeting other proteins (36). Although the compounds were effective at these low concentrations, they were not as specific as expected. I predicted that a specific inhibitor against Msi1 would only enhance luciferase activity of the *Firefly Luciferase-Numb-3'UTR* sample and not affect the activity of the sample transfected with the control-vector. However, all 3 compounds also increased the activity of the control sample,

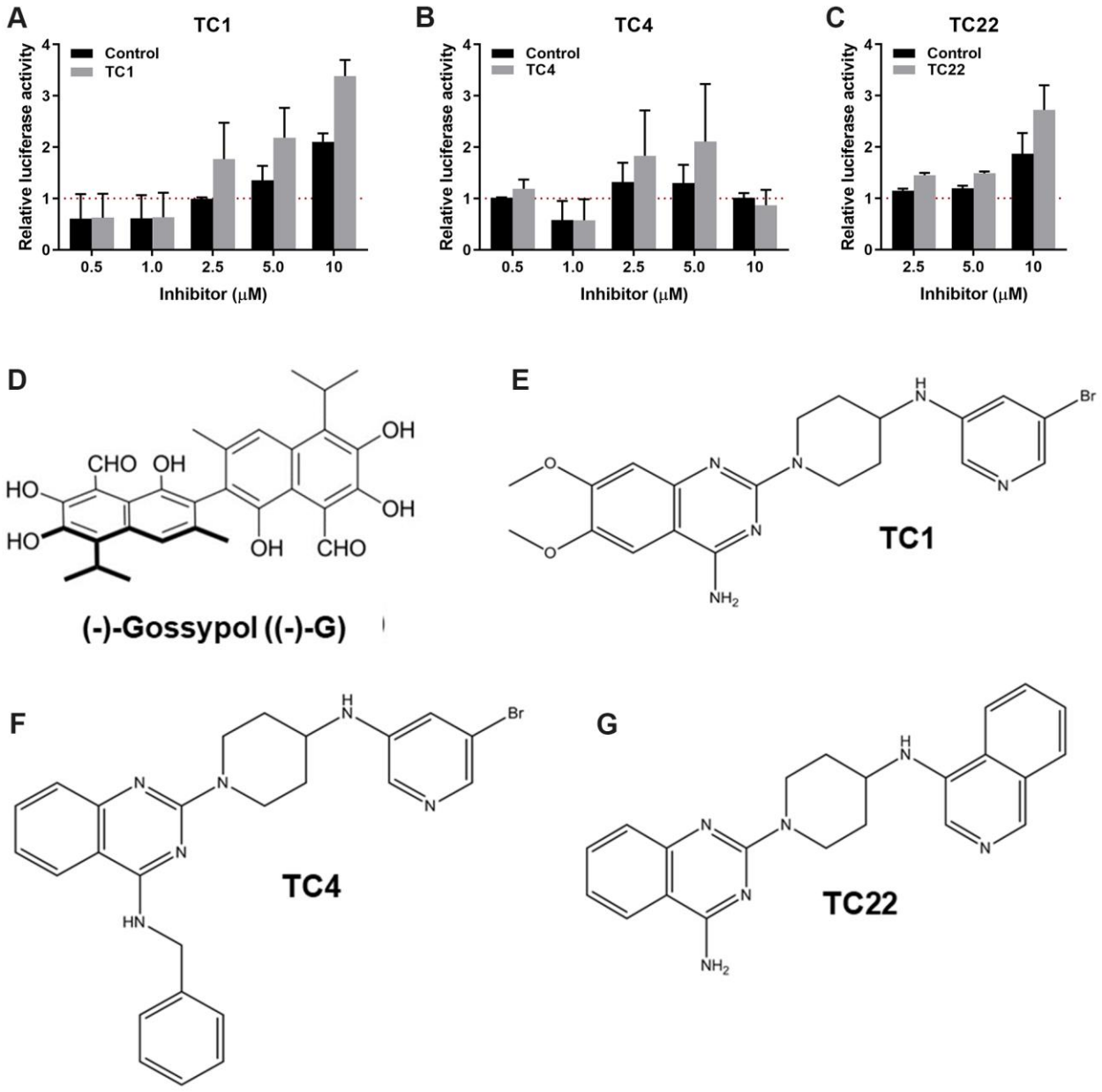

Figure 7.3: Dose-response analysis and molecular structures of potential hits. (A-C) Dose-response analysis of TC1, TC4, and TC22 inhibitors that had more luciferase activity in lysate from cells transfected with the Numb 3'-UTR-containing plasmid than in those with the control plasmid. Error bars represent SEM. Sample size: n = 2 independent assays for 0.5 and 1.0 μM; n = 3 independent assays for 2.5, 5, and 10 μM. **(D)** The positive control (-)-Gossypol **(E)** Molecule TC1 (CCT130193) **(F)** Molecule TC4 (CCT130155) **(G)** Molecule TC22 (CCT135153).

suggesting that they were also altering the translation of the plasmid backbone sequence. Strikingly, TC1 and TC4 do not affect the luciferase activity of control sample at 2.5 μM and 0.5 μM, respectively.

To test if the small molecules affect the control plasmid vector, in future studies I can transfect cells with the control *Firefly luciferase* plasmid and treat the cells with different doses of TC1, TC4, and TC22. Then I would analyze the amount of luciferase protein in each sample using a Western blot. If the amount of the luciferase protein changes in a dose-dependent manner, then I would need to redo the luciferase assays using a plasmid with a backbone sequence which is not affected by the small molecules.

MATERIALS AND METHODS

Cell culture

HCT116βW colon cancer cells were seeded in a 12-well plate at ~40% confluency in media consisting of 90% McCoy's 5A (Corning, #10-050-CV) and 10% fetal bovine serum (FBS, Atlanta biologicals, #S10350), and incubated at 37 ^{o}C for 20.5 hours. Media was then aspirated from cells and replaced with fresh media for 3.5 hours. Cell transfections were performed when cells were ~80% confluent (24 hours after seeding). GeneExpresso in vitro DNA transfection Reagent (Excellgen, #EG-1031) was used for transfections as recommended by the manufacturer. The amount of DNA used for transfections is shown in Table 7.1.

6 wells were transfected with the control transfection mixture, while the remaining 6 wells were transfected with the pGVP2-Numb-3'UTR transfection mixture. After addition of transfection mixture, cells were incubated at 37 ^{o}C for 6 hours. Cells were then analyzed quickly under a microscope to determine if the wells had approximately the same number of green-fluorescent cells. This GFP signal from the pEGFP-SV40-NLS plasmid was used to determine transfection efficiency. Afterwards, the media was aspirated from one well at a time and

replaced with the fresh media containing the small molecule at a final concentration of 20 µM. Then cells were incubated at 37 ^{o}C for 24 hours.

Table 7.1: Cells were transfected with either the control or Numb-3'-UTR vector in addition to pRL-TK Renilla (Promega, #E2241) and pEGFP-SV40-NLS plasmids. We used equal number of molecules (2.889 x 10^{10}) of plasmid DNA to account for the differences in plasmid size between the pGL3-promoter (Promega, #E1761) and pGVP2-Numb-3'-UTR (gift from Okano). pRL-TK Renilla is a transfection control for the Firefly luciferase plasmids. pEGFP-SV40-NLS plasmid was used for checking transfection efficiency.

	Luciferase construct	**pRL-TK Renilla**	**pEGFP-SV40-NLS**
Control (pGL3-Promoter)	200 ng	10 ng	0.5 ng
pGVP2-Numb-3'UTR	156.2 ng	10 ng	0.5 ng

Cell lysate preparation and luciferase assay

The media was aspirated from wells and cells were washed twice with cold 1X PBS (Corning, #21-040-CV). The cell lysis and luciferase assays were performed using the Dual-Luciferase Reporter Assay System (Promega, #E1960) according to the manufacturer's instructions. Briefly, 60 µL of 1X Passive Lysis Buffer (Promega, #E194A) was added to each well and the plate was incubated on a rocker at room temperature for 10 minutes. Cells were scraped from bottom of the wells, transferred to 0.6 ml Eppendorf tubes, snap-frozen in liquid nitrogen and then placed on ice for thawing. Thawed samples were vortexed for 15 seconds, and 20 µl of cell lysates was added to a 96-well white opaque plate. The assay was performed in duplicates for each cell lysate sample. Luciferase activity was measured using a Synergy HT Multi-Detection Microplate Reader and KC4 reduction data software.

Data analysis

Data for Firefly and Renilla luciferase activities were analyzed using Excel and GraphPad Prism 8. The Firefly luciferase activity was normalized to the Renilla luciferase activity in order to account for differences in transfection efficiency. Then the normalized Firefly/Renilla values for

the duplicate samples were averaged, before they were normalized to the average Firefly/Renilla value for the DMSO-treated sample. Samples treated with effective small molecule inhibitors would have a normalized value >1.

ACKNOWLEDGMENTS

I would like to thank Dr. David Davido for providing the Synergy HT Multi-Detection Microplate Reader.

References

1. Mills CC, Kolb Ea, Sampson VB. Development of chemotherapy with cell-cycle inhibitors for adult and pediatric cancer therapy. Cancer Res. 2018 Jan 15;78(2):320–5.

2. Pearce A, Haas M, Viney R, Pearson S-A, Haywood P, Brown C, et al. Incidence and severity of self-reported chemotherapy side effects in routine care: A prospective cohort study. PLoS ONE. 2017 Oct 10;12(10):e0184360.

3. Hanahan D, Weinberg RA. The hallmarks of cancer. Cell. 2000 Jan;100(1):57–70.

4. Imai K, Takaoka A. Comparing antibody and small-molecule therapies for cancer. Nat Rev Cancer. 2006 Sep;6(9):714–27.

5. Zhong S, Jeong J-H, Chen Z, Chen Z, Luo J-L. Targeting tumor microenvironment by small-molecule inhibitors. Transl Oncol. 2020 Jan;13(1):57–69.

6. MacKenzie MJ, Hirte HW, Goss G, Maroun J, Goel R, Jr WHM, et al. A phase II trial of ZD1839 (IressaTM) 750 mg per day, an oral epidermal growth factor receptor-tyrosine kinase inhibitor, in patients with metastatic colorectal cancer. Invest New Drugs. 2005 Mar;23(2):165-170

7. Schindler T, Bornmann W, Pellicena P, Miller WT, Clarkson B, Kuriyan J. Structural mechanism for STI-571 inhibition of abelson tyrosine kinase. Science. 2000 Sep 15;289(5486):1938–42.

8. Corbin AS, Buchdunger E, Pascal F, Druker BJ. Analysis of the structural basis of specificity of inhibition of the Abl Kinase by STI571. J Biol Chem. 2002 Aug 30;277(35):32214–9.

9. Bazzoni G, Carlesso N, Griffin JD, Hemler ME. Bcr/Abl expression stimulates integrin function in hematopoietic cell lines. J Clin Invest. 1996 Jul 15;98(2):521–8.

10. Bedi A, Zehnbauer BA, Barber JP, Sharkis SJ, Jones RJ. Inhibition of apoptosis by BCR-ABL in chronic myeloid leukemia. Blood. 1994 Apr 15;83(8):2038-44.

11. Clark S, McLaughlin J, Timmons M, Pendergast A, Ben-Neriah Y, Dow L, et al. Expression of a distinctive BCR-ABL oncogene in Ph1-positive acute lymphocytic leukemia (ALL). Science. 1988 Feb 12;239(4841):775–7.

12. Pendergast AM, Quilliam LA, Cripe LD, Bassing CH, Dai Z, Li N, et al. BCR-ABL-induced oncogenesis is mediated by direct interaction with the SH2 domain of the GRB-2 adaptor protein. Cell. 1993 Oct 8;75(1):175-85.

13. Muto J, Imai T, Ogawa D, Nishimoto Y, Okada Y, Mabuchi Y, et al. RNA-binding protein Musashi1 modulates glioma cell growth through the post-transcriptional regulation of Notch and PI3 Kinase/Akt signaling pathways. PLoS ONE. 2012 Mar 12;7(3):e33431.

14. Vo DT, Subramaniam D, Remke M, Burton TL, Uren PJ, Gelfond JA, et al. The RNA-binding protein Musashi1 Affects medulloblastoma growth via a network of cancer-related genes and is an indicator of poor prognosis. Am J Patholology. 2012 Nov;181(5):1762–72.

15. Uren PJ, Vo DT, de Araujo PR, Pötschke R, Burns SC, Bahrami-Samani E, et al. RNA-binding protein Musashi1 Is a central regulator of adhesion pathways in glioblastoma. Mol Cell Biol. 2015 Sep 1;35(17):2965–78.

16. Chen H-Y, Lin L-T, Wang M-L, Laurent B, Hsu C-H, Pan C-M, et al. Musashi-1 enhances glioblastoma cell migration and cytoskeletal dynamics through translational inhibition of Tensin3. Sci Rep. 2017 Dec;7(1):8710.

17. Sureban SM, May R, George RJ, Dieckgraefe BK, McLeod HL, Ramalingam S, et al. Knockdown of RNA binding protein Musashi-1 leads to tumor regression in vivo. Gastroenterology. 2008 May;134(5):1448-1458.e2.

18. Li N, Yousefi M, Nakauka-Ddamba A, Li F, Vandivier L, Parada K, et al. The Msi family of RNA-binding proteins function redundantly as intestinal oncoproteins. Cell Rep. 2015 Dec;13(11):2440–55.

19. Wang X-Y, Penalva LO, Yuan H, Linnoila RI, Lu J, Okano H, et al. Musashi1 regulates breast tumor cell proliferation and is a prognostic indicator of poor survival. Mol Cancer. 2010;9(1):221.

20. Lagadec C, Vlashi E, Frohnen P, Alhiyari Y, Chan M, Pajonk F. The RNA-binding protein Musashi-1 regulates proteasome subunit expression in breast cancer- and glioma-initiating cells: Musashi-1 controls CSC regulated proteasome subunit expression. Stem Cells. 2014 Jan;32(1):135–44.

21. Katz Y, Li F, Lambert NJ, Sokol ES, Tam W-L, Cheng AW, et al. Musashi proteins are post-transcriptional regulators of the epithelial-luminal cell state. eLife. 2014;3:e03915

22. Rezza A, Skah S, Roche C, Nadjar J, Samarut J, Plateroti M. The overexpression of the putative gut stem cell marker Musashi-1 induces tumorigenesis through Wnt and Notch activation. J Cell Sci. 2010 Oct 1;123(19):3256–65.

23. Cambuli FM, Correa BR, Rezza A, Burns SC, Qiao M, Uren PJ, et al. A mouse model of targeted Musashi1 expression in whole intestinal epithelium suggests regulatory roles in cell cycle and stemness. Stem Cells. 2015 Dec;33(12):3621–34.

24. Chiou G-Y, Yang T-W, Huang C-C, Tang C-Y, Yen J-Y, Tsai M-C, et al. Musashi-1 promotes a cancer stem cell lineage and chemoresistance in colorectal cancer cells. Sci Rep. 2017 Dec;7(1):2172.

25. Imai T, Tokunaga A, Yoshida T, Hashimoto M, Mikoshiba K, Weinmaster G, et al. The neural RNA-binding protein Musashi1 translationally regulates mammalian numb gene expression by interacting with its mRNA. Mol Cell Biol. 2001 Jun 15;21(12):3888–900.

26. Ohyama T, Nagata T, Tsuda K, Kobayashi N, Imai T, Okano H, et al. Structure of Musashi1 in a complex with target RNA: the role of aromatic stacking interactions. Nucleic Acid Res. 2012 Apr;40(7):3218–31.

27. Zearfoss NR, Deveau LM, Clingman CC, Schmidt E, Johnson ES, Massi F, et al. A conserved three-nucleotide core motif defines Musashi RNA binding specificity. J Biol Chem. 2014 Dec 19;289(51):35530–41.

28. Spears E, Neufeld KL. Novel double-negative feedback loop between Adenomatous Polyposis Coli and Musashi1 in colon epithelia. J Biol Chem. 2011 Feb 18;286(7):4946–50.

29. Battelli C, Nikopoulos GN, Mitchell JG, Verdi JM. The RNA-binding protein Musashi-1 regulates neural development through the translational repression of p21WAF-1. Mol Cell Neurosci. 2006 Jan;31(1):85–96.

30. Nahas GR, Murthy RG, Patel SA, Ganta T, Greco SJ, Rameshwar P. The RNA-binding protein Musashi 1 stabilizes the oncotachykinin 1 mRNA in breast cancer cells to promote cell growth. FASEB J. 2016 Jan;30(1):149–59.

31. Kuwako K, Kakumoto K, Imai T, Igarashi M, Hamakubo T, Sakakibara S, et al. Neural RNA-binding protein Musashi1 controls midline crossing of precerebellar neurons through posttranscriptional regulation of Robo3/Rig-1 expression. Neuron. 2010 Aug;67(3):407–21.

32. Lin J-C, Tsai J-T, Chao T-Y, Ma H-I, Liu W-H. Musashi-1 Enhances glioblastoma migration by promoting ICAM1 translation. Neoplasia. 2019 May;21(5):459–68.

33. Cragle CE, MacNicol MC, Byrum SD, Hardy LL, Mackintosh SG, Richardson WA, et al. Musashi interaction with poly(A)-binding protein is required for activation of target mRNA translation. J Biol Chem. 2019 Jul 12;294(28):10969–86.

34. Kawahara H, Imai T, Imataka H, Tsujimoto M, Matsumoto K, Okano H. Neural RNA-binding protein Musashi1 inhibits translation initiation by competing with eIF4G for PABP. J Cell Biol. 2008 May 19;181(4):639–53.

35. Lan L, Appelman C, Smith AR, Yu J, Larsen S, Marquez RT, et al. Natural product (−)-gossypol inhibits colon cancer cell growth by targeting RNA-binding protein Musashi-1. Mol Oncol. 2015 Aug;9(7):1406–20.

36. Weiss WA, Taylor SS, Shokat KM. Recognizing and exploiting differences between RNAi and small-molecule inhibitors. Nat Chem Biol. 2007 Dec;3(12):739–44.

CHAPTER 8: CONCLUSIONS AND FUTURE DIRECTIONS

This dissertation work focuses on the RNA-binding protein Msi1 and the characterization of a versatile mouse model that facilitates Cre-inducible overexpression of Msi1. Our lab initially designed this Msi1 “knock in” line for the study of the proto-oncogenic properties of Msi1. But mice ubiquitously overexpressing Msi1 unexpectedly displayed a stunted growth phenotype. My analysis revealed that ubiquitous overexpression of Msi1 impairs mouse early postnatal development and results in stunted growth of several organs including the brain and intestines. I demonstrated that ubiquitous Msi1-overexpressing (Ubc-Msi1$^{O/E}$) intestines had diminished epithelial cell proliferation and growth rates in small intestine villi and colon crypts. Mechanistically, I showed that downregulation of *Cdc20* in intestinal epithelial cells could underlie these growth defects. Decreased intestinal cell proliferation and early mortality have been reported in Cdc20-knockout mice (1), and these phenotypes are similar to those observed in our Ubc-Msi1$^{O/E}$ mice. For future experiments, it would be interesting to elucidate the mechanisms underlying decreased *Cdc20* RNA levels in Msi1$^{O/E}$ mice. Future work will investigate whether Msi1 can directly bind to *Cdc20* RNA and the consequences of this interaction, or if Msi1 influences expression of *Cdc20* indirectly.

The decreased IEC proliferation in ubiquitous Msi1$^{O/E}$ mice implies that upregulation of Msi1 does not provide a growth and survival advantage in normal cells, in contrast to cancer cells. It possible that diminished *Cdc20* expression in IECs is a result of a control mechanism that prevents uncontrolled cell division of the Msi1$^{O/E}$ IECs. Examples of control mechanisms in normal cells which are related to cell cycle include oncogene-induced senescence, DNA damage response, and the various cell cycle checkpoints. Cdc20 is essential for cell cycle progression from metaphase to anaphase, and loss of Cdc20 has been shown to induce mitotic arrest and cell death (1). Thus, I propose that Msi1$^{O/E}$ intestinal epithelial tissue has fewer proliferative IECs due to decreased *Cdc20* expression, which is causing mitotic arrest and

possibly cell death of transit amplifying cells (Fig 8.1A). To investigate whether Msi1$^{O/E}$ IECs are being arrested in metaphase, we could do a DAPI staining on the intestinal epithelial tissue and analyze chromosome appearance under high magnification. If there is mitotic arrest, we expect that Msi1$^{O/E}$ tissue would have more progenitor cells in the metaphase stage when compared to the control tissue. During the metaphase-to-anaphase transition, Cdc20 binds to the anaphase-promoting complex/cyclosome (APC/C) and activates degradation of cyclin B and securin (2,3). Therefore, we could analyze the protein levels of cyclin B and securin in the intestinal crypts by immunohistochemistry. If the Msi1$^{O/E}$ progenitor cells are being arrested in metaphase, we would expect the levels of cyclin B and securin to be elevated in the Msi1$^{O/E}$ tissue. Lastly, cell death as a result of mitotic arrest could be analyzed by doing TUNEL assay or staining for Annexin V, and we would expect increased apoptotic cells in the intestinal crypts of Msi1$^{O/E}$ mice.

To further analyze the role of Msi1 on tissue development and postnatal growth, we could induce Msi1 upregulation in older mice. This will allow us to determine whether the growth defects that we observed in Ubc-Msi1$^{O/E}$ mice are restricted to the early postnatal period or not. If older Ubc-Msi1$^{O/E}$ mice are able to survive longer than their counterparts, we would then utilize this model for its originally intended purpose of elucidating proto-oncogenic effects of Msi1. Long-term viability is necessary to allow for the development of polyps in mice.

We also discovered that Msi1 affects intestinal epithelial cell (IEC) differentiation along the intestinal tract in a region-specific manner. The ileum tissue was the region most responsive to ubiquitous Msi1 overexpression when compared to the jejunum and colon tissues. Enterocyte cell differentiation increased in the ileum tissues at the expense of secretory cells. I showed that increased *Hes1*-to-*Math1* ratio and consequently Notch signaling could underlie the increase in enterocyte differentiation in Msi1-overexpressing mice. Although the high *Hes1*-to-*Math1* ratio suggested Notch activation, more work is needed to determine whether the changes in ileum

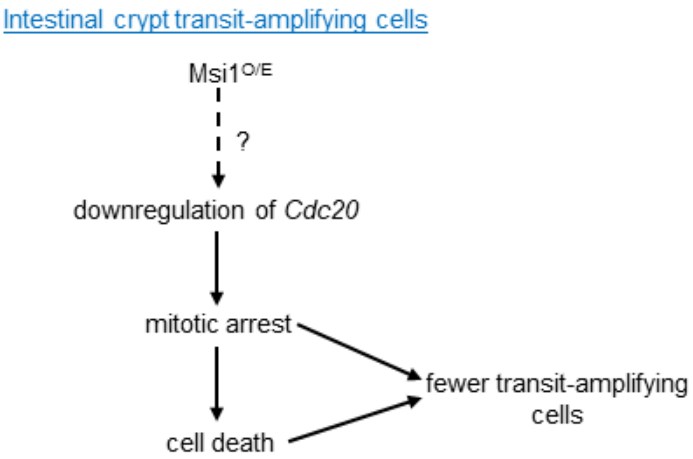

Figure 8.1: Hypothetical model for decreased intestinal epithelial cell proliferation in ubiquitous Msi1$^{O/E}$ ilea. Diminished *Cdc20* RNA levels were detected in ubiquitous Msi1$^{O/E}$ in ileal IECs. I hypothesize that the reduction in *Cdc20* expression induces mitotic arrest which would result in fewer transiting-amplifying cells, either directly or indirectly by inducing cell death. This model will be tested in future experiments.

IEC differentiation were due to modulations of Notch signaling or on transcription factors that function downstream of Hes1 and Math1. Possible transcription factors that could promote enterocyte differentiation downstream of Hes1 include *Caudal type homeobox 2* (*Cdx2*) *Hepatocyte nuclear factor-4-alpha* (*Hnf4a*), and *Hepatocyte nuclear factor-4-gamma* (*Hnf4g*) (4,5). It has been shown that Msi1 protein binds to *Cdx2*, *Hnf4a* and *Hnf4g* RNAs (4), but the effect of the binding has not yet been determined. Therefore, we could analyze expression of these three transcription factors and compare their levels between controls and Msi1-overexpressing mice, as well as among the three tissue regions. This will be the first step in unravelling the complicated region-specific effects of Msi1 upregulation on intestinal epithelial cell differentiation.

Another remarkable phenotype that we observed in the Ubc-Msi1$^{O/E}$ mice was the discrepancy in goblet cell differentiation analysis in the ileum tissue. The Alcian blue staining showed increased goblet cell numbers, whereas expression of the goblet marker *Muc2* was significantly lower in ilea epithelial cells. To understand this discrepancy, we could analyze RNA expression of other goblet cell markers such as *Trefoil factor 3* (TFF3). Another method of goblet cell analysis would be immunofluorescence staining for Muc2 in the ileum tissue. We could then determine whether the number of Muc2-positive cells correlates with the diminished *Muc2* expression in Ubc-Msi1$^{O/E}$ ileum tissue.

Using the Ubc-Msi1$^{O/E}$ mice, I also showed that Msi1 upregulation results in increased RNA and protein expression of intestinal ion transporters. Movement of ions through these transporters is important for water reabsorption into the intestinal epithelial cells. Although my experiments showed no evidence of dehydration in Ubc-Msi1$^{O/E}$ mice, these experiments showed enhanced expression of Dra, Nhe3 and Atp12a upon Msi1 upregulation. Future studies could focus on elucidating the mechanisms underlying increased expression of these 3 ion transporters. *Dra* and *Nhe3* RNAs are targets of Msi1 (6), but the regulatory effects of Msi1 on

these transcripts is unknown. Therefore, we would start by validating that the transcripts are true binding targets of Msi1 and then analyze effects of the binding on *Dra* and *Nhe3* RNA stability and translation.

Using our Msi1 knock-in model and an intestine-specific inducible strain, we showed that the growth phenotype of young Ubc-Msi1$^{O/E}$ mice differs from that of intestinal-specific Msi1 overexpressing mice (Vil-Msi1$^{O/E}$). Although we have not performed an in-depth analysis of the early postnatal development of Vil-Msi1$^{O/E}$ mice, our preliminary findings clearly show that intestinal-specific overexpression of Msi1 does not cause stunted growth nor early mortality. These results imply that non-intestinal tissue-derived factors could be influencing the stunted growth phenotype of Ubc-Msi1$^{O/E}$ mice. Remarkably, we observed unilateral kidney enlargement in female Vil-Msi1$^{O/E}$ mice. Given that Vil1 reporter expression has been reported in the kidney epithelium (7,8), it is possible that our Vil-Msi1$^{O/E}$ mice have upregulated Msi1 expression in their renal epithelia tissue. For future experiments, we could analyze Msi1 expression in the kidney tissue and then compare expression levels between controls and Vil-Msi1$^{O/E}$ mice, and between Vil-Msi1$^{O/E}$ females and males.

Lastly, we will continue investigating the potential proto-oncogenic effects of Msi1 upregulation in the intestinal epithelial tissue. First, we will analyze the intestinal tissue that was harvested at 15-weeks post-tamoxifen injections for any polyp formation. Second, we will supplement the drinking water of mice with dextran sodium sulfate (DSS) to induce inflammation and promote polyp formation in the colon tissue. If the Vil-Msi1$^{O/E}$ mice end up with more polyps than control mice, then we could conclude that Msi1 promotes polyp formation and/or tumor progression. Results from the first study without DSS will allow us to determine whether Msi1 promotes polyp formation or tumor progression. If Msi1 upregulation results in intestinal polyp formation, we could utilize the Vil-Msi1$^{O/E}$ mice to test small molecule inhibitors as potential therapeutics for colon cancer.

In conclusion, our conditional and inducible Msi1 knock-in line is an invaluable tool that can be used to analyze the regulatory functions of Msi1 in any tissue of interest using tissue-specific Cre-inducible lines. This work implicates Msi1 in early mouse postnatal development and intestinal tissue homeostasis including intestinal growth, proliferation, and differentiation. In addition, our findings demonstrate a potential role of Msi1 in regulating intestinal ion transporter expression and water reabsorption. Most importantly, our novel findings showing that Msi1 regulates intestinal cell differentiation in a region-specific manner highlight the importance of analyzing the intestinal tissue sections as separate entities. I hope that this dissertation will further the field's understanding of the regulatory roles of Msi1 in tissue development and tumorigenesis.

REFERENCES

1. Manchado E, Guillamot M, de Cárcer G, Eguren M, Trickey M, García-Higuera I, et al. Targeting Mitotic Exit Leads to Tumor Regression In Vivo: Modulation by Cdk1, Mastl, and the PP2A/B55α,δ Phosphatase. Cancer Cell. 2010 Dec;18(6):641–54.

2. Qiao R, Weissmann F, Yamaguchi M, Brown NG, VanderLinden R, Imre R, et al. Mechanism of APC/C ^{CDC20} activation by mitotic phosphorylation. Proc Natl Acad Sci USA. 2016 May;113(19):E2570–8.

3. Li M, York JP, Zhang P. Loss of Cdc20 causes a securin-dependent metaphase arrest in two-cell mouse embryos. MCB. 2007 May;27(9):3481–8.

4. Chen L, Toke NH, Luo S, Vasoya RP, Fullem RL, Parthasarathy A, et al. A reinforcing HNF4–SMAD4 feed-forward module stabilizes enterocyte identity. Nat Genet. 2019 May;51(5):777–85.

5. San Roman AK, Aronson BE, Krasinski SD, Shivdasani RA, Verzi MP. Transcription Factors GATA4 and HNF4A Control Distinct Aspects of Intestinal Homeostasis in Conjunction with Transcription Factor CDX2. J Biol Chem. 2015 Jan 16;290(3):1850–60.

6. Li N, Yousefi M, Nakauka-Ddamba A, Li F, Vandivier L, Parada K, et al. The Msi Family of RNA-Binding Proteins Function Redundantly as Intestinal Oncoproteins. Cell Rep. 2015 Dec;13(11):2440–55.

7. Rutlin M, Rastelli D, Kuo WT, Estep JA, Louis A, Riccomagno MM, et al. The Villin1 Gene Promoter Drives Cre Recombinase Expression in Extraintestinal Tissues. CMGH Cell Mol Gastroenterol Hepatol. 2020;10(4):864-867.e5.

8. El Marjou F, Janssen K-P, Hung-Junn Chang B, Li M, Hindie V, Chan L, et al. Tissue-specific and inducible Cre-mediated recombination in the gut epithelium. Genesis. 2004 Jul;39(3):186–93.